Samples collected from the floor of Jezero Crater with the Mars 2020 Perseverance Rover

J. Simon, K. Hickman-Lewis, B. Cohen, L. Mayhew, D. Shuster, V. Debaille, E. Hausrath, B. Weiss, T. Bosak, M.-p. Zorzano, et al.

JGR Planets

RESEARCH ARTICLE
10.1029/2022JE007474

Special Section:
The Mars Perseverance Rover Jezero Crater Floor Campaign

Samples Collected From the Floor of Jezero Crater With the Mars 2020 Perseverance Rover

J. I. Simon[1], K. Hickman-Lewis[2,3], B. A. Cohen[4], L. E. Mayhew[5], D. L. Shuster[6], V. Debaille[7], E. M. Hausrath[8], B. P. Weiss[9], T. Bosak[9], M.-P. Zorzano[10], H. E. F. Amundsen[11], L. W. Beegle[12], J. F. Bell III[13], K. C. Benison[14], E. L. Berger[15], O. Beyssac[16], A. J. Brown[17], F. Calef[12], T. M. Casademont[11], B. Clark[18], E. Clavé[19], L. Crumpler[20], A. D. Czaja[21], A. G. Fairén[10,22], K. A. Farley[23], D. T. Flannery[24], T. Fornaro[25], O. Forni[26], F. Gómez[10], Y. Goreva[12], A. Gorin[7], K. P. Hand[12], S.-E. Hamran[11], J. Henneke[27], C. D. K. Herd[28], B. H. N. Horgan[29], J. R. Johnson[30], J. Joseph[31], R. E. Kronyak[12], J. M. Madariaga[32], J. N. Maki[12], L. Mandon[33], F. M. McCubbin[34], S. M. McLennan[35], R. C. Moeller[12], C. E. Newman[36], J. I. Núñez[29], A. C. Pascuzzo[37], D. A. Pedersen[28], G. Poggiali[38], P. Pinet[26], C. Quantin-Nataf[39], M. Rice[40], J. W. Rice Jr.[13], C. Royer[19], M. Schmidt[41], M. Sephton[42], S. Sharma[12], S. Siljeström[43], K. M. Stack[12], A. Steele[44], V. Z. Sun[12], A. Udry[8], S. VanBommel[45], M. Wadhwa[12,13], R. C. Wiens[29], A. J. Williams[46], and K. H. Williford[47]

[1]Center for Isotope Cosmochemistry and Geochronology, Astromaterials Research and Exploration Science, NASA Johnson Space Center, Houston, TX, USA, [2]The Natural History Museum, London, UK, [3]Dipartimento BiGeA, Università di Bologna, Bologna, Italy, [4]NASA Goddard Space Flight Center, Greenbelt, MD, USA, [5]Department of Geological Sciences, University of Colorado Boulder, Boulder, CO, USA, [6]University of California, Berkeley, Berkeley, CA, USA, [7]Universitélibre de Bruxelles, Brussels, Belgium, [8]Department of Geosciences, University of Nevada, Las Vegas, Las Vegas, NV, USA, [9]Department of Earth, Atmospheric, and Planetary Sciences, Massachusetts Institute of Technology, Cambridge, MA, USA, [10]Centro de Astrobiologia (CAB), CSIC-INTA, Madrid, Spain, [11]University of Oslo, Norwegian Research Council, Oslo, Norway, [12]Jet Propulsion Laboratory, California Institute of Technology, Pasadena, CA, USA, [13]Arizona State University, Tempe, AZ, USA, [14]West Virginia University, Morgantown, WV, USA, [15]Texas State University, Jacobs JETS, NASA Johnsons Space Center, Houston, TX, USA, [16]Institut de Minéralogie, Physique des Matériaux et Cosmochimie, CNRS UMR 7590, Sorbonne Université, Muséum National d'Histoire Naturelle, Paris, France, [17]Plancius Research, Severna Park, MD, USA, [18]Space Science Institute, Boulder, CO, USA, [19]CELIA, Université de Bordeaux, CNRS, CEA, Bordeaux, France, [20]New Mexico Museum of Natural History and Science, Albuquerque, NM, USA, [21]Department of Geology, University of Cincinnati, Cincinnati, OH, USA, [22]Department Astronomy, Cornell University, Ithaca, NY, USA, [23]California Institute of Technology, Pasadena, CA, USA, [24]Queensland University of Technology, Brisbane, QL, Australia, [25]INAF-Astrophysical Observatory of Arcetri, Florence, Italy, [26]Institut de Recherche en Astrophysique et Planétologie (IRAP), Université de Toulouse, CNRS, UPS, CNES, Toulouse, France, [27]Danmarks Tekniske Universitet, National Space Institute, Lyngby, Denmark, [28]Department of Earth and Atmospheric Sciences, University of Alberta, Edmonton, AB, Canada, [29]Department of Earth, Atmospheric, and Planetary Sciences, Purdue University, West Lafayette, IN, USA, [30]Johns Hopkins University Applied Physics Laboratory, Laurel, MD, USA, [31]Cornell University, Ithaca, NY, USA, [32]Department of Analytical Chemistry, University of the Basque Country (UPV/EHU), Leioa, Spain, [33]LESIA, Observatoire de Paris, Université PSL, CNRS, Sorbonne Université, Université de Paris, Meudon, France, [34]Astromaterials Research and Exploration Science, NASA Johnson Space Center, Houston, TX, USA, [35]Department of Geosciences, Stony Brook University, Stony Brook, NY, USA, [36]Aeolis Research, Chandler, AZ, USA, [37]Malin Space Science Systems, San Diego, CA, USA, [38]INAF-Astrophysical Observatory of Arcetri, Firenze, Italy, [39]Laboratoire de Géologie de Lyon, Université Lyon, Bâtiment Géode, Villeurbanne, France, [40]Western Washington University, Bellingham, WA, USA, [41]Department of Earth Sciences, Brock University, St. Catharines, ON, Canada, [42]Department of Earth Science and Engineering, Imperial College London, London, UK, [43]RISE Research Institutes of Sweden, Stockholm, Sweden, [44]Earth and Planetary Laboratory, Carnegie Institution for Science, Washington, DC, USA, [45]McDonnell Center for the Space Sciences, Department of Earth and Planetary Sciences, Washington University in St. Louis, St. Louis, MO, USA, [46]Department of Geological Sciences, University of Florida, Gainesville, FL, USA, [47]Blue Marble Space Institute of Science, Seattle, WA, USA

Abstract The first samples collected by the Mars 2020 mission represent units exposed on the Jezero Crater floor, from the potentially oldest Séítah formation outcrops to the potentially youngest rocks of the heavily cratered Máaz formation. Surface investigations reveal landscape-to-microscopic textural, mineralogical, and geochemical evidence for igneous lithologies, some possibly emplaced as lava flows. The samples contain major rock-forming minerals such as pyroxene, olivine, and feldspar, accessory minerals including oxides and phosphates, and evidence for various degrees of aqueous activity in the form of water-soluble salt, carbonate, sulfate, iron oxide, and iron silicate minerals. Following sample return, the compositions and ages of these

L. W. Beegle was formerly at Jet Propulsion Laboratory, California Institute of Technology, Pasadena, CA, USA.

Key Points:

- Nine samples, consisting of four pairs of rock cores and a tube of atmospheric gas, were collected from the floor of Jezero Crater, Mars
- In situ observations of crater floor outcrops, used as proxies for the samples, reveal aqueously altered igneous lithologies
- Perseverance will leave one sample from each pair at the Three Forks depot and retain a second to be cached with future samples

Supporting Information:

Supporting Information may be found in the online version of this article.

Correspondence to:

J. I. Simon,
justin.i.simon@nasa.gov

Citation:

Simon, J. I., Hickman-Lewis, K., Cohen, B. A., Mayhew, L. E., Shuster, D. L., Debaille, V., et al. (2023). Samples collected from the floor of Jezero Crater with the Mars 2020 Perseverance rover. *Journal of Geophysical Research: Planets*, *128*, e2022JE007474. https://doi.org/10.1029/2022JE007474

Received 20 JUL 2022
Accepted 29 JAN 2023

Author Contributions:
Conceptualization: J. I. Simon
Data curation: J. I. Simon, K. Hickman-Lewis, A. Steele, V. Z. Sun, A. Udry
Investigation: J. I. Simon, K. Hickman-Lewis, S.-E. Hamran, S. Siljeström, K. M. Stack, A. Steele, V. Z. Sun, A. Udry
Methodology: J. I. Simon, S.-E. Hamran
Supervision: S.-E. Hamran
Validation: K. Hickman-Lewis, S. Siljeström, K. M. Stack, A. Steele, V. Z. Sun, A. Udry
Writing – original draft: J. I. Simon, K. Hickman-Lewis, A. Steele, V. Z. Sun, A. Udry
Writing – review & editing: J. I. Simon, K. Hickman-Lewis, S. Siljeström, K. M. Stack, A. Steele, V. Z. Sun, A. Udry

variably altered igneous rocks are expected to reveal the geophysical and geochemical nature of the planet's interior at the time of emplacement, characterize martian magmatism, and place timing constraints on geologic processes, both in Jezero Crater and more widely on Mars. Petrographic observations and geochemical analyses, coupled with geochronology of secondary minerals, can also reveal the timing of aqueous activity as well as constrain the chemical and physical conditions of the environments in which these minerals precipitated, and the nature and composition of organic compounds preserved in association with these phases. Returned samples from these units will help constrain the crater chronology of Mars and the global evolution of the planet's interior, for understanding the processes that formed Jezero Crater floor units, and for constraining the style and duration of aqueous activity in Jezero Crater, past habitability, and cycling of organic elements in Jezero Crater.

Plain Language Summary Here we provide a narrative of sample collection and associated in situ rover observations for the rocks collected by the Perseverance rover to provide a preliminary description of the first samples of the Mars 2020 mission. These rocks collected in Jezero Crater represent the first samples from Mars with a known geologic context, the first collected with the potential to be returned to Earth for laboratory analysis, and the first cores from rock outcrops on another planet. Remote and proximal analyses indicate that all crater floor outcrops investigated are igneous in origin. Laboratory analyses of these rocks will be useful to study the planet's interior at the time of emplacement, characterize martian magmatism, and place timing constraints on geologic processes, both in Jezero Crater and more widely on Mars. All collected rocks have interacted with water and contain secondary geochemical and mineralogical evidence that can be used to understand aqueous environments in the crater and the potential conditions of habitability for ancient life on Mars.

1. Mars Sample Return From Jezero Crater

Mars 2020 has successfully collected eight rock cores from several locations on the crater floor and an atmospheric sample (Figure 1), all described herein. These samples collected during the Crater Floor Campaign, the first Science Campaign of the Perseverance rover (see Sun et al., 2022), will be returned to Earth as part of the Mars Samples Return Program and studied to address high-priority science questions posed by the Mars science community (cf. Beaty et al., 2019).

1.1. Mars Sample Return

The Mars 2020 mission is the first step in a multi-stage international effort towards Mars Sample Return (MSR), which has been a high priority of the international planetary science community for decades (e.g., Kminek et al., 2022; Meyer et al., 2022). While several different approaches to MSR have been considered in the past, the National Research Council (2011) Vision and Voyages for Planetary Science in the Decade 2013–2022 recommended the collection of well-documented samples from a selected site on Mars by a rover capable of mineralogic and geochemical characterization. These MSR decadal survey plans enable the planetary science community to better develop methods and approaches for sample analyses on Earth.

The principal objective of the Mars 2020 mission is to create high science value sample caches for potential return to Earth (Farley et al., 2020). A scientifically return-worthy sample cache will include distinct sample suites or individual samples selected to represent the diversity of the area explored by the Perseverance rover. This cache will address the science objectives of MSR described by iMOST (2018), in general, and, more specifically, the astrobiological potential, geologic history, and evolution of Mars as reflected in the Jezero Crater region. The scientific aim for MSR is to maximize the science return and to go beyond the minimal scientifically return-worthy sample collection. This could include returning a sample collection that contains complementary samples, for example, one that constrains the emplacement timing of a second sample with high astrobiological potential, a suite of samples that record changing conditions through time, or rocks from outside Jezero Crater that improve our understanding of those collected in Jezero (see description of scientifically return-worthy sample cache in MEPAG at https://mepag.jpl.nasa.gov/announcements/SRW_Intro_Eval.pdf). Future elements of the MSR Campaign include the MSR Program, which is tasked with the goal of bringing a scientifically return-worthy set of martian samples to Earth, and the Sample Receiving Project, which would coordinate preliminary sample analyses (e.g., Haltigin et al., 2022; Tait et al., 2022), including those required for sample safety assessment (Kminek et al., 2022) within a Sample Receiving Facility.

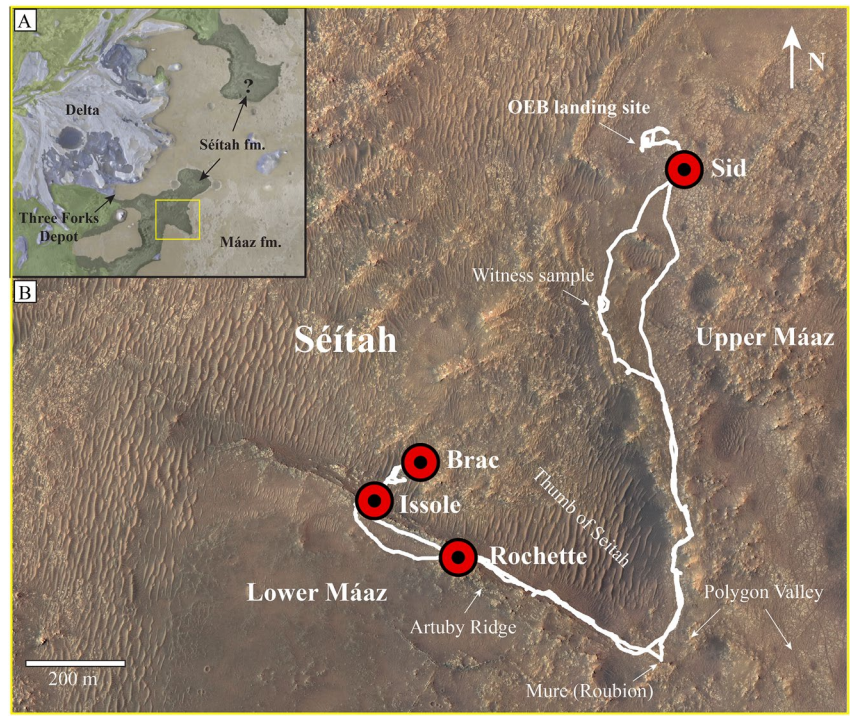

Figure 1. *Crater Floor Science Campaign area explored by the Perseverance rover*: (a) Inset shows western edge of Jezero Crater, location of Three Forks sample depot, and explored region in yellow box. (b) High Resolution Imaging Science Experiment image shows the location of outcrop sample targets and rover path. Octavia E. Butler landing site, first witness sample location, and prominent crater floor features are labeled.

1.2. Science Rationale

The selection of Jezero Crater as the landing site was guided by several factors. First, the biosignature preservation potential of shallow subaqueous sedimentary environments (including lakes) is known to be high (Hays et al., 2017; Wacey et al., 2009; Westall et al., 2015), and Jezero is a depositional basin with one or more stages of fluvial activity during the Noachian and the Hesperian (Goudge et al., 2012; Schon et al., 2012). Second, the delta stratigraphy in Jezero contains diverse geologic units with a clear stratigraphic context (Ehlmann et al., 2008; Goudge et al., 2015; ground-truth evidence reported by Mangold et al. (2021)), therefore providing a record of environmental conditions during formation/deposition. Third, the inlet river channels from the outside Jezero watershed were active during the valley network-forming era on early Mars (Goudge et al., 2015), and therefore the delta stratigraphy provides a record of environmental conditions during the time when river valley networks existed on Mars. Fourth, the Fe/Mg-smectite-rich delta stratigraphy at Jezero may have exceptionally high biosignature preservation potential and may provide an ideal location to explore for concentrated and preserved martian organic carbonaceous materials (e.g., McMahon et al., 2018; Summons et al., 2011). Fifth, although carbonates are generally scarce on Mars, orbital reflectance spectra of the Jezero area show strong absorptions from carbonate minerals (Brown et al., 2010; Ehlmann et al., 2008; Goudge et al., 2015; B. H. N. Horgan et al., 2020; Zastrow & Glotch, 2021); carbonates are known to be powerful archives of paleodepositional geochemistry and may also preserve biosignatures with high fidelity (Bosak et al., 2021). Finally, the sedimentary geology is superimposed upon bedrock exposures of the Jezero Crater floor that have been hypothesized to be igneous in origin and therefore, collectively, reflect a diversity of rock types and geological processes (Goudge et al., 2015; B. H. N. Horgan et al., 2020; Schon et al., 2012; Shahrzad et al., 2019). This general geology has been broadly confirmed by observations made thus far during the Mars 2020 mission (Bell et al., 2022; Farley et al., 2022; Liu et al., 2022; Mangold et al., 2021; Wiens et al., 2022).

This ensemble of criteria strongly suggest that variably altered igneous samples the Mars 2020 mission has collected from the floor of Jezero Crater are valuable members of a scientifically return-worthy cache. These Crater Floor Campaign samples are well suited for returned sample science studies that will satisfy several

important MSR objectives: (a) to better understand the differentiation and magmatic history of early Mars, (b) to determine the geochronology of the Jezero Crater floor and therefore the lake and delta timing, and (c) to address questions surrounding astrobiology, paleoenvironment and paleoclimate, based on the presence of minerals produced by the interactions of igneous minerals with water (including some carbonates, sulfates, and smectites) and the presence of organic materials.

The initial working hypothesis regarding geochronology proposed that the currently-exposed crater floor had an igneous origin, and a similar composition to other martian basalts, but was emplaced ~2.5 to 4.0 Ga ago, a time currently unrepresented in meteorite collections (e.g., Udry et al., 2020). Support for this hypothesis comes from spectral signatures consistent with other exposures of Hesperian ridged plains (mixtures of olivine and pyroxene; Goudge et al., 2012), the range of crater retention ages spanning ~2.5 to 3.5 Ga (Goudge et al., 2012; Shahrzad et al., 2019), and a younger inferred age of the crater floor compared to the implied cessation age of valley network activity at ~3.8 Ga (Fassett & Head, 2008). The spectral signatures of igneous rocks are common for Mars and not diagnostic of age. Returned sample analysis is thus required to obtain critical evidence related to the petrogenesis, composition, age, cooling rates, alteration, and ultimately the origin, of these units.

1.3. Exploration of Crater Floor Geology

Remote sensing and in situ science conducted by the Mars 2020 Perseverance rover show that the rocks exposed at the floor of Jezero Crater are in fact igneous, but have distinct formation histories (Bell et al., 2022; Farley et al., 2022; Liu et al., 2022; Scheller et al., 2022; Tice et al., 2022; Wiens et al., 2022). Hypotheses related to the origin of Mars and the evolution of its interior and surface motivated by both meteorite and Mars mission work will be further tested by Earth-based analyses of rock samples collected by Perseverance following MSR (Kminek et al., 2022; Meyer et al., 2022). As presented below and detailed in supporting studies contained in this special volume, the analyses conducted by Perseverance, particularly on abrasion sites, show that the bedrock units in Jezero are igneous in origin. Rocks of the Séítah formation represent an olivine-rich cumulate formed from the differentiation of an intrusive body or thick lava flow or impact melt (Farley et al., 2022; Liu et al., 2022; Wiens et al., 2022). By contrast, the much more ferroan rocks of the Máaz formation, rich in pyroxene and plagioclase, may represent either the differentiated upper portion of the Séítah magma body or a separate, younger series of lavas emplaced on top of the Séítah formation (Farley et al., 2022; Wiens et al., 2022). These bedrock units were variably altered by aqueous processes (Farley et al., 2022; Scheller et al., 2022; Tice et al., 2022) and were likely covered by sediment at an ancient shoreline (Mangold et al., 2021; Sholes et al., 2022) and possibly a crater lake. The igneous bedrock may have erupted from a vent within the crater but could also include contributions from volcanism originating outside of Jezero. These materials could have been transported into the crater either as primary eruptions or as volcanoclastic materials, although the latter is not supported by Perseverance observations described herein and in this volume. Regardless, laboratory analysis of these samples will provide critical geochemical and geochronological evidence for reconstructing the history of Mars, and will help constrain the regional geology, potentially including the timing of younger depositional episodes and aqueous events in the crater and potential crater lake.

2. The Collection of Jezero Crater Floor Samples

2.1. Overview of Mars 2020 Operations in Jezero Crater

The Perseverance rover landed in Jezero Crater on 18 February 2021 and completed ~90 days of commissioning activities (Figure 1). The Mars 2020 team conducted its first science campaign, the Crater Floor Campaign, to explore the units currently exposed on the Jezero Crater floor. This campaign explored the region to the south and east of the landing site for approximately 10 months, ending on sol 380, as described in detail by Sun et al. (2022, this volume). During the Crater Floor Campaign, four pairs of rock cores were collected, two each from four distinct outcrops; and one atmospheric sample was collected (Figure 2). Pairs of samples were collected so that one sample from each pair can be deposited in a "contingency" cache on the crater floor while the rover continues to collect samples beyond the delta front and outside Jezero Crater. Each sample target, sample core, and associated outcrop abrasion site was named (see sample stratigraphy in Figure 2, sampling protocol outlined in Table 1, and complete list of rock unit, target, core, and abrasion site names in Table 2).

Starting from the Octavia E. Butler (OEB) landing site, Perseverance drove south towards its first sampling location in the lower Máaz formation. On sol 120 the bit carousel witness tube assembly that recorded contam-

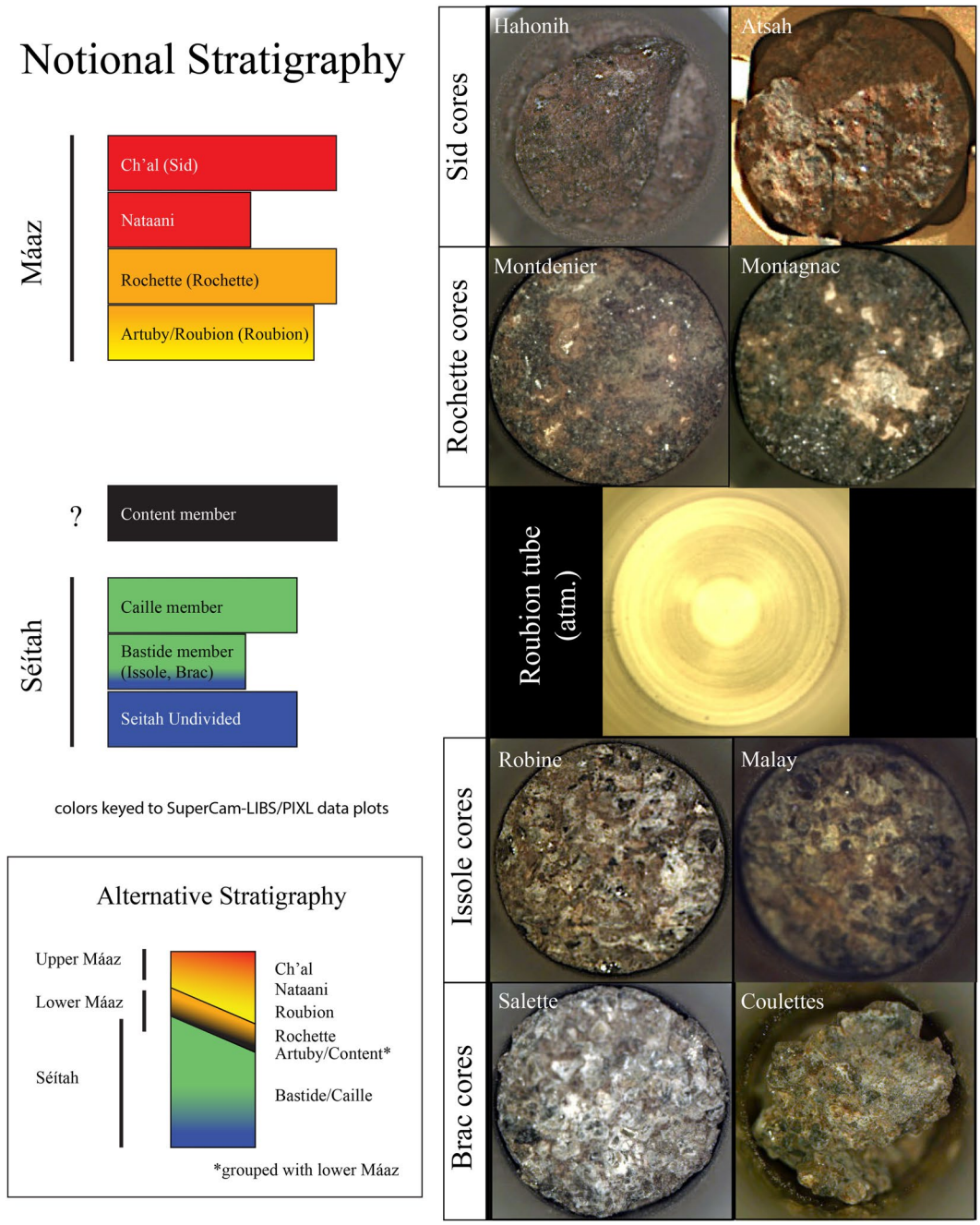

Figure 2. *Samples from Jezero Crater floor collected by Perseverance*: CacheCam images of rock sample cores from Séítah and Máaz units and tube of atmospheric gas prior to sealing. Core diameters are approximately 1.3 cm. Notional and alterative crater floor stratigraphic relationships of sampled units shown for reference (see Crumpler et al. (2023) and B. Horgan et al. (2022)).

ination during final assembly, testing, launch, cruise, and landing was sealed. Between sols 159 and 168, Perseverance successfully conducted the Guillaumes abrasion and attempted to drill the Roubion target. although no rock was acquired in the sample tube due to the weak nature of the rock and its presumed disaggregation during drilling. Nonetheless, this sample tube was retained as an atmospheric sample, which is considered a high-priority science target for MSR (e.g., Swindle et al., 2022). Subsequently, Perseverance continued west along the contact between the Máaz and Séítah formations, partly defined by the Artuby Ridge, *en route* to a location where outcrops of the Séítah formation could be accessed and investigated. Between sols 181 and 199,

Table 1
STOP List for Nominal Sampling Sol Path

Instrument	ZCAM	WATSON	WATSON	SHERLOC	PIXL	ZCAM	SCAM	WATSON	SCAM	ZCAM
Nominal sol #	S-6	S-4 and S-3	S-3	S-3	S-3	S-2	S-2	S + 1	S + 1	S + 1
Target	Workspace, includes both abrasion and coring targets	Abraded site	Coring targets	Abraded site, co-registered with PIXL	Abraded site, co-registered with WATSON, SHERLOC	Abraded site	Abraded site	Borehole #1	Borehole #1, tailings/inner wall	Borehole #1 tailings
Rationale	Workspace documentation	Rock texture documentation; for close approach	Coring target documentation (pre-drill), each core site for paired samples		Lithology, chemistry, and mineralogy documentation	Required to support SCAM observations	Lithology documentation	Borehole documentation, only 1 borehole imaging for paired samples	Rock borehole/ tailings chemistry and mineralogy	Chemistry and mineralogy

Note. S = sol that first core is collected. Second core collected following S + 1 Borehole and Tailings observations and has no additional STOP list observations.

Perseverance attempted sampling again, this time in the Rochette member at the Citadelle locality, representing a resistant caprock layer within the Máaz formation. This resulted in successful abrasion of the Bellegarde target and acquisition of the mission's first two rock cores—Montdenier and Montagnac. Perseverance then drove further westward and northeast into the Séítah formation, where the target Garde was abraded on sol 206, shortly before a pause in operations due to solar conjunction. Perseverance thereafter drove further into Séítah and between sols 250 and 277 abraded the Dourbes target, acquiring two more rock cores—Salette and Coulettes—from the Bastide member of the Séítah formation. Between sol 286 and 290, Perseverance performed the Quartier abrasion on the Issole outcrop (Issole member, Séítah formation) and acquired a second Séítah sample pair—Robine and Malay—near the Séítah-Máaz contact as it headed south and exited the South Séítah region. In order to efficiently complete the Crater Floor Campaign and to take the quickest route to the location at which the Delta Campaign would begin, Perseverance then retraced its path toward the OEB landing site. *En route*, Perseverance collected a final crater floor sample pair from the crater-retaining Ch'ał member within Máaz. This last pair of rock cores—Hahonih and Atsah—along with a corresponding abrasion site named Alfalfa, were collected between sols 371 and 377 just east of the OEB.

2.2. Notional Mars 2020 Standardized Observation Protocol for Sample Collection

During mission operations, a standardized set of minimum required activities and observations are undertaken to fully document a sample, once the sampling target has been identified (Table 1). These activities are termed the Standardized Observation Protocol, or STOP list. The STOP list includes imagery at multiple scales along with chemical and mineralogical analyses of the outcrop surface. Outcrop characterization is performed utilizing several payload instruments on the rover and is primarily focused on imaging (workspace context, targeted, and multispectral), compositional (X-ray fluorescence, laser induced breakdown spectroscopy, and luminescence), and mineralogical (Raman and VISIR) observations. The full names and a detailed discussion of the instrumentation used to explore and sample the rock targets, for example, Mastcam-Z, PIXL, SCS, SuperCam, RIMFAX, and WATSON/SHERLOC, can be found in the following overviews: PIXL, Allwood et al. (2020); Mastcam-Z, Bell et al. (2021) and Maki et al. (2020); SHERLOC, Bhartia et al. (2021); RIMFAX, Hamran et al. (2020); SuperCam, Maurice et al. (2021) and Wiens et al. (2021); and SCS, Moeller et al. (2021). Because rock surfaces are frequently coated with dust or other materials, an approximately 1 deep and 5 cm diameter wide abrasion is created within a few tens of centimeters of each sample target in the same lithology. In this “sample proxy” site, high-resolution images and detailed maps of elemental composition, mineralogy, and potential organic matter are obtained. After coring, an image is taken of the sample in the tube (Figure 2), the amount of sample is estimated, and the tube is hermetically sealed (Moeller et al., 2021). Unique serial numbers are readily visible on the tube and seal exteriors to ensure confident identification even decades after acquisition.

Each sample is documented in two main products: The Sample Dossier and the Initial Report. The Sample Dossier contains all observations from the STOP list, along with relevant rover data (e.g., temperatures, rover location, rover arm position and actions, etc.). Uploaded to the NASA Planetary Data System (PDS) with a regular cadence, the Sample Dossier primarily consists of instrument-specific and engineering data products. These data are independently delivered to the PDS, and thus the dossier acts as a “one stop shop” for sample-specific results. The Initial Report is a description of each sample in a standardized narrative format, written by the Science Team. This initial report is written within weeks of sample acquisition to capture the reasoning for sampling and to describe the interpretations available at the time of sampling and at the completion of the STOP list. The Initial Report should be thought of as a set of field notes associated with each sample. Initial Reports are archived in the NASA PDS as an element of each Sample Dossier, providing critical inputs to the sample catalogs that will ultimately be produced for each of the samples when they return to Earth.

Table 2
Perseverance Crater Floor Core Characteristics

Core Name(s)	Formation	Member	Outcrop	Abrasion	Rock type	Latitude, longitude, elevation	Length (cm)	Headspace gas (mol)[a]	Sol and time sealed
Roubion	Máaz	Roubion	Roubion	Guillaumes	Igneous basalt	18.42769°, 77.45165°, −2585.0 m	0 (disaggregated)	4.9×10^{-6}	SOL-0164M14:12:47.041
Montdenier and Montagnac	Máaz	Rochette	Rochette	Bellegarde	Igneous basalt	18.43074°, 77.44437°, −2574.6 m	59.6 and 61.5 mm	1.2×10^{-6} and 1.3×10^{-6}	SOL-0190M12:29:34.349 and SOL-0196M15:53:23.786
Salette and Coulettes	Séítah	Bastide	Brac	Dourbes	Ultramafic cumulate	77.44301°, 18.43397°, −2569.2 m	62.9 and 33.5 mm	1.1×10^{-6} and 2.5×10^{-6}	SOL-0262M15:30:24.958 and SOL-0271M15:25:59.868
Robine and Malay	Séítah	Issole	Issole	Quartier	Ultramafic cumulate	77.44133°, 18.43264°, −2574.3 m	60.8 and 30.7 mm	1.1×10^{-6} and 2.7×10^{-6}	SOL-0295M15:32:36.230 and SOL-0337M14:58:24.024
Hahonih and Atsah	Máaz	Ch'al	Sid	Alfalfa	Igneous andesite	77.45242°, 18.44386°, −2568.3 m	65.5 and 60.0 mm	1.0×10^{-6} and 1.3×10^{-6}	SOL-0371M14:53:54.458 and SOL-0377M13:58:03.427

Note. Witness tube (M2020-109-1 WB1) sealed 16:25:55 LMST, Sol 120, Ls 61.4, Latitude 18.43907°, Longitude 77.44940°, Elevation −2568.073 m.
[a]In order to characterize the gas content of the tube and the environment to which solid samples were most recently exposed, a suite of atmospheric measurements are made to supplement the "STOP" list activities (see Text S1 & Figure S1 in Supporting Information S1).

3. Geological Context of Jezero Crater Floor Samples

During the Crater Floor Campaign, the eight core samples were collected from rocks that are interpreted to be stratigraphically below (i.e., older than) the delta sediments, from regions initially identified as within either the Crater floor fractured (Cf-f1/2) or Crater floor fractured rough (Cf-fr) units of Stack et al. (2020). Proximal and remote analyses suggest that all crater floor outcrops investigated are igneous in origin and dominantly ultramafic to mafic in composition. The stratigraphically lower Séítah formation (i.e., Cf-f1/2) is an olivine and pyroxene-bearing unit containing minor amounts (<10%) of secondary Mg-Fe carbonates. It is interpreted as a coarsely crystalline olivine cumulate. The overlying pyroxene- and plagioclase-dominated Máaz formation (i.e., Cf-fr) is interpreted to be a sequence of basaltic to basaltic andesite lava flows (Farley et al., 2022; Liu et al., 2022; Wiens et al., 2022). The following section describes the geologic context of the samples collected, a narrative of the "fieldwork" that includes some first-time mission activities, and examples in which rover operations deviated from the STOP list during sample collection. Some of these details may be important for interpretation of sample analyses in the future.

3.1. Séítah Outcrop Targets

The Séítah formation comprises an irregular region of the crater floor consisting of NE–SW-trending ridges surrounded by megaripples, loose rocks, and boulders (Figure 1). "Séítah" is the Navajo language term for "amidst the sands." The topography of the Séítah region was largely considered unacceptable for rover traversability, therefore rover observations were limited to a narrow corridor, approximately 200 m in length, in southern Séítah. Three outcrops (Bastide, Brac, and Issole) were investigated; of these, Brac and Issole were chosen as localities for sampling. Most outcrops in the Bastide member of the Séítah formation exhibit tabular layers with relatively consistent thickness on the centimeter–decimeter scale. No layers were noted in the overlying Content member, outcrops of which overlie a possible angular unconformity, but are comparably rubbly and exhibit pits that might represent vesicles. No proximity analyses were conducted on Content member materials. SuperCam remote micro-imager (RMI) images of Séítah outcrops show a rock texture comprised of relatively equant 1.0–3.5 mm dark gray-green particles separated by interstitial lighter-toned materials. This texture is particularly evident at Bastide (see Beyssac et al., 2023; Wiens et al., 2022).

Following the Garde abrasion of Bastide, its outcrop geometry and relief were considered unsuitable to conduct the full suite of proximity science required prior to sampling (i.e., the STOP list), and thus the decision was made to seek another, similar, outcrop for the next sampling attempt. A suitable candidate (Brac, within the Bastide member) was identified near the contact with the overlying Content member (Figure 3, anaglyph Figures S2, S3 in Supporting Information S1, outcrop map Figure S11 in Supporting Information S1). Based on its morphology, concordance with surrounding outcrops, and estimated dip consistent with that of the wider Séítah region, the Brac outcrop was confidently interpreted to be a portion of the Séítah bedrock. Perseverance conducted outcrop analysis, abrasion (the Dourbes abrasion site), and sampling at Brac, leading to the acquisition of the two rock cores—Salette and Coulettes. The Salette core is a full-length sample (~6 cm), whereas the Coulettes core is considerably shorter (~3.5 cm). A disc-shaped fragment detached from the base of the Salette core after sampling, perhaps due to fracturing along a layer boundary or other plane of weakness.

The second Séítah sampling locality, the Issole outcrop, is located near the boundary between the underlying Séítah and overlying Máaz formations; because the boundary is covered by regolith, the nature of the contact remains unknown (Figure 4, anaglyph Figure S4 in Supporting Information S1, outcrop map Figure S11 in Supporting Information S1). Perseverance conducted outcrop analysis, abrasion (the Quartier abrasion site)

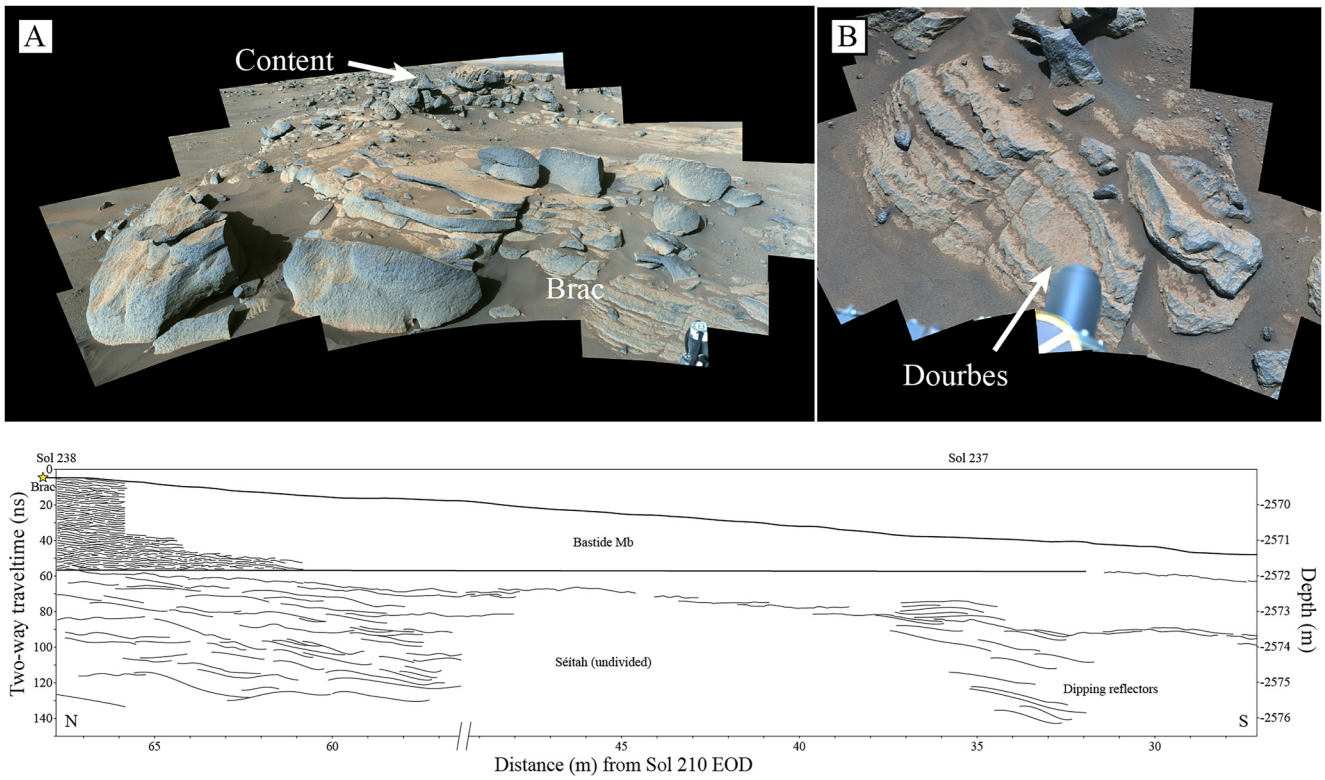

Figure 3. *Mastcam-Z workspace mosaics and interpreted RIMFAX subsurface for Brac*: The Séítah formation outcrop target at the highest elevation reached by Perseverance and possibly the oldest sample collected. (a) View looking north of the Content member that appears to be lying unconformably on top of the Bastide member (see text). (b) Sloped-surface within Brac where Dourbes abrasion was made is approximately 10 cm from top-to-bottom.

and sampling at Issole, leading to the acquisition of the two cores–Robine and Malay. Following the sampling of Robine, the acquisition of the planned second core Pauls was prevented by a fault during the transfer of the sample tube into the Adaptive Caching Assembly, precluding its processing. Subsequently, it was found that a few fragments of the Pauls core had become lodged in the bit holder, likely having fallen out of the sample tube. These fragments prevented the coring bit from being fully seated into the bit holder and the team decided to expel the Pauls core and re-sample the adjacent Malay region using the same sample tube. The Robine core is a full-length sample (~6.5 cm), whereas the Malay core is considerably shorter (~3 cm). CacheCam images of both cores suggest that they are intact and unfractured (see Figure 1).

The interpreted subsurface stratigraphy from estimated permittivity values of the RIMFAX radargram of Séítah targets on the 201 and 237–238 sol paths are shown in Figures 3 and 4. Estimated densities around 3.5 g/cm^3 are in accordance with the olivine-rich Séítah lithology observed at all three outcrops studied (Hamran et al., 2022). The subsurface appears to represent a sequence of SW-dipping to subhorizontal rocks from approximately 3 m below the surface level to >8 m burial depth interpreted as an extension of the Issole member that also appears to extend below Artuby Ridge further south. This lower unit appears to be truncated by an angular unconformity. The potential unconformity is overlain by a 2–3 m thick sequence that is more clearly bedded and that outcrops at the surface as the Bastide member (containing the Bastide and Brac outcrops).

3.2. Máaz Outcrop Targets

The Máaz formation, named for Navajo language term for "Mars," is a widespread unit in the crater that, from High Resolution Imaging Science Experiment (HiRISE) camera orbital views, appears fractured in a distinctive meter-scale polygonal pattern. Broadly, the Máaz formation exhibits a smooth lower morphology and a rougher, more massive, rubbly, and cratered upper morphology. The Máaz formation stratigraphy varies from layered, to homogenous and massive in nature and has been subdivided into five members: Roubion, Artuby, Rochette, Nataani, and Ch'ał (see Sun et al., 2022). Several possibilities exist for the Máaz stratigraphy, including

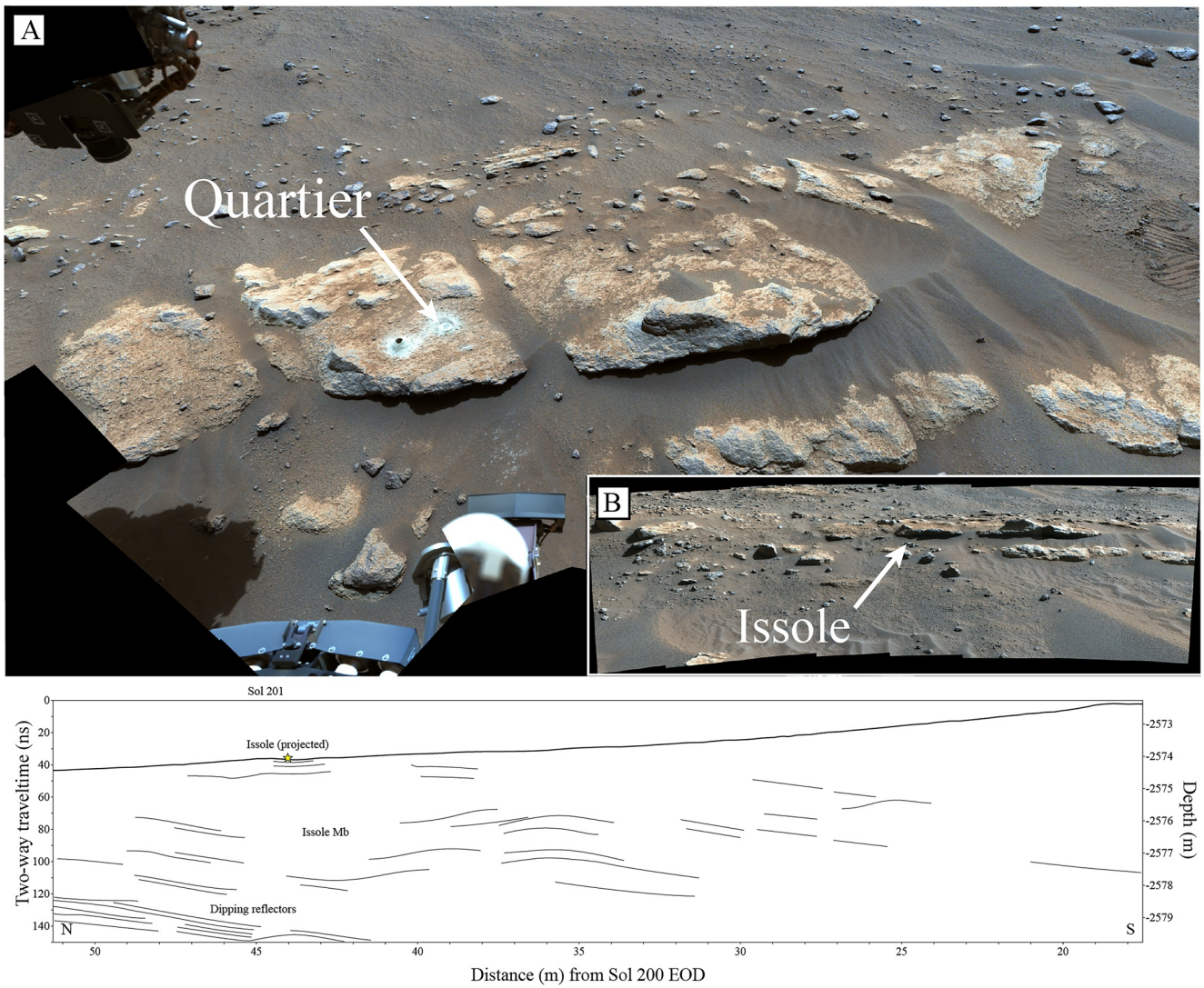

Figure 4. *Mastcam-Z workspace mosaics and interpreted RIMFAX subsurface for Issole*: The Séítah formation outcrop target near the Séítah/Máaz contact. (a) Sample borehole (~1.3 cm diameter) and Quartier abrasion site (~5 cm diameter) in workspace image provide scale of targeted outcrop features. (b) View of Issole looking south from Séítah towards base of the Artuby Ridge (not seen).

one that is largely based on elevation (the sequence as listed above, from bottom to top) and one in which Roubion is stratigraphically between Rochette/Artuby ("lower Máaz") and Nataani/Ch'ał ("upper Máaz"). This grouping is supported by spectral and compositional similarities within the upper and lower groups, where lower Máaz members are more mafic and pyroxene-dominated, and upper Máaz members are more silicic and plagioclase-dominated, with Roubion exhibiting intermediate properties (see B. Horgan et al., 2022). In this model, Roubion and some portions of upper Máaz are found at elevations below Rochette and Artuby due to infill by "upper Máaz" of paleotopography carved into the "lower Máaz." This supports the hypothesis that, at least locally, upper Máaz may fill an eroded surface, that is, a "paleovalley," in lower Máaz near the Séítah "Thumb" area (Figure 1). Another common feature of the Máaz formation is that it is observed at elevations that are below the highest portions of the putatively older Séítah rocks.

The Roubion coring attempt, the Guillaumes abrasion site, and the associated STOP list activities, were undertaken on a very low relief rock (Figure 5, anaglyph Figures S6, S7 in Supporting Information S1, outcrop map Figure S11 in Supporting Information S1) selected largely to meet first-time engineering requirements for sampling. Coring at Roubion produced a hole and tailings pile, and the entire coring and sealing process completed nominally. However, the Perseverance volume probe indicated no sample, this was confirmed by CacheCam images

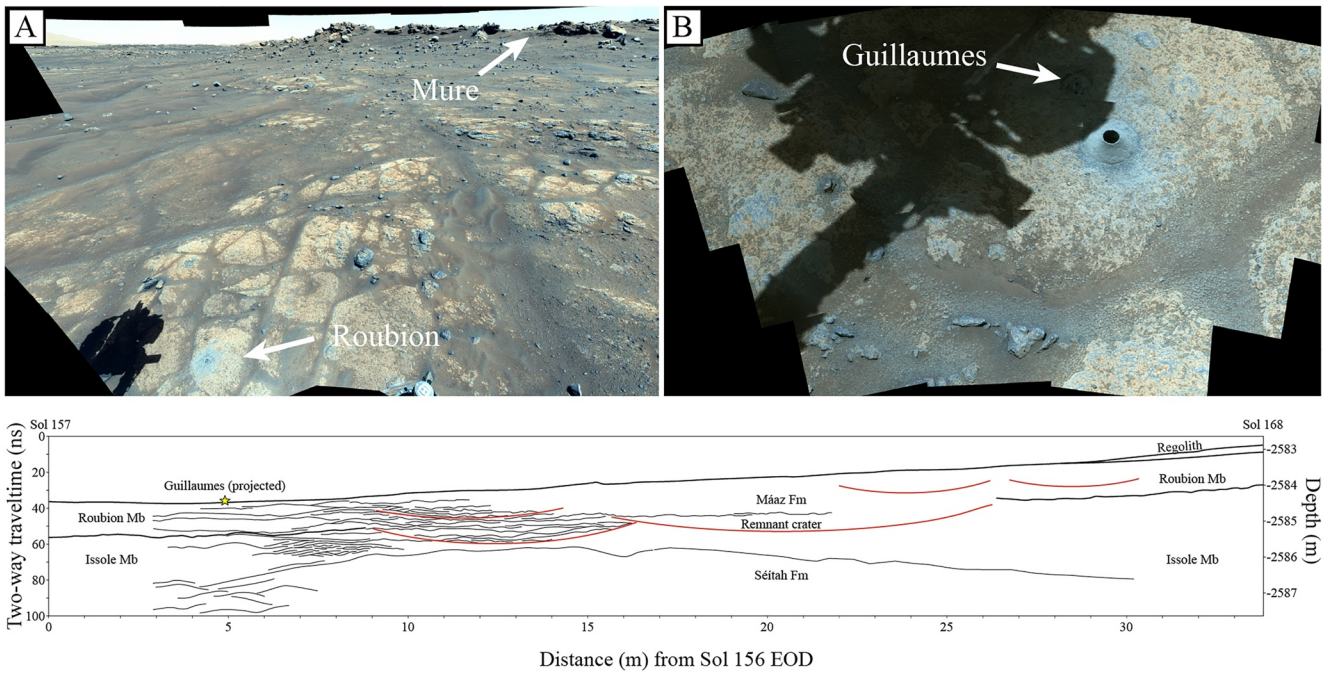

Figure 5. *Mastcam-Z workspace mosaics and interpreted RIMFAX subsurface for Roubion*: The Máaz formation outcrop target at the lowest elevation reached by Perseverance and the first sample target where the sample disaggregated, and an atmospheric sample was collected. (a) Shows low-lying Roubion member and exposure of rough, layered, and rubbly upper Máaz outcrop named Mure in the distance. (b) Nearfield outcrop scale indicated by Guillaumes abrasion and borehole of Roubion as in Figure 4.

documenting an empty sample tube (Figure 2), that is, no core was recovered. In the absence of a core or core fragments on the ground, the most likely explanation is that the rock disaggregated during coring and either contributed to the tailings pile or fell back to the bottom of the borehole. Further coring at this location was abandoned. Although no rock core was obtained, the tube has several dozen ∼10 μm sized particles and the sealed Roubion sample inadvertently provides a returnable sample of approximately 4.9 μmol of martian atmosphere.

The interpreted subsurface stratigraphy from estimated permittivity values of the RIMFAX radargram for the 157–168 sol path are shown in Figure 5. The ∼2.5–2.8 g/cm^3 densities estimated are similar to that of basaltic material (Hamran et al., 2022). The radargram shows surface parallel reflectors and fine-scale layering below the smooth morphology down to a burial depth of approximately one m. Arcuate structures observed in radargrams may represent small, buried impact craters. Deeper reflectors (>3 m into the subsurface) appear to dip southward and may be associated with Séítah sequences.

After an unsuccessful first attempt to collect a rock sample from low-lying Máaz outcrops at Roubion, Perseverance traversed approximately 450 m NW along the base of Artuby Ridge, a ∼1 km long NW-SE trending linear ridge exposing on its NE side a several meter high cliff of the crater floor stratigraphy (Figure 1). In HiRISE images, the trough at the base of Artuby defines the morphological boundary between the southern edge of Séítah and exposures of Máaz. The team decided to target the relatively high-standing Máaz formation rocks along the top of Artuby, which define the Rochette member for sampling.

The rocks forming Artuby Ridge are variably layered to massive. Thick (10s of cm), laterally discontinuous layered rocks occur along the NE-facing slope of Artuby Ridge; thin (cm-scale), planar layered rocks are observed near the crest of Artuby Ridge. These layered rocks appear to transition into more massive exposures both laterally and up-section within Artuby Ridge (see Alwmark et al. (2023)). The appearance of thin, laterally continuous layering within the rocks of Artuby Ridge indicates a notable transition from the apparently massive rocks observed from OEB to Roubion, that is, in the upper Ch'ał member.

The interpreted subsurface stratigraphy from estimated permittivity values of RIMFAX radargrams acquired during the rover's drive along Artuby Ridge (sol 177), ascent of Artuby Ridge and arrival at Citadelle (sol 178), and after the short bump to Rochette (sol 180), are shown in Figure 6 (see anaglyph Figures S7, S8 in Supporting

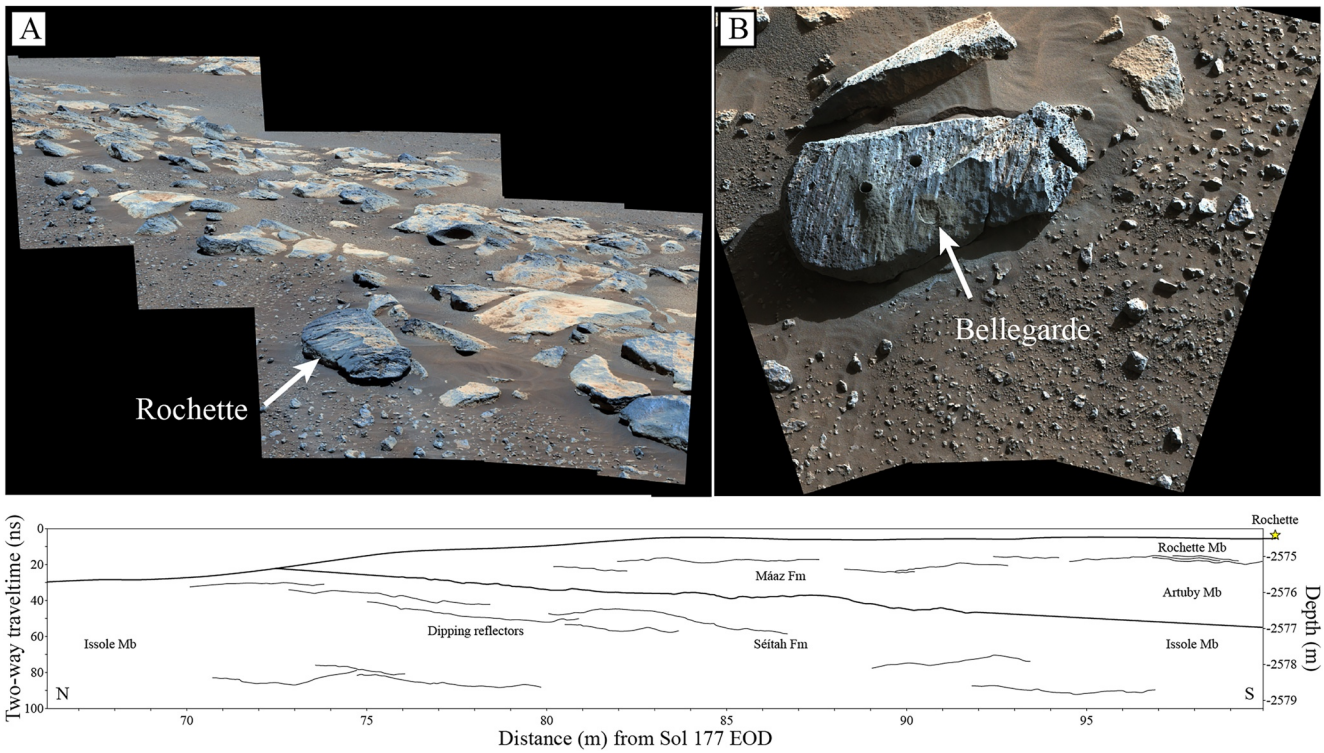

Figure 6. *Mastcam-Z workspace mosaics and interpreted RIMFAX subsurface for Rochette*: The Máaz formation outcrop target on top of Artuby Ridge and the first successful sample collected. (a) Shows Rochette that forms part of a NW—SE-trending band of similar boulders. (b) Rochette in which Bellegarde abrasion site and boreholes provide scale as in Figure 4.

Information S1, outcrop map Figure S11 in Supporting Information S1). While driving along the base of Artuby Ridge, RIMFAX observed a sequence of SW-dipping reflectors that dominate the subsurface stratigraphy from approximately surface levels to >10 m burial depth. Starting on sol 178, the radargram shows a relatively thin horizontal capping layer, consistent with the Rochette outcrop at the surface. It remains unclear whether the deeper layers, south of Rochette, are horizontal like the surface layer or SW-dipping. The estimated permittivity suggests that the horizontal, near surface layers are similar to basaltic material whereas those at depth exhibit greater density consistent with an olivine-rich lithology (Hamran et al., 2022), suggesting that rocks similar to Séítah (e.g., Issole member?) are present at depth (see Figure 6 caption for details).

The first fully successful sampling event occurred at Citadelle where Montdenier and Montagnac, the pair of rock cores representing the second sample target of the Mars 2020 mission, were collected (Figure 6, anaglyph Figures S7, S8 in Supporting Information S1, outcrop map Figure S11 in Supporting Information S1). The cores, and their companion Bellegarde abrasion site, were acquired on a small tabular boulder (Rochette, ∼40 cm across) forming part of a NW—SE-trending band of similar boulders and outcrops on the SW side of the Artuby Ridge crest. These blocks appear morphologically consistent with a degraded lava flow (Figure 6). Rochette (the block from which the samples were acquired) moved slightly during coring, confirming that it is not currently anchored to in-place outcrop. Although Rochette may have been displaced from its original location, the lateral extent and similarity of the blocks near Rochette suggest that this displacement is likely small, and an estimated emplacement position may still provide a useful constraint for some studies. Rochette was selected in part because it is stratigraphically higher than Séítah on Artuby Ridge, and therefore likely younger. As discussed above, the capping layer of Artuby Ridge that contains Rochette is located at a higher elevation than Roubion where the Guillaumes abrasion was made, but it remains unclear whether the Rochette member is actually younger or whether the Roubion member, along with upper Máaz formation material, filled paleotopography of eroded Rochette and Artuby member stratigraphy of the lower Máaz formation near Mure and the Thumb of Séítah.

Given the unexpected outcome of the Roubion sampling attempt, coring of Montdenier included an unusual step to confirm the presence of a sample in the tube with Mastcam-Z images prior to tube sealing. In the intervening

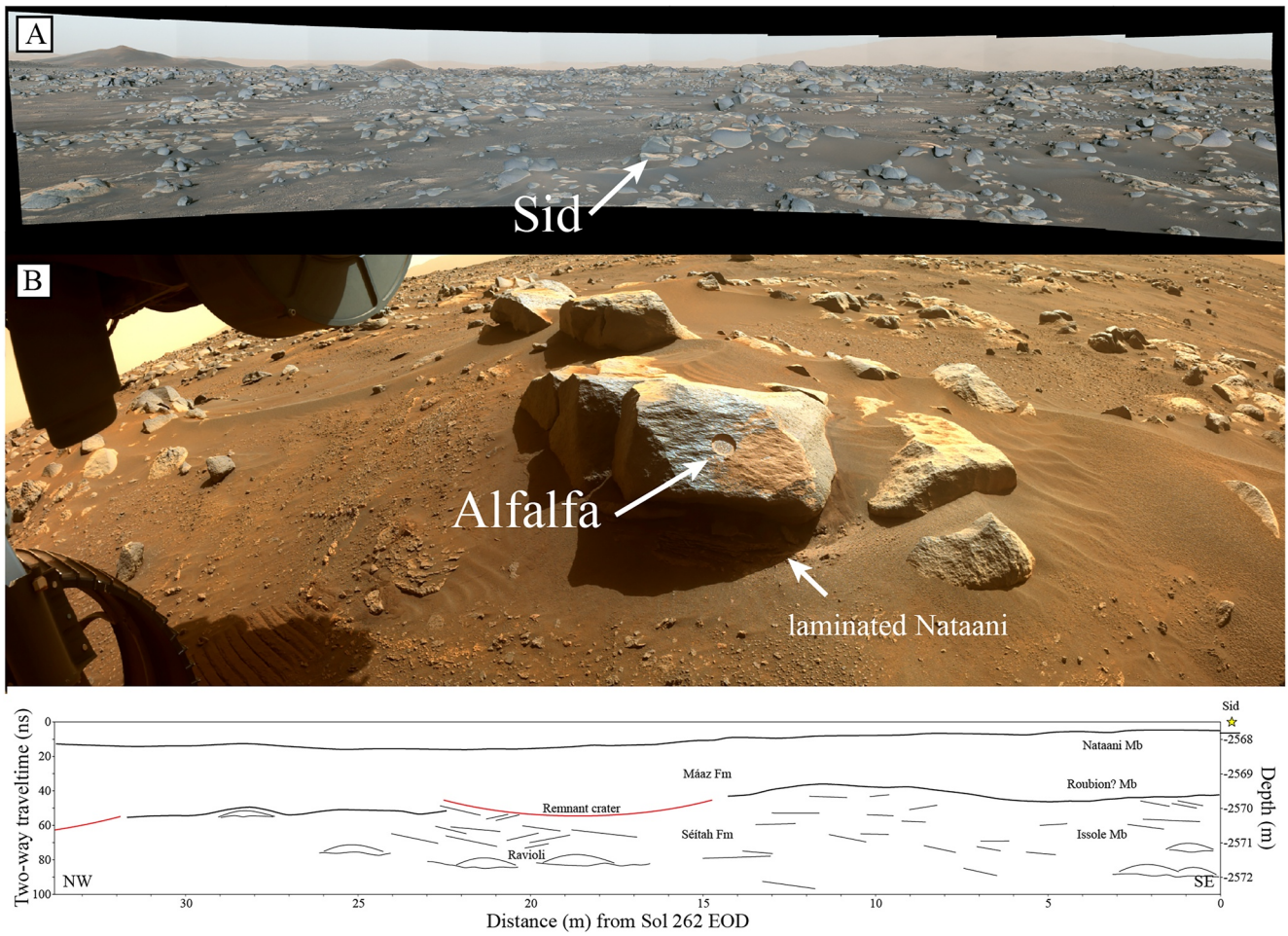

Figure 7. *Mastcam-Z workspace mosaics and interpreted RIMFAX subsurface for Sid*: The uppermost Máaz formation outcrop target that lies directly on top of Nataani and likely represents the youngest sample collected. (a) View looking east shows massive rocks of the Ch'ał member that form hummocks and ridges outcropping east of the Octavia E. Butler and the southward traverse to Mure. (b) Nearfield outcrop scale of Sid indicated by Alfalfa abrasion as in Figure 4.

4-sol period, the sample was exposed to the martian environment. This exposure is a notable deviation from the notional sampling sol path in which the tube is sealed autonomously within hours of coring. The paired core Montagnac was collected and sealed on sol 196 following the normal automated procedure and without visual confirmation prior to acquisition. Coring of Montagnac produced a hole and tailings pile of expected appearance, and the entire coring and sealing process completed nominally. The volume probe indicated full length, that is, ~6.0 cm or ~8.5 cm^3, cores in each sample tube.

The final pair of rock cores from the crater floor was collected from the morphologically rough upper Ch'ał member of the Máaz formation. The Ch'ał member comprises massive rocks that form hummocks and ridges outcropping east of the OEB and the southward traverse to Séítah. The Ch'ał member was recognized early in the mission as a morphologically distinct unit from the low-lying, polygonally jointed rocks (Nataani member) on which the rover landed and traversed. Named for a large rock observed on Sol 78, the Ch'ał member generally presents as angular, massive, cobble to boulder-sized, dark-hued rocks with scattered pits, which might represent vesicles, but otherwise little apparent internal structure. Ch'ał-type rocks are observed to overlie Nataani member rocks and, in many places, dark-hued, ventifacted "nubs" project upward from Nataani member outcrops (Figure 7). These nubs may be residual products of in-place weathering of Ch'ał rocks. The Ch'ał rocks were known from the early part of the mission to have the most evolved compositions of those observed on the crater floor (Wiens et al., 2022).

Several locations and rock types were considered for Ch'ał sampling as the rover traversed north in the last leg of the Crater Floor Campaign. Throughout the campaign, exposures of the Ch'ał unit were observed in east-facing viewsheds, for example, east of the Roubion sample location. The expression of these topographic highs and their

visible/near-infrared spectral properties in Mastcam-Z multispectral images can be clearly tied to at least one well-defined cratered region on the surface of the Máaz formation to the south and east in HiRISE and CRISM images (Figure 1). The team evaluated candidates for sampling based on their morphologic and topographic similarities to the Ch'ał archetype and evidence that the rock was in place. As the rover passed southeast of OEB, the team identified several blocks of Ch'ał-type material in direct contact with underlying Nataani rocks, including a boulder named Sid (Figure 7, anaglyph Figures S9, S10 in Supporting Information S1, outcrop map Figure S11 in Supporting Information S1). The relatively large size of Sid and other rocks in the area, and their direct contact with the underlying flat rocks of the Nataani member, imply that Sid may be derived directly from the receding Ch'ał member and may not have been moved or rotated significantly after deposition. This satisfied the above criteria for collecting a sample.

Outcrops of Ch'ał member blocky material at topographic highs overlying the recessive polygonal rocks, such as Nataani and Roubion, appear to form a coherent layer in subsurface sounding in RIMFAX radargrams (Figure 7). In the subsurface, the uppermost ∼2 m represents the Máaz formation, where the deposits are dominated by horizontal layering and polygons visible at the surface. Intra-polygon fractures are not visible in the radargram, suggesting that these fractures may be very shallow. Bowl-shaped reflector geometries in the Máaz formation are interpreted to represent remnant impact structures. Based on density estimates and interpretations of subsurface radargram geometry, underlying Séítah formation strata potentially lie between ∼2 and 7 m burial depth (e.g., Hamran et al., 2022). To avoid traversability hazards, the rover avoided high standing Ch'ał member outcrops; as such, the sample target was not directly characterized by RIMFAX radar observations.

4. In Situ Analyses of Sampled Outcrops

In the following section, we present the main observations made on the abrasion sites and associated natural surfaces of the sampled outcrops, which are intended to serve as proxies for the rock samples collected. We present key data highlighting the textures, compositions, and mineralogies of the crater floor bedrock to enable comparisons among the collected rock samples and those to be collected later in the mission. Table 3 lists the key attributes of the crater floor samples available for return to Earth.

4.1. Primary Rock Type of Sampled Séítah Outcrops

Identification of large (∼1–3.5 mm) olivine crystals exposed on relatively fresh natural surfaces of Séítah rocks were confirmed in the Dourbes and Quartier abraded sites at Brac and Issole, respectively (Figures 8 and 9). This cumulate texture includes euhedral to subhedral olivine crystals surrounded by intercumulus pyroxene. Co-registered WATSON images and PIXL X-ray fluorescence maps on abraded surfaces reveal a concentrated network of olivine crystals that accounts for up to 60% of the rock (Figure 9). These observations are expanded on by coordinated SHERLOC (plus the Autofocus and Context imager [ACI]), SuperCam-LIBS/VISIR spectroscopy, and Mastcam-Z multispectral observations. In Dourbes (and Garde), the crystals are equant, whereas in Quartier some olivine crystals appear more elongated (Liu et al., 2022; Wiens et al., 2022).

PIXL X-ray element maps indicate Fo_{55} olivine compositions and intercumulus material that is dominated by monocrystalline and crystallographically oriented augitic pyroxenes that grew around and among the olivine grains (Liu et al., 2022; Tice et al., 2022), which is within the range of $Fo_{44–66}$ calculated using CRISM orbital data (Brown et al., 2020). At grain boundaries and within interstitial spaces defined by the olivine and pyroxene crystals, Na-rich and K-rich feldspar, as well as accessory Fe-Cr-Ti oxides and Ca-phosphates were observed. More detailed and refined mineral compositions are presented in Liu et al. (2022) and Wiens et al. (2022). The mesostasis likely represents crystallization of late-stage melt enriched in incompatible elements (Liu et al., 2022), but some of the phases may be secondary.

Bulk sum analysis of the PIXL mapping data obtained in selected scans of the Dourbes (Garde) and Quartier abrasion sites (Figure 10; PIXL scans in Figure 9) are shown in Table 4. These analyses include a mixture of likely primary igneous mineralogy together with secondary phases arising from later alteration. PIXL mapping focused on the primary mineralogy of abrasion sites shows that the SiO_2 contents of 30–50 wt.% and $Na_2O + K_2O$ contents of ∼0–2 wt.% are relatively constant across the Dourbes and Quartier sites. SuperCam-LIBS analyses were undertaken on both the natural surfaces and abraded sites of Séítah. SuperCam-LIBS analyses of the natural surfaces indicate SiO_2 contents of ∼45 wt.% and $Na_2O + K_2O$ contents ∼2 wt.%. Although the SiO_2 abundance is approximately the same in the abraded sites, alkalis measured using SuperCam-LIBS on the abraded Séítah

Table 3
Summary of Crater Floor Sample Characteristics

Sample	Lithologic description	Petrologic description	Primary mineralogy	Secondary mineralogy	Organic materials	Key returned sample science rationale
Roubion	Polygonal, low-lying, granular-weathering "pavers" in lower elevation Máaz fm	~0.5–1.0 mm evenly sized grains, and holes, possibly secondary cavity-filled or primary mineral replacement	Fe-rich augitic pyroxene (possible second mafic phase), plagioclase, Fe-Cr-Ti oxides (PIXL)	Fe/Mg-phyllosilicates (SuperCam-VISIR, SuperCam-Raman Ca/Mg-sulfate (PIXL, SHERLOC) halides (PIXL) perchlorate (PIXL, SHERLOC)	One- and two or more-ring aromatic molecules	*Atmosphere:* modern composition and weathering agents
Montdenier and Montagnac	Variably massive to layered to pitted resistant cap rocks along Artuby ridge	~0.2–0.5 mm evenly sized grains, possibly secondary cavity-filled or primary mineral replacement	Fe-rich augitic pyroxene (possible second mafic phase), plagioclase, Fe-Cr-Ti oxides (PIXL)	Fe/Mg-phyllosilicates (SuperCam-VISIR) Ca/Mg-sulfate (PIXL, SHERLOC) halides (PIXL) perchlorate (PIXL), perchlorate or phosphate (SHERLOC), Na-perchlorate (SuperCam-Raman) silicate (SHERLOC)	Mix of organic compounds or a single heterocyclic compound; One- and two or more-ring aromatic molecules	*Igneous Petrogenesis:* elemental and isotopic composition of crustal ± mantle melts and emplacement mechanisms, *Aqueous Alteration*: secondary mineralogy and weathering history, *Geochronology:* timing constraints on crater and regional geology, *Paleomagnetism*: timing of planetary dynamo, and *Astrobiology:* salt minerals relate to potentially habitable conditions

Table 3
Continued

Sample	Lithologic description	Petrologic description	Primary mineralogy	Secondary mineralogy	Organic materials	Key returned sample science rationale
Salette and Coulettes	Layered rocks comprising middle-lower part of Martre outcrop	1–3.5 mm olivine-rich cumulate	Olivine intercumlate pyyroxene (PIXL, SHERLOC)	Fe/Mg-phyllosilicates (SuperCam-VISIR, PIXL) Ca/Mg-sulfate (PIXL, SHERLOC, SCAM?) carbonate (SHERLOC) ferric oxide (WATSON-ACI, Mastcam-Z) perchlorate (PIXL), perchlorate or phosphate (SHERLOC), silicate (SHERLOC).	Two or more- ring aromatic molecules	*Igneous Petrogenesis: elemental and isotopic composition of crustal ± mantle melts and emplacement mechanisms*, *Aqueous Alteration*: secondary mineralogy and weathering history, Geochronology: age relationship with Máaz fm, *Paleomagnetism*: timing of planetary dynamo, and *Astrobiology:* carbonate and salt minerals relate to potentially habitable conditions

Table 3
Continued

Sample	Lithologic description	Petrologic description	Primary mineralogy	Secondary mineralogy	Organic materials	Key returned sample science rationale
Robine and Malay	Layered rocks comprising middle-lower part of Martre outcrop	1–3.5 mm olivine-rich cumulate	Olivine intercumlatepyyroxene (PIXL),olivine (SHERLOC)	Fe/Mg-phyllosilicates (SuperCam-VISIR), Ca/Mg-sulfate (PIXL, SHERLOC) Fe-(hydr)oxides (WATSON-ACI, Mastcam-Z) Mg/Ca/Fe-carbonate (SuperCam-VISIR, SHERLOC) perchlorate or phosphate (SHERLOC), silicate (SHERLOC), carbonate (SHERLOC)	Mix of organic compounds or a single heterocyclic compound; two or more-ring aromatic molecules	*Igneous Petrogenesis: elemental and isotopic composition of crustal ± mantle melts and emplacement mechanisms*, *Aqueous Alteration:* secondary mineralogy and weathering history, *Geochronology*: age relationship with Máaz fm, *Paleomagnetism:* timing of planetary dynamo, and *Astrobiology:* carbonate and salt minerals relate to potentially habitable conditions
Hahonih and Atsah	Massive, blocky, "hummocky" rocks found predominantly east of OEB	~0.5–3.5 mm porphryitic texture, relatively large euhedral feldspars, a few mm long, within a finer-grained (~0.5–1.0 mm) matrix	Fe-rich augitic pyroxene (possible second mafic phase), plagioclase, Fe-Cr-Ti oxides (PIXL), pyroxene (SHERLOC)	Fe-phyllosilicates (SuperCam-VISIR, PIXL), Mg-OH (SuperCam-VISIR), Al-phyllosilicate?—SuperCam-VISIR), ferric oxide (Mastcam-Z, SuperCam-LIBS, WATSON-ACI?), akaganeite (SuperCam-VISIR?), carbonate (SHERLOC), perchlorate or phosphate (SHERLOC), silicate (SHERLOC)	One- and two or more-ring aromatic molecules	*Igneous Petrogenesis: elemental and isotopic composition of crustal ± mantle melts and emplacement mechanisms*, *Aqueous Alteration*: secondary mineralogy and weathering history, *Geochronology:* stratigraphic constraint on age of Jezero delta and Mars crater calibration defined by uppermost surface of Máaz fm, and *Paleomagnetism:* timing of planetary dynamo

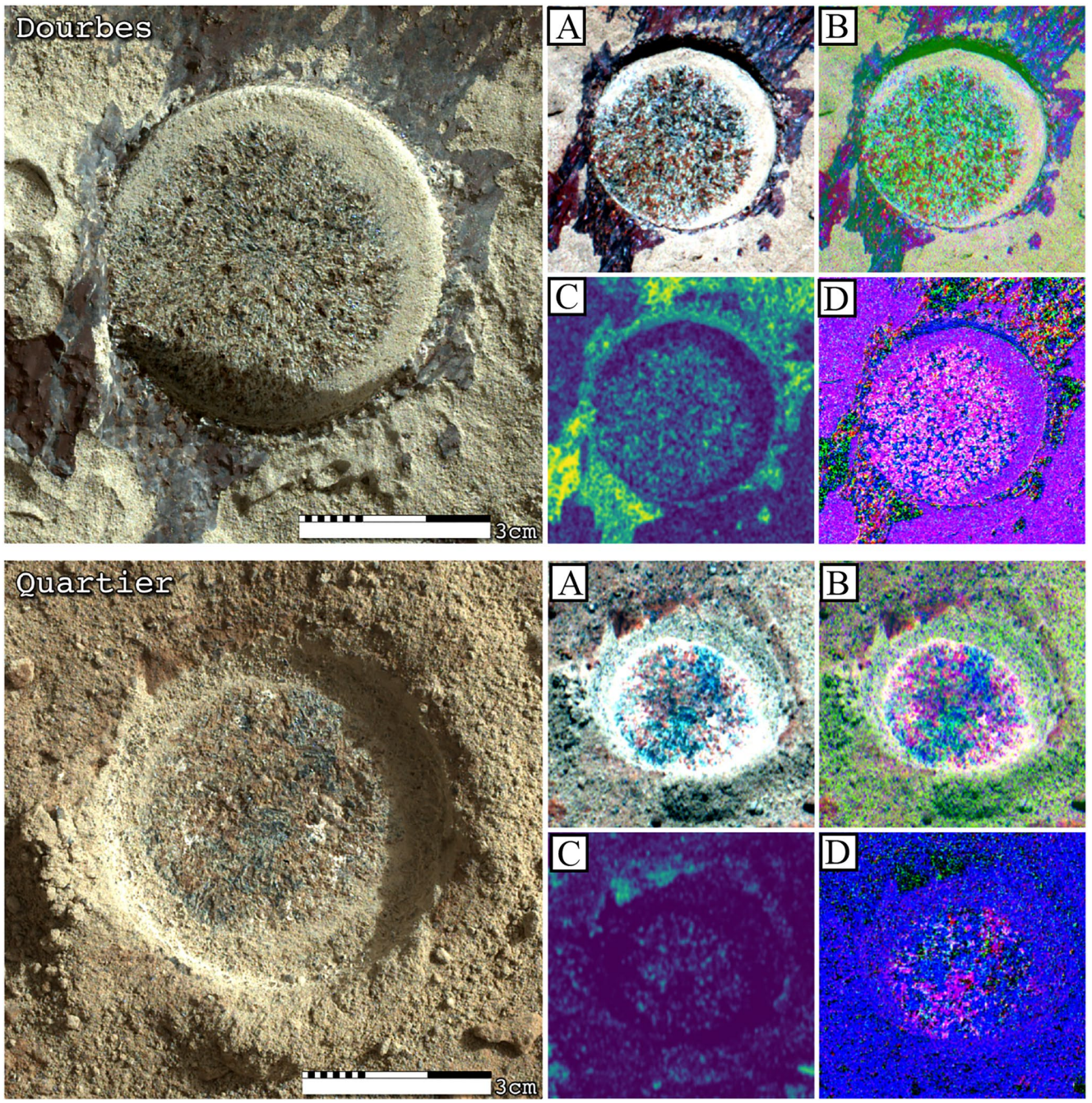

Figure 8. *WATSON* (*~25* cm *standoff*) *image paired with a quad of Mastcam-Z multispectral images for Séítah formation abrasion sites*: (a): L256 enhanced color, where white indicates abraded olivine or salts, red indicates oxidized grains, and dark blue to gray grains are unaltered mafic minerals (olivine, pyroxene, and oxides). (b): L256 decorrelation stretch highlights these color differences. (c): Band depth in L5 (528 nm) relative to shoulders at L6 (442 nm) and L4 (605 nm), typically indicating iron oxides (crystalline and nanophase). (d): Mafic parameter combination, where red = R0R/R1 (630/800 nm); green = band depth at 910 nm; and blue = R1/R5 (800/978 nm). Dourbes shows clear rounded olivine grains (magenta) surrounded by pyroxene (blue). Quartier shows similar relationships but with possible cm-scale layering, based on the strong dark stripe with more pyroxene signatures across the center of the site, indicating layer-to-layer differences in olivine versus pyroxene abundances.

sites (<1 wt.%) are generally lower than the natural surfaces. SuperCam-LIBS and Raman spectra indicate olivine $Fo_{55–60}$ (Beyssac et al., 2023; Wiens et al., 2022). As shown by the oxide ternary diagram (PIXL data, Figure 10) and total alkali versus silica diagram (SuperCam-LIBS data, Figure 11), the bulk compositions of the Séítah targets are consistent with an ultramafic rock modified by some degree of aqueous alteration.

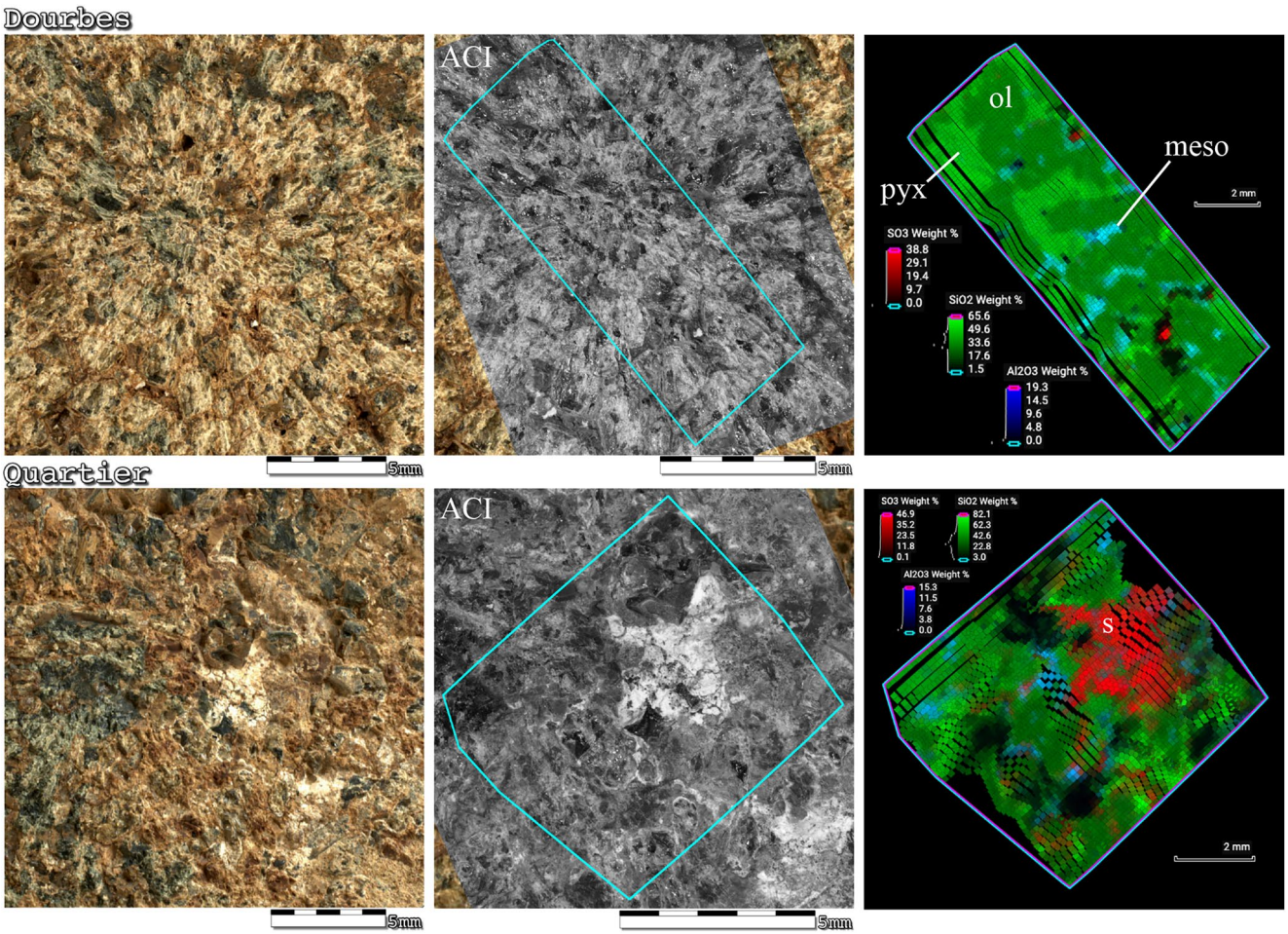

Figure 9. *Close up observations of Séítah abrasion sites by WATSON* (*~4* cm *standoff*), *Autofocus and Context imager*, *and PIXL*: Compositional X-ray map of SO_3 (red), SiO_2 (green), and Al_2O_3 (blue) concentrations, generally correspond to primary olivine (ol) = dark green and pyroxene (pyx) = light green, compositionally evolved intercumulus mesostasis (meso) = blue and secondary sulfate (s) = red, respectively (see text and Figures S12–S16, Table S1 in Supporting Information S1 for additional information).

4.2. Primary Rock Type of Sampled Máaz Outcrops

Rock textures observed in the Guillaumes, Bellegarde, and Alfalfa abrasion sites of Máaz formation rocks indicate grain sizes that vary between ~0.2 and 0.5 mm for Rochette, ~0.5 and 1.0 mm for Roubion, and ~0.5 and 3.5 mm for Sid (Figures 12 and 13). Light and dark grains or crystals comprise most of the abraded surfaces. The light materials have at least two distinct morphologies and tones: some have angular shapes, including potential elongated feldspar laths, whereas others (especially those that are brightest white) have a more irregular outline. The latter suggests a secondary cavity-filling or replacement phase. Excluding evidence of secondary alteration, the light and dark grains appear roughly equal in size with an obvious spatial heterogeneity in relative abundance. There is little evidence of a fine-grained "microlite" matrix in the Máaz rocks, but rather a more uniform grain size distribution. There is no compelling evidence of the intergranular porosity or cements common to many sedimentary rocks. Taken together, these observations are consistent with fine-grained gabbro or holocrystalline basalt. The exception is the porphyritic texture observed in Alfalfa of the upper Máaz, Ch'ał member that exhibits relatively large euhedral feldspar crystals, several millimeters in length, within a finer-grained feldspar- and pyroxene-dominated matrix. Although the matrix observed in Alfalfa is similarly coarse to that of other Máaz rocks, its grains are more elongated than those in Guillaumes and Bellegarde. Collectively, these observations suggest that Alfalfa represents a more rapidly cooled lava (see Figure 13). In all Máaz rock targets, abrasion surfaces exhibit evidence for a homogeneous distribution of interlocking grains suggesting textures consistent with crystallization from a magma (Figure 13).

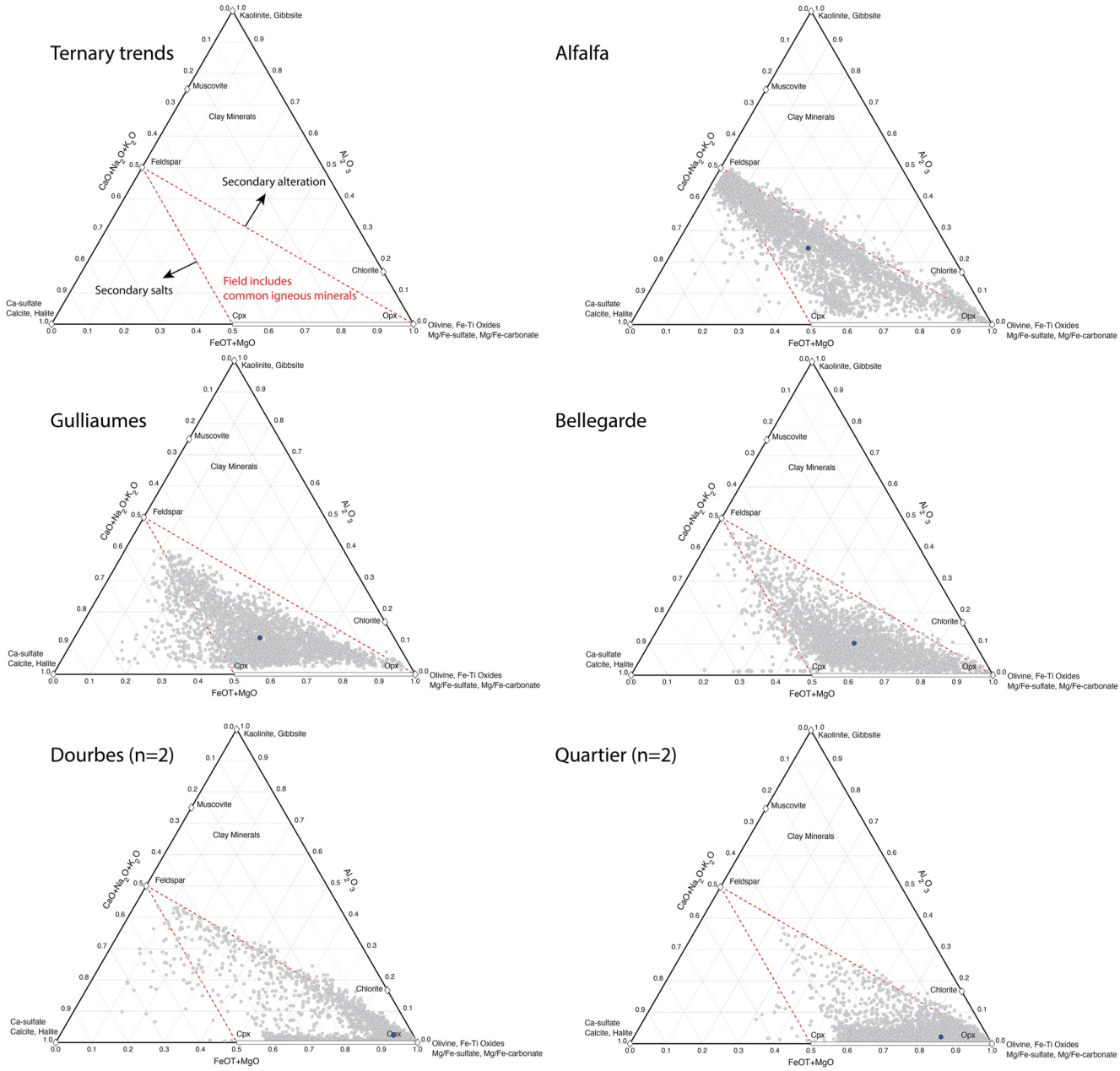

Figure 10. *Abrasion site PIXL data*: Plotted by pixel and as bulk sum composition (blue circle) on a ternary diagram of molar abundances $Al_2O_3 - (CaO + Na_2O + K_2O) - (FeO_T + MgO)$. Common primary igneous minerals (olivine, pyroxene, feldspar, and Fe-Ti-oxides) are typically found within dashed red inner triangle area whereas common clay minerals fall above the upper red dashed line. Several additional secondary minerals (e.g., Fe-Mg-Ca-sulfates/carbonates, halite) are also plotted for reference.

Coordinated PIXL X-ray mapping and WATSON images, SuperCam-LIBS, SHERLOC-Raman spectroscopy, and Mastcam-Z multispectral data indicate that the minerals present in Máaz rocks include at least two pyroxene compositions, likely an Fe-rich augitic and an Fe-rich but less Ca-rich pyroxene like pigeonite, plagioclase feldspar, a third mafic silicate phase (olivine or orthopyroxene?), and Fe-Ti-oxides, together with secondary iron oxides and/or silicates, sulfates, Na-Cl and/or Na-ClO_4 salts, and phosphates (Figures 9–13; see Clavé et al., 2022, this volume; Meslin et al., 2022, this volume). More detailed and refined mineral compositions are presented in Udry et al. (2022); Tice et al. (2022); and Fe-bearing minerals detected by Mastcam-Z multispectral data and CRISM hyperspectral data in Máaz are presented in B. Horgan et al. (2022, this volume). Accessory phases

Table 4
Bulk Sum Averages for PIXL Scan Areas

	Guillaumes (sol 167)			Bellegarde (sol 187)			Dourbes (sol 257)			Dourbes2 (sol 270)			Quartier1 (sol 294)			Quartier2 (sol 301)			Montpezat2 (sol 350)			Alfalfa (sol 369)		
	wt %	1s error (wt%)	std	wt %	1s error (wt%)	std	wt %	1s error (wt%)	std	wt %	1s error (wt%)	std	wt %	1s error (wt%)	std	wt %	1s error (wt%)	std	wt %	1s error (wt%)	std	wt %	1s error (wt%)	std
Na_2O	5.71	0.72	3.10	4.76	0.56	1.59	1.70	0.56	0.38	2.24	0.54	2.21	2.27	0.77	1.39	1.93	0.60	1.21	3.40	0.97	1.70	5.28	0.66	2.29
MgO	2.63	0.56	1.08	2.19	0.64	1.16	19.73	0.99	2.14	18.53	0.93	1.97	15.86	0.80	3.80	13.13	0.66	2.68	6.15	0.31	1.75	0.76	0.32	0.52
Al_2O_3	7.56	0.38	3.02	6.96	0.35	3.62	1.96	0.51	5.16	3.08	0.56	5.96	1.50	0.44	1.87	2.35	0.55	1.88	5.82	0.29	2.77	11.88	0.60	5.69
SiO_2	38.28	1.92	7.12	43.78	2.19	10.65	40.36	2.02	3.11	38.08	1.91	4.10	34.13	1.71	14.70	41.36	2.07	7.30	44.95	2.25	6.16	57.16	2.86	11.32
P_2O_5	1.64	0.54	1.41	2.75	0.56	2.46	0.29	0.25	8.83	0.74	0.29	9.20	0.42	0.24	1.76	0.29	0.25	0.57	1.09	0.43	1.45	0.98	0.37	1.51
SO_3	2.69	0.56	2.90	3.21	0.56	5.84	0.52	0.21	1.13	1.15	0.36	3.33	8.61	0.46	11.60	1.70	0.47	1.81	0.93	0.35	0.47	1.96	0.51	1.16
Cl	3.50	0.54	4.14	1.52	0.44	0.84	0.62	0.34	1.81	0.74	0.25	0.74	1.15	0.48	0.85	0.96	0.36	0.60	0.79	0.27	0.71	1.05	0.34	1.51
K_2O	0.75	0.26	0.47	1.06	0.34	0.76	0.12	0.14	0.90	0.26	0.23	0.56	0.12	0.14	0.33	0.21	0.21	0.40	0.73	0.25	0.69	1.93	0.51	1.28
CaO	7.80	0.39	3.86	7.64	0.38	4.34	3.89	0.49	5.93	1.58	0.45	1.26	2.75	0.56	4.48	6.09	0.31	5.92	9.08	0.46	4.97	4.42	0.40	3.42
TiO_2	1.48	0.54	2.27	2.49	0.58	2.18	0.39	0.24	1.08	0.32	0.23	2.91	0.25	0.23	0.79	1.01	0.33	2.29	1.06	0.42	2.03	0.68	0.29	1.61
Cr_2O^3	0.03	0.06	0.07	0.01	0.03	0.02	0.30	0.25	1.33	0.22	0.21	1.03	0.05	0.06	0.33	0.30	0.24	1.25	0.07	0.09	0.16	0.02	0.05	0.02
MnO	0.47	0.20	0.37	0.44	0.23	0.21	0.73	0.31	0.28	0.62	0.22	0.23	0.70	0.24	0.28	0.59	0.24	0.23	0.52	0.21	0.31	0.32	0.25	0.38
FeO-T	18.76	0.94	10.94	23.26	1.16	11.27	30.01	1.50	10.48	30.04	1.50	10.12	30.16	1.51	13.56	26.35	1.32	10.95	20.86	1.04	12.31	11.34	0.57	13.66

occur at grain boundaries between plagioclase and pyroxene and may be late-stage primary, secondary, or both (Kizovski et al., 2022).

X-ray fluorescence mapping by PIXL was undertaken in selected areas of the Guillaumes, Bellegarde, and Alfalfa abrasion sites (Figure 10; PIXL scans in Figures 9 and 13). The bulk sum analysis of each scanned abrasion surface is shown in Table 4. Note, as for the Séítah observations, that these analyses include a mixture of what are likely primary igneous mineral grains along with secondary phases suggestive of later alteration. PIXL analyses of abrasion sites show SiO_2 contents of 30–70 wt.% and $Na_2O + K_2O$ contents of ~2–9 wt.%. These data, especially those for Guillaumes and Bellegarde, show considerable spread, likely attesting to a significant salt contribution to their bulk compositions. These are therefore unreliable for an igneous rock classification as presented. SuperCam-LIBS analyses undertaken on natural surfaces and abraded sites at each sampled Máaz formation locality also show considerable spread in composition, but the targeting nature of the LIBS approach appears to reflect a more representative analysis of the primary rocks and indicates that Ch'ał is relatively evolved (see Figure 11, Wiens et al., 2022).

The Máaz rock compositions span from basaltic to andesitic with evidence of some addition of salt and aqueous activity recorded in the bulk chemical signatures, as shown by the oxide ternary diagram (PIXL data, Figure 10) and total alkali versus silica diagram (SuperCam-LIBS data, Figure 11). Although no abrasion or sample core was collected from the Content member atop Séítah rocks, its composition as determined by SuperCam-LIBS generally matches other Máaz units, is distinct from Séítah, and therefore may have implications for the hypothesized stratigraphy and formation of crater floor rock (cf. Wiens et al., 2022).

4.3. Alteration of Crater Floor Rocks

Both the Séítah and Máaz formations have undergone variable degrees of post-emplacement aqueous alteration. The presence of reddish-brown staining and the identified SCAM VISIR hydration peaks are consistent with aqueous deposition of iron oxides or Fe silicate (see Section 5.2; Mandon et al., 2022, this volume). Surface coatings are common on Jezero Crater floor rocks (Bell et al., 2022; Wiens et al., 2022). Mastcam-Z and SuperCam RMI images reveal several brown to reddish domains, ranging in areal extent from patches to regions with more continuous coatings. Some areas have thicker coating layers. These coatings are spectrally and thus compositionally distinct from the underlying rock (e.g., see Garczynski et al., 2022, this volume). The elemental compositions of the coatings are similar to those of Mars global dust.

Although natural surfaces of Séítah appear to have elevated alkalis compared to the corresponding abraded surfaces in SuperCam-LIBS observations (see Figure 11), the degree of alteration of samples collected from Séítah appears relatively minor because much of the geochemistry and textures of the primary rocks have been retained, that is, the dissolution of olivine crystals, if it occurred at all, is minimal (Liu et al., 2022).

Imaging and chemical investigations of the Brac outcrop indicate the presence of multiple, varied alteration phases. High-resolution WATSON imaging of the Dourbes abraded surface reveals a reddish, likely Fe-bearing, secondary phase filling interstitial spaces among primary

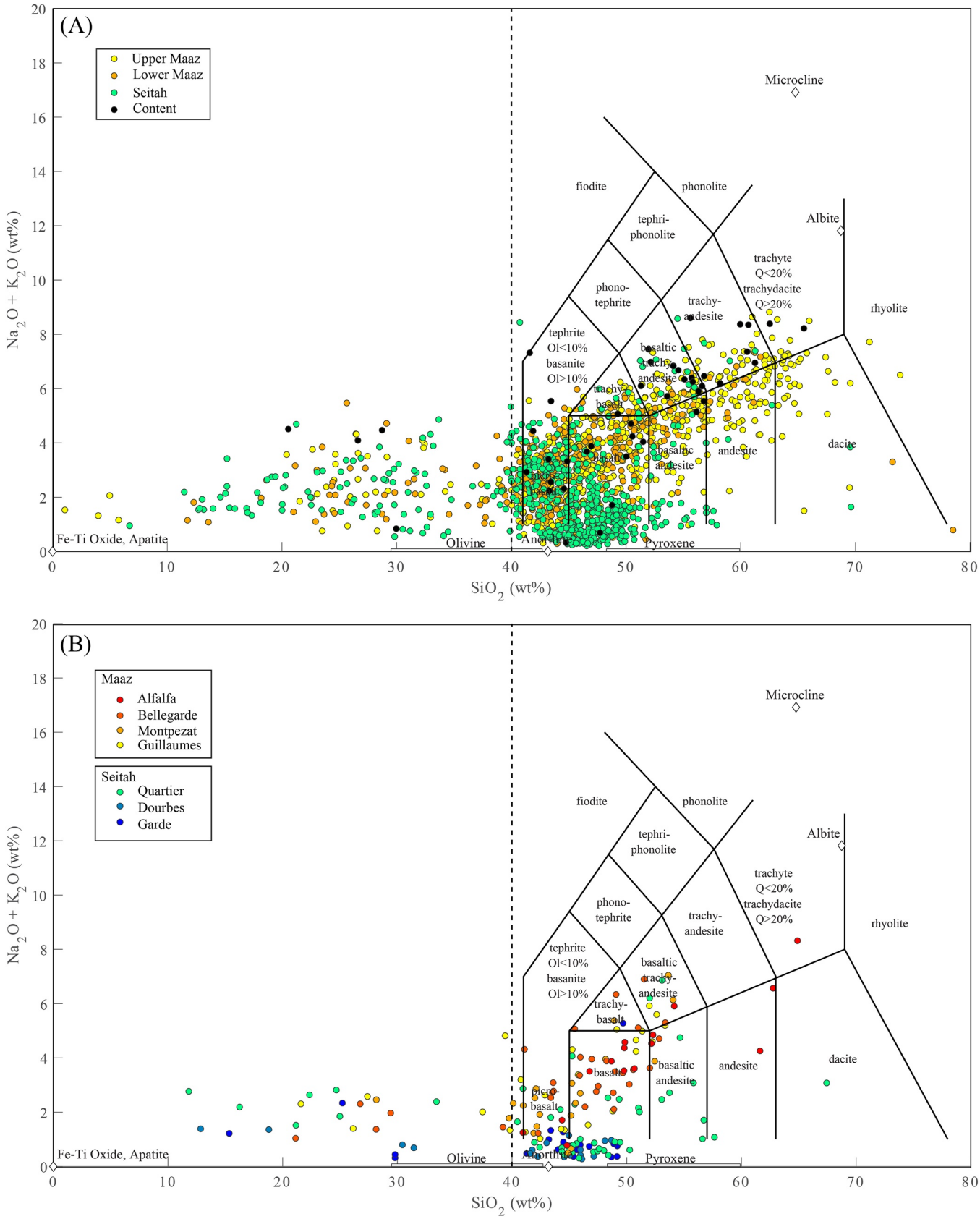

Figure 11.

minerals (Figures 8 and 9). Mastcam-Z multispectral imaging of the natural surface mainly reflects the dust coverage on the outcrop while similar analyses of the Dourbes abrasion site reveals spectral signatures of a secondary phase, likely ferric oxides (Figure 8). SuperCam-VISIR data suggest the presence of Fe- and Mg-bearing phyllosilicates (Figure 14). Both the ferric oxide and Fe-bearing phyllosilicate phases are consistent with WATSON observations. Mineral compositions inferred from PIXL data, while dominated by primary phases, also show evidence of secondary phases, such as sulfate, calcite, and halite (Figure 10). Spots of concentrated $CaSO_4$ and $MgSO_4$*nH_2O as well as an occurrence of perchlorate were documented by PIXL (Tice et al., 2022). Similarly, a carbonate phase in the abrasion site was also identified by SuperCam-LIBS/VISIR and SHERLOC-Raman (Figures 14 and 15). A hydration signature consistent with Fe-(hydr)oxide and phyllosilicate phases, is also apparent in SHERLOC-Raman and SuperCam-VISIR data (see Mandon et al., 2022, this volume).

The Quartier abrasion site on Issole shows characteristics of alteration similar to those observed in Dourbes on Brac (Figures 8, 14, and 15). Purple-hued areas in WATSON images of the natural surface, which are likely indicative of a surface coating, have a spectral signature consistent with ferric iron. The reddish-brown material in the abrasion sites (Figure 8) attributed to Fe-oxyhydroxides via Mastcam-Z multispectral data appears to surround a pale-brown/white phase, which has been identified as a sulfate (possibly Mg/Ca/Fe-bearing) by SHERLOC (Figure 15). Similar to Dourbes, possible Fe-phyllosilicates, Mg-phyllosilicates, and carbonate were detected by SuperCam-VISIR (Figure 14). Raman data from SHERLOC also point to the presence of carbonate and Mg-sulfate in these rocks, particularly in the Quartier abrasion site (Figure 15). A large (approximately 4 mm^2) area of what is thought to be nearly pure Mg/Ca-sulfate was detected in one PIXL scan, but a second scan of a more representative portion of primary mineralogy of the Quartier abrasion site resulted in much lower average SO_3 concentrations, in-family with Jezero samples analyzed to this point (Cl/S ratio [atom/atom] > 1.0).

The samples from the Máaz formation (Montdenier, Montagnac, Hahonih, and Atsah), as well as the three Máaz abrasion sites (Bellegarde, Alfalfa, and Guillaumes) all share some common evidence of alteration, but also possess evidence of alteration that is specific to individual samples, best described as variability in their degree of alteration. The Roubion target extends this range as it exhibits pervasive alteration and secondary mineralogy; this factor may have led to its disaggregation during coring. Reddish staining is present in all Máaz abrasion sites (Figure 9) and is consistent with iron oxide detected by Mastcam-Z, PIXL, and SuperCam-LIBS. This phase often occurs as an alteration rind around grains and/or voids. The degree of oxidation in Máaz abrasion sites varies significantly, as shown based on 525 nm band depth in Figure 12. Clear signatures of fine-grained hematite are detected in Alfalfa, while oxidation consistent with nanophase hematite is detected in Bellegarde, and no significant oxidation is detected in Montpezat (an abrasion within the Artuby member of Máaz formation at the base of Artuby Ridge), suggesting highly variable oxidation during emplacement or later weathering.

Spectral signatures of Fe- and/or Mg-phyllosilicates and a hydration signal are also evident in SuperCam-VISIR data from all abrasion sites (Figure 14). Analysis presented in Wiens et al. (2022) indicates that from the observations across the Máaz formation, up to 20%–25% of the MgO and a lower percentage of the CaO are due to accumulation of sulfates and other precipitates. Bellegarde and Alfalfa contain possible Al-phyllosilicates evidenced in data from PIXL and SuperCam, respectively (see Figure 5 and Wiens et al., 2022). The Guillaumes and Bellegarde abrasion sites contain voids that are sometimes filled with white materials as seen in WATSON images (Figures 12 and 13). The Guillaumes abrasion site appears particularly flaky and granulated compared to the other abrasions. Voids are noticeably absent from the Alfalfa abrasion site.

Ca-sulfates, perchlorates, silicates, carbonates, and phosphates are potential void-filling secondary phases detected in abrasion sites from the Máaz formation. All of these phases were identified by SHERLOC while detections of sulfates are supported by SuperCam-VISIR data (Figure 14) and PIXL data suggest the presence of carbonates, halides, sulfates, and perchlorate (Figure 10). The average S and other elemental abundances for Bellegarde, Rochette, and Guillaumes are approximately equivalent (Table 4) with the exception of the Guillaumes abrasion site, which indicates

Figure 11. *SuperCam-LIBS total alkalis versus silica plots for natural and abraded surfaces of rocks sampled during the Crater Floor Campaign*: (a) laser spot data from natural surfaces of "upper Máaz," "lower Máaz," Séítah, and Content. (b) Laser spot data from within abrasion sites. The individual data points represent ∼250 μm LIBS laser spots and therefore represent a mixture of one or more primary and secondary minerals. Endmember igneous mineral compositions shown as diamonds and lines for those with solid solution for reference. The underlying igneous classification scheme does not apply to the individual data points and simply provides a frame of reference for comparing samples (data included in Tables S2–S6 in Supporting Information S1). Color coding of sample symbols matched to those of stratigraphic column units shown in Figure 2.

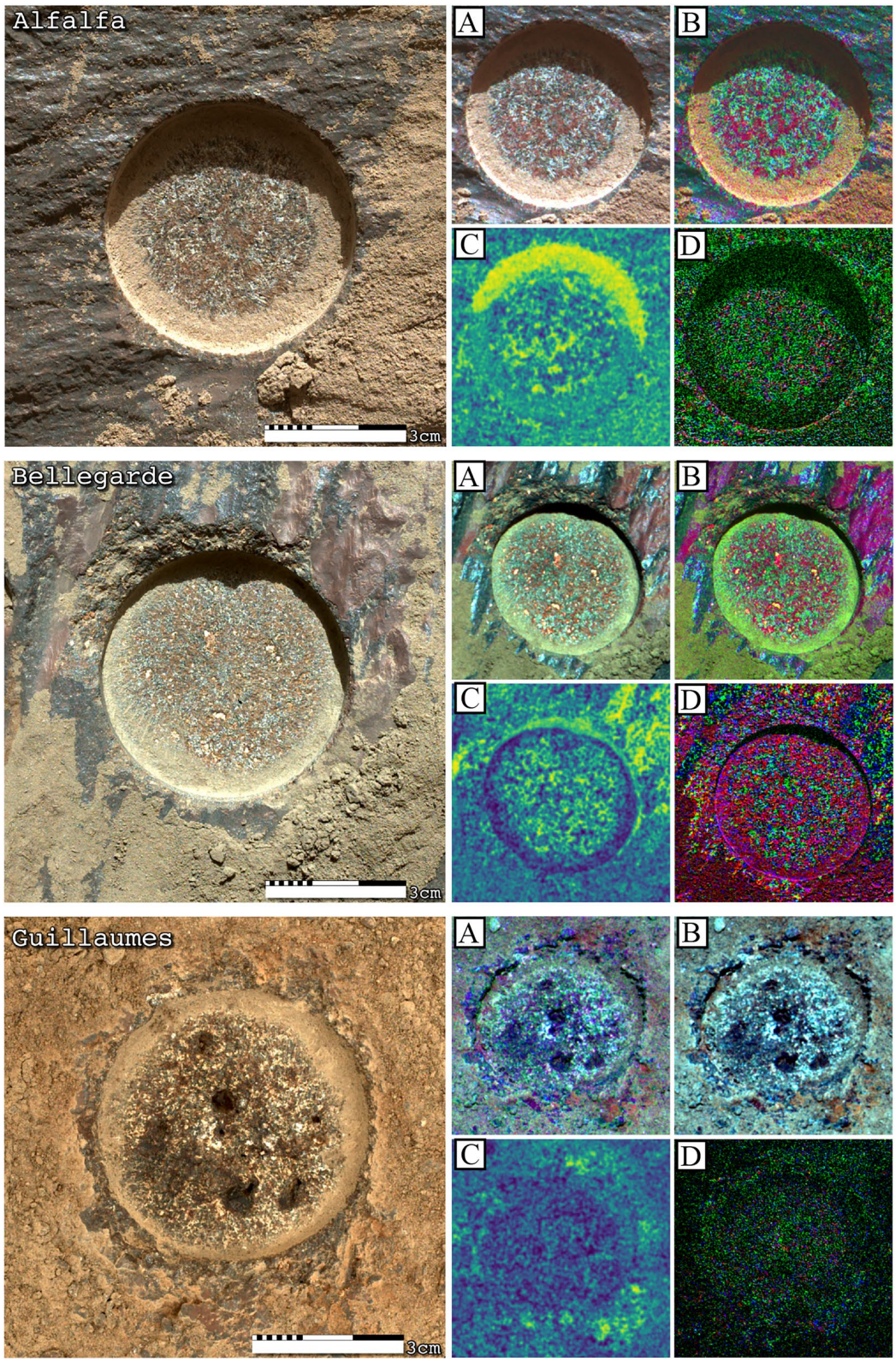

Figure 12.

a much higher (>2x) concentration of Na and Cl. Sulfate and perchlorate salts occupied the largest volume in the Guillaumes abrasion site (i.e., the unsuccessful rock core sample), where perchlorate, including sodium perchlorate, was also detected by SuperCam-Raman (see Meslin et al., 2022, this volume) and SHERLOC-Raman (see Murphy et al., 2022 and Corpolongo et al., 2023). The oxidized anions in these salts indicate a later origin relative to the deposition of the primary igneous minerals that contain reduced iron such as pyroxene and olivine and the spatially and volumetrically limited precipitation of iron(II)-containing carbonate in Séítah. In other abrasion sites, significant concentrations of Cl at the sub-mm scale were detected with PIXL scans, but correlations with Na were weak or absent, whereas a weak association with Fe was sometimes indicated. Most of the salt phases identified elsewhere were not detected in Alfalfa and voids are noticeably absent, further attesting to its minimal degree of alteration.

Visible and IR spectroscopy of the crater floor rocks and the compositional and Raman spectroscopic maps of all abraded sites from Séítah did not reveal any veins or even mm-scale accumulations of salts with sulfate or oxychlorine anions. PIXL and SHERLOC detected smaller sites of sulfate and oxychlorine salts in the rocks sampled from both Máaz and Séítah (Figures 9, 13, and 15). The coexistence of oxidized and reduced phases in the same rocks suggests multiple episodes of aqueous alteration under changing redox conditions or electrochemical reactions occurred that were capable of producing both such phases from a single fluid (e.g., Steele et al., 2018). Analyses in Earth-based laboratories are required to address when these episodes occurred, whether they involved fluids with different organic contents and whether and how they preserved organics.

Fluorescence spectroscopy, as obtained with SHERLOC, can be used to detect and characterize diverse aromatic compounds within samples and perform preliminary classification based on number of rings (Bhartia et al., 2008). Abrasion sites in both Máaz and Séítah show similar fluorescence features (single band at 270–295 nm, single band at 335–350 nm, and doublet at ∼303 and 325 nm, two peaks at ∼290 and 330 nm) (Figure 15). The 270–295 nm feature likely originates from single-ring aromatics, and in many cases is co-located with the single band at 335–350 nm. The 335–350 nm features likely originate from double-ring aromatics and/or Ce^{3+} fluorescence emissions from inorganic mineral phases like phosphates (Scheller et al., 2022). The doublet at 303 and 325 nm most likely originates from single- or double-ring aromatics, though the possibility of mineral (Ce^{3+}) fluorescence emission contribution is still being investigated. The two peaks at ∼290 and 330 nm could represent a one- or two-ringed aromatic compound. The fluorescence spectra may be attributed to aromatic organic compounds with a fairly low average abundance, comparable to detections in some martian meteorites (e.g., Koike et al., 2020; Jaramillo et al., 2019; Steele et al., 2012, 2016, 2018, 2022). The most significant difference in fluorescence signals between the two formations is the close to order of magnitude more detections in Máaz versus Séítah (see Sharma, Beegle, et al., 2022; Sharma, Roppel, et al., 2022). The 335–350 nm feature is observed in all targets while the fluorescence doublet at 305 and 325 nm is only detected in the Bellegarde and Quartier targets, in which it is associated with sulfates, and the 290 and 330 nm features are found associated with carbonates and silicates. The other two fluorescence features (270–295, 335–350 nm) have less clear associations with minerals although the 335–350 nm feature seems to be preferentially associated with grain and 270–295 nm with brown-toned alteration material.

SHERLOC deep UV Raman analysis also detected peaks that may be due to organic carbon on multiple targets. Raman spectroscopy is less sensitive than fluorescence spectroscopy, so the signal-to-noise ratio and number of detections is expectedly lower. In two of the targets, Garde and Quartier, the Raman detections were correlated with the strongest fluorescence detections. In the third, Montpezat, a possible G band (i.e., C-C bond) was detected.

5. Returned Sample Science Potential

The Mars 2020 Science Team has prioritized key science questions to be addressed by the samples collected by Perseverance upon their return to Earth. As the first suite of samples returned to Earth from a known locality on Mars, these samples represent the opportunity for the global scientific community to address major outstanding

Figure 12. *WATSON (∼25* cm *standoff) image paired with a quad of Mastcam-Z multispectral images for Máaz formation abrasion sites*: (a): L256 enhanced color, where red indicates oxidized grains, light-toned grains are salts or feldspar, and dark blue to gray grains are unaltered mafic minerals (pyroxene and oxides). (b): L256 decorrelation stretch highlights these color differences. (c): Band depth in L5 (528 nm) relative to shoulders at L6 (442 nm) and L4 (605 nm), typically indicating iron oxides (crystalline and nanophase). (d): Mafic parameter combination, where red = R0R/R1 (630/800 nm); green = band depth at 910 nm; and blue = R1/R5 (800/978 nm). Alfalfa is dominated by hematite and unoxidized pyroxenes (green and magenta/blue), Guillaumes exhibits low spectral contrast due to weathering (black), and Bellegarde is dominated by Fe-rich pyroxenes (magenta/red).

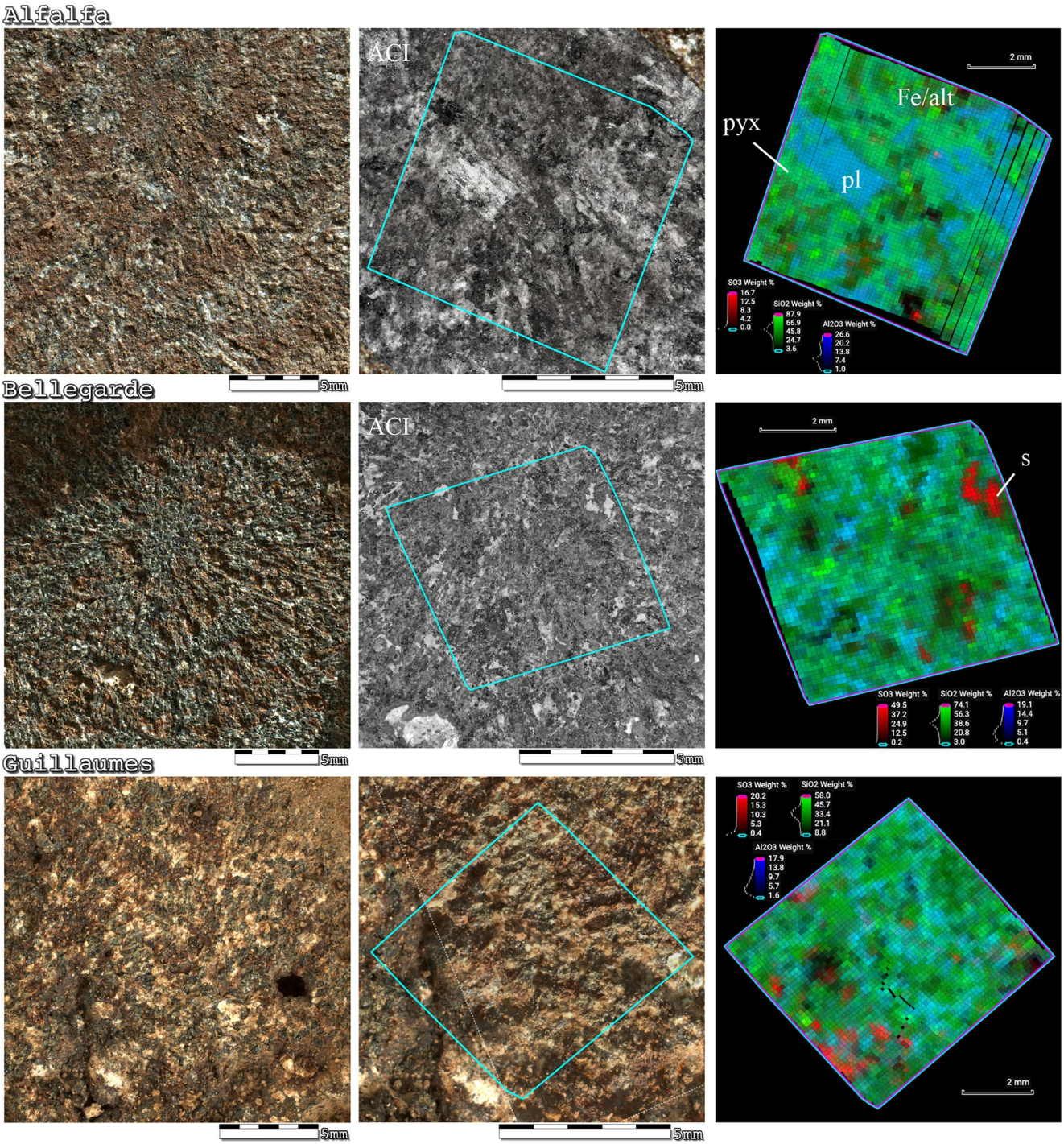

Figure 13. *Close up observations of Máaz abrasion sites by WATSON (~4 cm standoff), Autofocus and Context imager (ACI), and PIXL*: Compositional X-ray map of SO_3 (red), SiO_2 (green), and Al_2O_3 (blue) concentrations, generally correspond to primary pyroxene (pyx) = light green, plagioclase (pl) = blue, and Fe-silicate/alt. olivine (Fe/alt) = green and secondary sulfate (s) = red, respectively (see text and Figures S12–S16, Table S1 in Supporting Information S1 for additional information). Colorized ACI used to improve image clarity for Guillaumes because of lighting conditions.

questions relating to geochemistry, geochronology, petrogenesis, paleomagnetism, planetary evolution, paleoenvironments, and potentially astrobiology from the early history of Mars (i.e., the Noachian-Hesperian period). Scientific rationales for the return of each collected sample are listed in Table 3. These mission goals align with longstanding MSR science objectives held by the international planetary science community. Earth-based

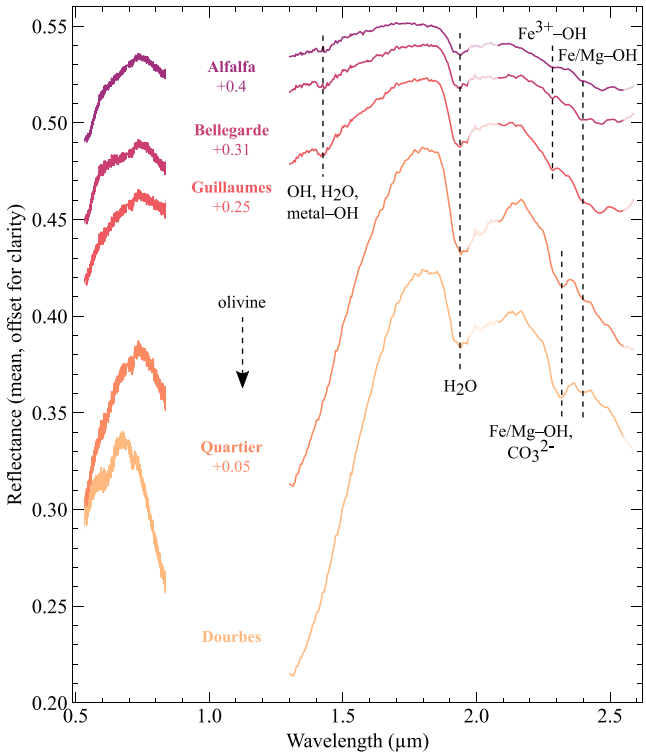

Figure 14. *SuperCam mean visible and infrared reflectance spectra of the abraded rocks sampled during the Crater Floor Campaign*: The main band attributions are annotated (see Mandon et al. (2022), this volume). Parts of the spectra are shown at lower opacity near ~2 μm owing to possible residual atmospheric CO_2 bands and past ~2.5 μm where calibration is uncertain (Royer et al., 2022, this volume).

analysis of igneous rocks of the Jezero Crater floor sample suite, described herein, will provide important constraints on a number of these questions as discussed below.

5.1. Igneous Jezero Crater Floor Bedrock Samples

Surface operations of the Mars 2020 mission have provided exceptional geological context for the igneous samples collected. From orbital observations, crater floor rocks are suggested to be related to widespread lithologies outside of Jezero (e.g., Brown et al., 2020; Mandon et al., 2020). Determination of similar (or distinct) lithologies and/or ages in Jezero and outside of Jezero rocks would help to constrain aspects of the regional geologic history, and potentially the planetary evolution of Mars, as described below (Section 5.4). Future rover operations outside Jezero Crater will further clarify these lithological relationships, but Earth-based analyses of the igneous lithologies from Jezero and samples from their plausible outside Jezero equivalents (i.e., the "olivine-carbonate" and/or "mafic cap" units of Mandon et al., 2020) would lead to a more comprehensive and robust reconstruction of regional geologic history and planetary evolution.

5.1.1. A Collection of Igneous Olivine Cumulate and Basaltic to Andesitic Samples

Typical igneous minerals and textures, ranging from cumulate with adcumulus growth in Séítah to aphanitic and porphyritic in Máaz, have been observed. The eight cores collected contain varying amounts of olivine, plagioclase, ortho- and clinopyroxene, as well as minor minerals such as oxides and phosphates. Textures and mineralogies of the samples can be used to partially constrain their petrogenesis; however, compositions, atomic structure, and bonding within individual minerals, as well as trace element and isotopic signatures widely used to constrain specific formation temperatures, pressures, source volatile contents, and ages will require levels of analytical precision and spatial resolution only afforded by returned sample laboratory analyses.

5.1.2. The First Rocks From Mars With Geologic Context

The age and composition of rocks from Mars provide insights into the geology of its surface and interior. More than 175 distinct martian meteorite samples (Udry et al., 2020) have been collected on Earth, and while they have greatly enhanced our understanding of the geological evolution of Mars, they are an inferior archive compared to samples collected directly by the Mars 2020 mission. The majority of martian meteorites (~88%) have crystallization ages of <600 Ma; this is at odds with the fact that >75% of the Martian surface rocks date to the Noachian or Hesperian Periods (≥3.2 Ga, Tanaka et al., 2014). Based on a few dominant cosmogenic exposure age populations, most martian meteorites likely represent less than approximately one dozen launch sites (e.g., McSween, 2015, and references therein). A vast majority of martian meteorite bulk compositions do not match compositions of Martian terrains investigated to date by either remote sensing or rover exploration (McSween, 2015). These three issues imply that martian meteorites represent neither the diversity of the martian surface nor that of the interior. This is further corroborated by considerations of the impact process by which martian meteorites are delivered to Earth, which demonstrate a bias towards younger, more competent igneous rocks (e.g., Walton et al., 2008; Warren & Kallemeyn, 1994; Udry et al., 2020, and references therein). Finally, no definitive link has yet been made between any of the martian meteorites and their source craters.

Although the emplacement timing of the crater floor rocks needs to be more precisely constrained, comparisons of the mineralogy, petrology, and geochemistry of the returned samples with martian meteorite lithologies also has the potential to provide fundamental insights into the range of mantle source compositions and conditions of melting present within Mars over time, and to elucidate the variety (or lack thereof) of eruptive compositions. It will place valuable constraints on the composition of the martian interior at a rather early to intermediate stage

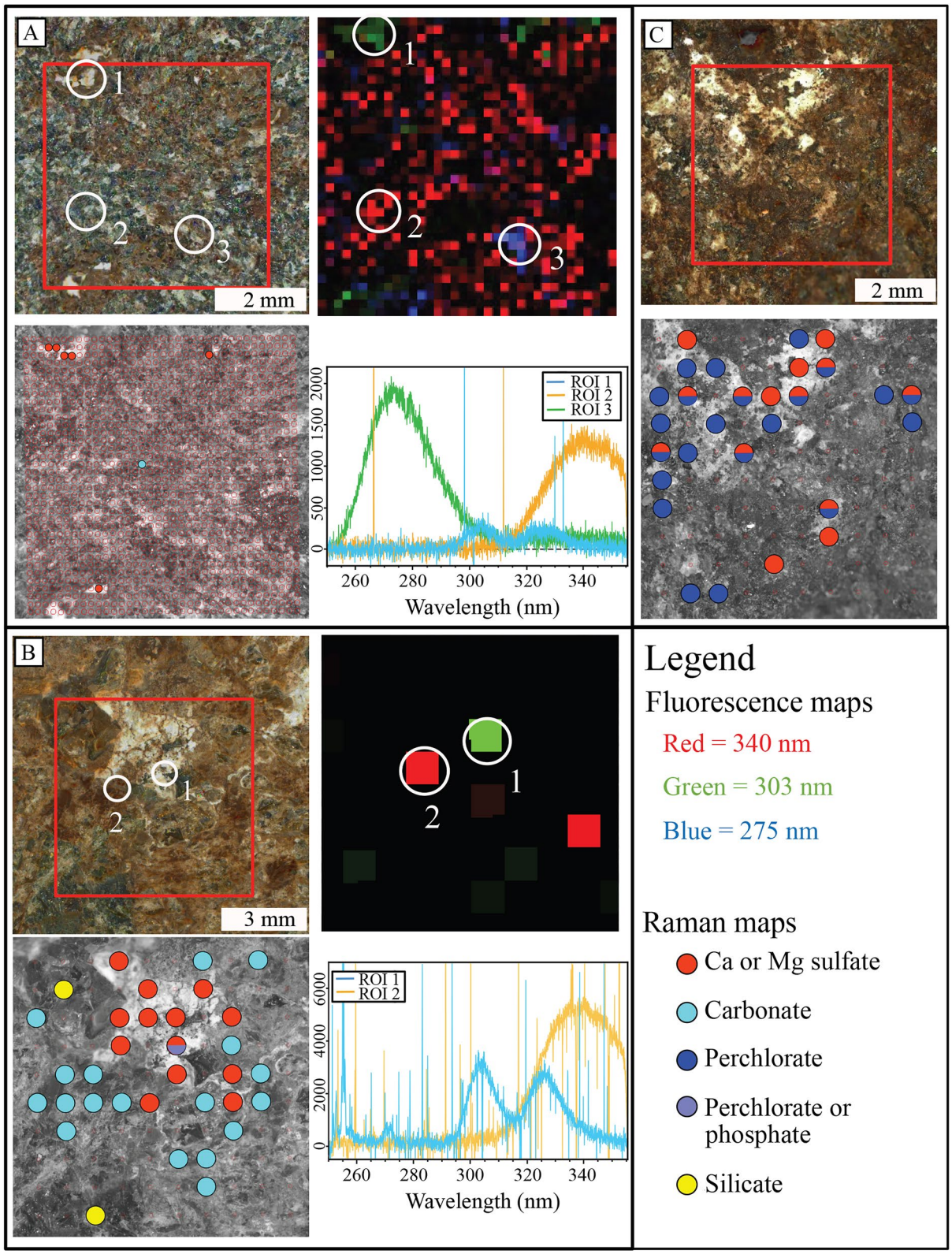

Figure 15.

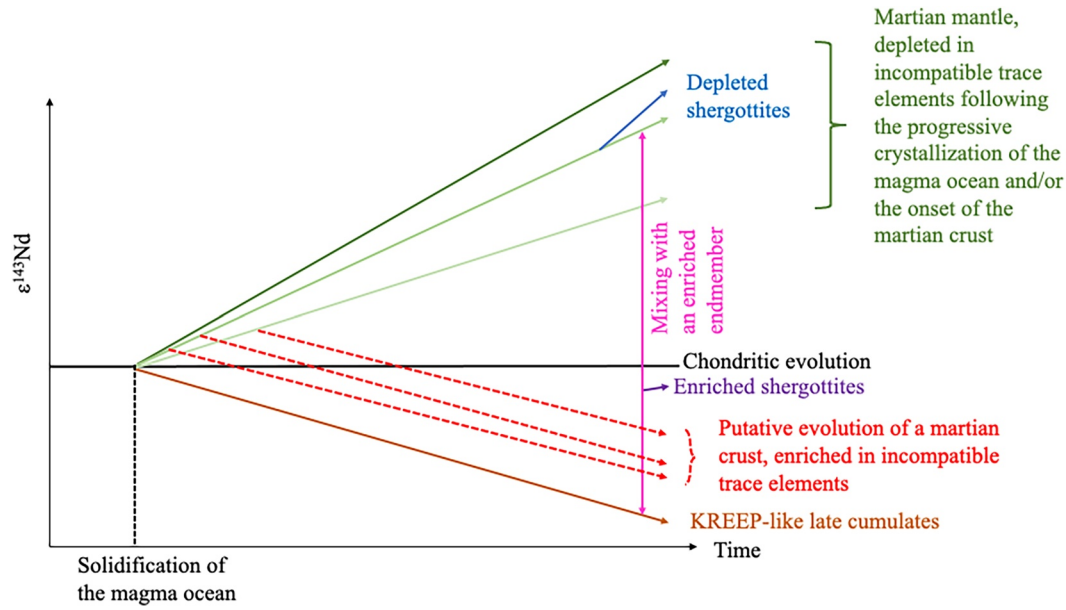

Figure 16. *Schematic geodynamical evolution of the martian interior* : Radiogenic ingrowth of $^{143}Nd/^{144}Nd$ depends on the variation in Sm/Nd in the reservoirs. The progressive solidification of the magma ocean resulted in several depleted reservoirs (in green) and ended up with enriched late cumulates (in brown), after Debaille et al. (2007). From the depleted martian mantle, a crust has been extracted, that is enriched in incompatible trace elements, as observed in NWA 7034 (Armytage et al., 2018). Depleted shergottites (in blue) directly sample a depleted reservoir while the enriched shergottites (in violet) represent a mixture (in pink) between depleted and enriched reservoirs.

of chemical differentiation (Clenet et al., 2013; Pinet & Chevrel, 1990). The olivine cumulate lithology represented by samples from Séítah (Salette, Coulettes, Robine, and Malay cores) appears to have similarities to the considerably younger chassignite and poikilitic shergottite subgroup of martian meteorites, at least at first look (Liu et al., 2022). The Máaz lithologies bear some similarities to basaltic shergottites, augite-rich shergottites, and alkali-rich igneous clasts found within NWA 7034 (e.g., Herd et al., 2017; Rubin et al., 2000; Santos et al., 2015; Tait & Day, 2018; Udry et al., 2017, 2022), although they are significantly more ferroan than all known martian meteorites (cf. Udry et al., 2020).

The apparent similarity between the preliminary composition of the Séítah formation and some martian meteorite lithologies suggests that similar conditions and mantle compositions existed during magmagenesis at the time of the formation of these units despite the large difference in likely formation age. However, the observation that Máaz formation rock lithologies are more ferroan than most martian meteorites suggests that some, if not all of the igneous rocks in Jezero, have distinct magmatic histories, perhaps derived from mantle source(s) with different bulk compositions, differing conditions of partial melting, ascent and emplacement, crustal assimilation, and/or involving melts produced by impact of altered surface rocks.

In addition to bulk mineral and major element analyses, trace element analyses will be crucial for constraining the possible source reservoirs of Jezero rocks and testing their magmatic petrogenesis. For example, trace element data may distinguish between a single differentiated system or separate magma generation events (cf. Farley et al., 2022). Trace element geochemistry can also be employed to understand why these rocks are so ferroan; rare earth elements could be used to test whether crustal assimilation was important to magmagenesis (Peters et al., 2015), and siderophile element abundances may denote the assimilation of chondritic meteorite materials and thus be used to test an impact melt origin hypothesis (e.g., Day et al., 2016; Goderis et al., 2016).

Figure 15. *SHERLOC analysis of abrasion targets*: (a) Bellegrade, (b) Quartier, and (c) Guillaumes showing a diversity of organic and alteration minerals detected in Máaz and Séítah. Panels (a and b) starting top left show colorized Autofocus and Context imager (ACI) (red squares indicate outlines of scan areas and white circles regions of interests), fluorescence maps with region of interest (ROIs), fluorescence spectra from ROIs, and Raman maps with confidently detected minerals indicated by colored circles. In panel (c), the top image is a colorized ACI image (the red square indicate outline of the scan area), while the bottom is a Raman map with confidently detected minerals indicated by colored circles. In each of the Raman maps, note that the filled colored circles are much larger than the ∼100 μm analysis spots (indicated by the small, unfilled red circles).

Investigating the petrogenetic history of samples from the Máaz and Séítah formations by trace element analyses (e.g., REE abundances) can help us better understand the igneous evolution of Mars. In situ analyses on Mars cannot distinguish whether Bellegarde or Dourbes are derived from depleted or enriched shergottite-like or nakhlite/chassignite-like mantle sources, or from entirely distinct mantle source types. This can only be determined in terrestrial laboratories.

5.1.3. Potential Isotopic Record of Jezero Crater Floor Igneous Rocks

In addition to trace elements, isotopic analyses will help to better constrain the number of source reservoirs in the martian interior (including the mantle and crust), their compositions, and possible mixing phenomena. Meteorite studies demonstrate the great possibility to perform high-precision analyses of Martian materials in Earth-based laboratories; for example, isotopic analyses help to constrain processes relating to the geodynamical evolution of Mars (e.g., Borg et al., 1997, 2016; Debaille et al., 2007; Harper et al., 1995; Moriwaki et al., 2020). Measuring the radiogenic ingrowth of elements such as Ca, Sr, Nd, Hf, and W provide constraints on both the differentiation of the planet into several internal reservoirs and the timing of such events (Figure 16). Such analyses require not only ultrasensitive instruments that need to be operated at conditions met only in specialized laboratories, but also highly specialized sample preparation prior to analysis. Although the absolute chronology of Mars may require calibration (see Section 5.5), it is expected that the returned igneous samples from the Jezero Crater floor would be between ~3.7 Ga (as indicated by the crater counting ages of the inlet valley; Fassett & Head, 2008) and ~3.96 Ga (crater counting of the Isidis basin age; Werner, 2008), hence they will help to fill in a large temporal gap observed in martian meteorites between ~2.4 (Herd et al., 2017) and ~4.1 Ga (Lapen et al., 2010). This will place new constraints on the geodynamical evolution of the Martian mantle, better defining our view of the geological evolution of the interior of Mars.

It has also been proposed from the study of martian meteorites that the early (and present?) martian mantle was much more chemically heterogeneous than Earth's mantle (Barnes et al., 2020; Blichert-Toft et al., 1999), likely related to the lack of martian plate tectonics (Debaille et al., 2013). The ancient igneous rocks collected by Perseverance can be used to probe the early stages of planetary differentiation, a record that no longer exists on Earth. Several major questions remain unresolved, for example, what is the duration of the magma ocean stage, which is estimated to have lasted from 35 (Borg et al., 2003) to 100 Ma (Debaille et al., 2007), how this timing compares to the fast differentiation hypothesized for Mars (Dauphas & Pourmand, 2011), and/or why did Mars transition into a "rigid-lid planet" (Moore et al., 2017). Also, igneous samples representative of a time and location distinct from that recorded by the meteorite record will provide a critical test of the "planetary-scale" mixing line observed in shergottites (Lapen et al., 2017), and whether it actually has global significance, and to address whether or not the origin of the enriched endmember is the martian crust (Humayun et al., 2013; Moriwaki et al., 2017), the late cumulates resulting from the magma ocean solidification (Armytage et al., 2018), or something else entirely.

Future insights from isotopic measurements of these martian rocks can be gained from the variations of stable isotopes of certain metals and halogens (e.g., Li, Cl, Mg, Ca, Fe, and Zn; see Johnson et al., 2004; Teng et al., 2017). These isotopic systems are sensitive to processes such as fractional crystallization, volatile degassing, and hydrothermal alteration and recorded by mass-dependent isotope fraction in igneous rocks (e.g., Bellucci et al., 2017; John et al., 2012; Kang et al., 2017; Paniello et al., 2012; Simon, 2022; Teng et al., 2011; Tomascak, 2004; Watkins et al., 2009). Recent work measuring Ca isotopes, an element that has both multiple stable and radiogenic isotopes, exemplifies the emerging applications of non-traditional stable isotope studies, as Ca isotopes can be used to test interpretations related to both thermal and chemical equilibrium by recording the degree of thermal and/or chemical metamorphism potentially modifying the original composition of the igneous rocks (Antonelli & Simon, 2020). Likewise, the combined measurement of non-traditional and traditional radiogenic elements such as Ca and Nd, that have distinct chemical behaviors, has been used recently to distinguish different planetary source reservoirs (e.g., mantle vs. crust) in some terrestrial igneous rocks where the isotopic signature of neither element alone can unambiguously be used to define their source reservoir (Mills et al., 2018).

5.1.4. Volatile Abundances in the Mantle Source Region of Jezero Crater Floor Igneous Rocks

The abundance and distribution of H_2O and other volatiles, in the martian interior is a key factor in understanding the thermochemical and geodynamic evolution of Mars (Breuer et al., 2016; Dreibus & Wanke, 1985; Elkins-Tanton, 2008; McCubbin et al., 2008; Ruedas et al., 2013). Additionally, the effects of magmatic degassing are important to climate change and thus planetary habitability. Studies of martian meteorites have demonstrated

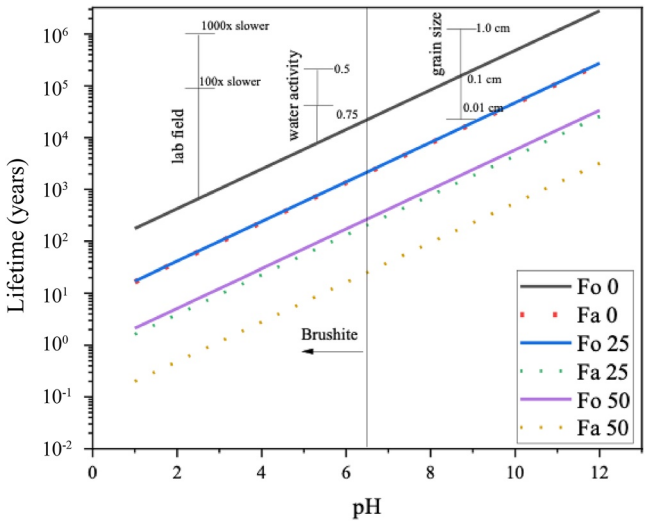

Figure 17. *Plot of mineral lifetimes for waters of varying pH*: For 1 mm diameter grains of forsterite (Fo) and fayalite (Fa) at temperatures of 0°C, 25°C, and 50°C at pH values ranging from 1 to 12 based on laboratory dissolution rates, also showing the effect of grain size, activity of water, and the lab-field effect. These types of calculations indicate the range of mineral lifetimes that can persist under different aqueous conditions.

that H-bearing mineral phases, such as glass within olivine-hosted melt inclusions and the minerals apatite and amphibole, can be used to constrain the abundances of H_2O in martian magmas and magmatic source regions when the hydrous phases can be measured with high-precision methods such as secondary ion mass spectrometry (Gross et al., 2013; McCubbin et al., 2010, 2012; Usui et al., 2012). Based on study of martian meteorites, the martian mantle is considered heterogeneous with respect to H_2O abundances (Black et al., 2022; Filiberto et al., 2016; McCubbin et al., 2016), and the prevailing hypothesis is that the martian mantle became progressively drier throughout its history (Balta & McSween, 2013).

Nearly all H_2O estimates from the martian interior come from samples with igneous crystallization ages ≤1.3 Ga. The Noachian ages of the ultramafic-mafic rocks in the collected Máaz and Séítah samples could help to establish additional estimates of the H_2O content of martian magmatic source region(s) at a time for which estimates do not currently exist for Mars. Both phosphates and olivine-hosted melt inclusions have been detected in rocks from Máaz and Séítah (Liu et al., 2022), providing at least two potential pathways to determine parental magmatic water abundances depending on the fidelity of any glass or phosphate phases in the returned samples. Additionally, H_2O abundances in nominally anhydrous minerals, such as the olivine and pyroxene observed in Máaz and Séítah, have been used to study the water contents of mantle source(s), for example, Peslier (2010). Similar types of volatile measurements in igneous feldspar have been used to estimate magmatic volatile abundances, for example, Mosenfelder et al. (2015). In combination with other trace element data, the parental magmatic H_2O abundances could be used to estimate H_2O abundances in the mantle source of Mars, similar to H_2O estimates in the interiors of other planetary bodies like the Moon and asteroid 4Vesta (e.g., Hauri et al., 2015; McCubbin et al., 2021; Saal et al., 2002; Simon et al., 2020).

5.2. Secondary Mineralogy and Geochemistry of Jezero Crater Floor Bedrock

5.2.1. Aqueous Activity Recorded by Jezero Crater Floor Rocks

Investigating the alteration minerals in the returned samples using laboratory-based analyses that have a higher spatial resolution and particular sensitivity to minor phases, trace elements, and isotopes will be key to answering additional questions related to the aqueous activity in both the Séítah and Máaz formations. A better understanding of the samples will allow constraints to be placed upon the past aqueous history of Jezero Crater floor including the timing of this activity in absolute terms as well as relative to the duration of lacustrine activity in Jezero Crater and the conditions of aqueous activity including temperature(s), fluid sources, as well as water distribution, cycling and storage during alteration episodes.

Evidence of aqueous alteration preserved in samples from the crater floor and investigated with high resolution laboratory techniques may indicate a number of generations of fluid alteration (Scheller et al., 2022; Tice et al., 2022). The primary ultramafic lithology of the Séítah formation appears to have undergone at least three separate episodes of alteration: (a) an earlier carbonation event followed by (b) a later brine event that partially filled the rocks with a complex mixture of sulfate and perchlorate minerals, finely crystalline and possibly amorphous silicates, and chloride minerals, and finally, (c) more recent surface oxidation. Given that olivine was identified as a primary phase in rocks of the Séítah formation (Figures 8 and 9) and that carbonate was detected as a secondary phase, the Fe- and Mg-phyllosilicates, carbonates, and possible amorphous silica may have resulted from an early stage of water-rock reaction (Brown et al., 2010). Deposition of salt phases is detailed below. The recent surface oxidation is apparent across Séítah (see Rice et al., 2022, this volume) and may be preserved as a weathering rind in the core samples. At least three separate episodes of alteration events are also identified in the primary mafic lithology of the Máaz formation: (a) formation of phyllosilicates, (b) salt precipitation including void filling, and (c) later oxidative weathering. The relative abundances and compositions of the secondary mineralogy in the Máaz formation appear to be distinct from the Séítah formation, and more variable.

The deposition of salt phases varies within the Maaz formation with most of the salts identified in the lower Máaz formation absent from the upper Máaz formation (i.e., Alfalfa). In contrast to the Séítah formation, the Fe- and Mg-phyllosilicates detected in the Máaz formation are likely to be serpentine group minerals and are found in association with fayalite and there is little to no associated carbonate.

Observations of salt minerals indicate the presence of saline solutions at some point in the geologic history of both the Séítah and Máaz units. Such solutions may have resulted from concentration by evaporation and these salt mineral phases may be the last evidence of water in Jezero Crater. If true, trace element and isotopic analyses of the salt minerals that appear more abundant in the lower Máaz members, possibly exemplified by those seen in the disaggregated Roubion target, will provide important constraints for the past aqueous environment(s) within Jezero Crater. Jezero samples generally have a Cl/S ratio (atom/atom) greater than 1.0; this is in contrast to martian global soils and almost all previous rocks and sediments analyzed on Mars which have Cl/S ~ 0.25 or lower (Yen et al., 2006). The predominance of chlorine over sulfur may indicate the progressive enrichment in residual brines of highly soluble chlorides and oxychlorines following sulfate deposition in the Jezero lacustrine environment. Mineral dissolution rates in the presence of brines have been shown to be much slower than in more dilute waters (Olsen et al., 2015; Pritchett et al., 2012; Steiner et al., 2016). Therefore, the rate of alteration of these rocks is dependent on the chemistry of the reacting fluid. Laboratory analyses that can help determine characteristics of the reacting fluids will help constrain the rate of alteration (Figure 17).

The record of distinct aqueous environments, such as brines versus dilute waters, can be interpreted by examining returned samples. Although we do not know for sure the volume of salt minerals in the Máaz cores, we anticipate that there is enough to study through the length of the core samples. The salt minerals were not a crust on the outcrop, as would be expected if they were a simple weathering rind. Rather, they were found in localized areas in the abraded patches, demonstrating that they are in the shallow subsurface of the rock. If the voids present in the sampled rocks formed by dissolution, estimates of the duration of the presence of liquid water can be calculated under different conditions using mineral lifetimes after Lasaga (1998) (Equation 1; Figure 17).

$$T = \frac{d}{Vr} \tag{1}$$

where t = the mineral lifetime in years, d = the grain diameter in m, V = the molar volume of the mineral, and r = the mineral dissolution rate. For the calculations presented in Figure 17, grain diameters were assumed to be 1 mm, the molar volume of forsterite and fayalite were taken from Robie et al. (1979), and dissolution rate laws of forsterite were taken from Bandstra and Brantley (2008), based on rates and published activation energies for olivine (Oelkers, 2001 and references therein). These results clearly show that olivine is expected to persist for different lengths of time under different pH and temperature conditions, as well as different conditions such as the activity of water, grain size, and the lab-field effect. Although the hydration state of salts may change during storage, the temperature constraints on the samples (temperatures required to be less than 60°C, and desired to be less than 40°C), will help in the preservation of potential sample constituents such as hydrated sulfates, zeolites, and amorphous material (iMOST, 2018).

5.2.2. Planetary Evolution of Aqueous Environments

The study of secondary mineral phases can also provide insights into planetary-scale processes and environments where rocks interact with water. The ability to interpret the geochemical processes and paleoenvironments of Jezero Crater from mineral assemblages and compositions may provide direct links to understanding similar rocks and mineral assemblages outside of the crater. Similarly, if investigation of orbital data and/or data from the extended mission were to reveal a stratigraphic relationship between units inside and outside of Jezero, the geochemical and environmental interpretations made from alteration phases in returned samples could help to constrain the broader geographic distribution of water.

The extent of interconnectivity of the hydrologic system at different points in martian history, including the potential for communication between surface and subsurface components of the system, remains an open question in planetary science (Carr & Head, 2010). Higher resolution investigation of the secondary mineral assemblages in the returned samples and the elemental composition of those minerals may reveal the presence of mineral phases and/or relationships between mineral phases that were not observable by the in situ instrumentation. This information will help address whether the samples experienced open or closed system alteration, cf. Clavé et al. (2022, this volume). Further constraining the fluid source and environment of alteration is key for under-

standing the potential habitability of any past water/rock systems. Sample measurements that would help constrain the near surface environmental conditions of Jezero Crater include: (a) Isotopic measurements of secondary minerals in returned samples to potentially distinguishing the source of reactant fluids (e.g., magmatic, groundwater, atmospheric). (b) Robust determination of alteration by atmospherically derived fluids would provide insights into the martian climate. (c) Measurement of alteration by groundwater to constrain the duration of the presence of groundwater and the temperatures at which alteration occurred, with implications for the potential habitability (Section 5.4) of subsurface water/rock systems. (d) Comparison of the aqueous alteration in returned samples with aqueous alteration observed in other locations on Mars (e.g., salts and veins observed with Mars Science Laboratory) to help shed light on the past global history of Mars.

5.3. Martian Atmospheric Composition

The relatively thin modern atmosphere of Mars evolved from one that was thick enough, in the past, to have supported liquid water at the surface. Its evolving elemental and isotopic compositions reflect the cumulative history of planetary outgassing, atmospheric escape, volatile-bearing mineral precipitation, and impacts (Lammer et al., 2013). There is an inherent scientific interest in returning an atmospheric sample (Jakosky et al., 2021; Swindle et al., 2022), as well as, ancient rocks that likely contain a record of this history, for example, Usui et al. (2012, 2015). The analysis of the martian gas will allow comparisons of noble gases (Xe, Kr, Ar, Ne) and light elements such as H, C, N, and O to the values of the elements in the solid samples of ancient Mars returned to Earth within the same cache collection, analyzed in martian meteorites, and studied by surface landers such as MSL (SAM in situ analysis). Although we have volatile measurements in recently (<1 Ma) formed impact glasses contained within martian meteorites, the gases sampled do not reflect unadulterated atmosphere–they include a combination of atmospheric, mantle, and spallation (in space) contributions (Bogard & Johnson, 1983; Bogard et al., 2001; Usui et al., 2012, 2015).

All sealed tubes contain a small amount of headspace gas, above the rock sample, captured inside the tube as the sample is sealed. During the attempt to seal the Roubion sample, no core was acquired, and the contents of this sealed tube thus consists only of martian air (with the exception of a few grains/dust remnants from the drilled rock). The estimated amount of martian atmosphere gas in the Roubion sample is: 4.9×10^{-6} mol, whereas for the other samples, with a full length (~6 cm) core, the number of moles may be approximately 1.0–1.3 $\times 10^{-6}$ mol (see Table 2, Text S1 and Figure S1 in Supporting Information S1). Although relatively small for many current analytical methods, future advancements in sample analyses are expected to maximize sample return science of gas volumes of this size.

5.4. Habitability and Astrobiological Potential

5.4.1. Organic Materials in Jezero Igneous Rocks

The structure, abundances, distribution, and isotopic composition of organic compounds in samples returned from Jezero Crater will be examined with the goal of understanding the martian carbon cycle and assessing the possibility of a past martian biosphere. Organic compounds have been detected in various martian meteorites (McKay et al., 1996; Sephton et al., 2002; Steele et al., 2012, 2016, 2022) and materials and lithologies from Gale Crater that were analyzed in situ (Eigenbrode et al., 2018; Freissinet et al., 2015; Millan et al., 2022). Although not considered the prime astrobiology targets of the mission, analyses of Jezero Crater floor samples may nonetheless enable the reconstruction of abiotic, prebiotic or biological processes that either synthesized the organics in situ or delivered them to the samples from endogenous (i.e., martian) or exogenous (i.e., asteroids and comets) sources (Flynn, 1996).

The collected cores, like igneous rocks studied from Earth, can preserve organic compounds primarily in the zones altered by fluids (e.g., Klein et al., 2015), or as minute fluid inclusions that contain methane with a high-temperature origin (Etiope & Whiticar, 2019; Klein et al., 2019; Reeves & Fiebig, 2020; Zhang et al., 2021). The crater floor samples have measurable abundances of organics: deep UV fluorescence measured by the SHERLOC instrument shows evidence of possible single- and double-ring aromatic organic compounds (Farley et al., 2022; Scheller et al., 2022). Multiple possible detections of aromatic organic materials have also been made by SHERLOC deep-UV Raman spectroscopy. Overall, Raman and fluorescence spectra revealed very low abundances of organics, where detected, comparable to those detected in Gale Crater, and often in association with salts and grain boundaries, suggesting the emplacement of organics during diagenetic episodes (see Corpolongo et al., 2023; Murphy et al., 2022; Sharma, Beegle, et al., 2022; Sharma, Roppel, et al., 2022). These

results provide insight into the distribution of minor/trace amounts of organics, but more robust interpretations based on mapping the distribution and characterizing the composition of organic matter present in either igneous or alteration phases of the samples from Jezero Crater floor will require techniques with nano- to micrometer scale spatial resolution and the ability to detect and determine the chemistry and structure of organic molecules. This highlights the need for return of these samples to interrogate the molecular structure of these compounds within, thereby understanding their formation, alteration, and degradation histories. Laboratory analyses of these samples and collected witness tubes could also help to establish the background content of organic material at the martian surface and in the subsurface. Such samples are required for comparisons of processes that have cycled carbon in the biosphere, hydrosphere and geosphere on Earth and any counterparts on Mars.

5.4.2. Astrobiological Potential of Observed Salts

Phanerozoic salts such as sulfate and chloride on Earth can preserve organic compounds and fossils (e.g., Benison & Bowen, 2006). They can also reliably archive characteristics of the paleo-depositional environment, as evidenced by the more than one-billion-years-old Paleoproterozoic sulfate deposits that have been used to probe seawater chemistry (e.g., Blattler et al., 2018). Salts, including those implicated in prebiotic surface-based chemical reactions on Earth (e.g., Benner et al., 2018), are typically found in large scale evaporite deposits that have not, thus far, been detected in Jezero Crater. Salts in the returned samples from Séítah (namely from Issole, the Robine and/or Malay cores) should be examined for the presence of fluid inclusions and organic matter. The potential of salts to record past fluid chemistry and preserve inclusions also motivates the search for more extensive salt deposits in the delta stratigraphy and areas outside of the Jezero Crater floor.

5.4.3. Carbonated Olivine, Source of H_2, and Energy for Life

Olivine carbonation-serpentinization processes occurring where water interacts with igneous minerals and changes the redox state of iron to generate hydrogen occur on Earth and are thought to be common throughout the Solar System, including Mars (Steele et al., 2022). These processes are indicated by in situ observations of Séítah rocks. Molecular hydrogen produced by these reactions can serve as an electron donor for microbial metabolic activities such as sulfate reduction and methanogenesis (Madigan et al., 2022). Exploration for environments and samples that were extensively altered in this manner will continue as Perseverance traverses the marginal deposits and portions of the delta that contain carbonate.

5.5. Geochronology and Paleomagnetism Recorded in Altered Igneous Rocks

Many of the science questions at Jezero Crater involve sequences of events and temporal evolutions over geologic timescales; these can be addressed with geochronology and paleomagnetic observations of returned samples of igneous rocks and their alteration products. For example, What is the history of igneous differentiation on Mars? What was the timing of aqueous activity in the Jezero Crater region? What is the history of the magnetic field on Mars, and how does the occurrence of a dynamo correlate with our knowledge of the martian atmosphere through time? What is the erosional and exhumation history of Nili Planum? What is the erosional history of the Jezero delta since its deposition?

5.5.1. Timing of Igneous Activity

The genetic relationship between Máaz and Séítah and between both units and the deltaic rocks is uncertain. The most straightforward interpretation is one where Séítah represents the oldest exposed crater floor unit. An alternate interpretation, consistent with its coarse-grained texture, is that Séítah represents an igneous sill or laccolith (Farley et al., 2022; Liu et al., 2022). In this case, Séítah could be younger than overlying Máaz, and injected into or below it. Whether an intrusion or slowly cooled lava, it is also unclear from field observations whether the contact between Séítah and Máaz represents a disconformity, or instead whether Máaz is a cogenetic, less mafic complement to a more mafic Séítah (Farley et al., 2022; Wiens et al., 2022). Furthermore, it is unknown whether Máaz and Séítah underlie or embay/intrude the delta. These issues can be directly tested by quantifying the crystallization ages of each formation. Since both formations are very likely to have crystallized after Jezero Crater formed, their crystallization ages will also provide a lower bound on the age of Jezero Crater itself.

The igneous rock samples collected from the Jezero Crater floor are each well-suited for geochronology and can therefore help to establish the absolute and relative timing of igneous activity in the region. Interpreted as

primary igneous rocks, these samples each contain a diversity of minerals and grain sizes (Farley et al., 2022; Liu et al., 2022; Wiens et al., 2022); including pyroxene, plagioclase, and likely accessory minerals that can be used to quantify the timing of their crystallization using parent-daughter systems such as K-Ar and U-Th-Pb. In addition, these same phases should enable thermochronology studies, for example, $^{40}Ar/^{39}Ar$ and (U-Th)/He), for quantitative constraints on post-crystallization cooling rates and exhumation history, which can inform models of their original emplacement depths.

5.5.2. Timing of Aqueous History

The temperatures and pressures at the surface of Mars today preclude the stability of liquid water for all but brief durations, yet there is clear evidence that liquid water has substantially modified the surface topography of Mars in the geologic past (e.g., Carr & Head, 2010), including the inlet and outlet channels and delta sedimentary deposits observed at Jezero Crater (e.g., Mangold et al., 2021). Because extended durations of liquid water stability are understood to be a requirement of the emergence of biological activity (Westall & Brack, 2018), some of the most important science questions at Jezero Crater relate to when, and for how long, liquid water was present: When were the delta sediments deposited, and thus, when was a lake present? How many sediment-delivery and lake-filling events occurred? Over what duration was the delta sediment deposited? In addition to these questions on the geomorphic evolution of the Jezero lake and delta, the timing of the secondary aqueous activity that appears to have modified the igneous rocks exposed at the crater floor will be addressed. Science questions include: When and over what durations did these aqueous alteration occur? Did chemical alteration of crater floor rocks occur when, or shortly after, the lake was present, or much later? Could the local conditions involving aqueous activity and rock alteration have supported biological activity?

Quantifying the timing, duration(s) and frequency of aqueous activity within Jezero Crater are among the most important objectives to be addressed with return sample science. These directly relate to questions on when, and for how long, environmental conditions for prebiotic activity, and potentially microbial life itself, may have once existed at Jezero. The samples collected from Séítah and Máaz can be used to quantify the timing of aqueous activity in two distinct ways: (a) by providing bounds on delta deposition timing, thus the timing of Jezero lake filling event(s) and (b) via geochronology applied to secondary chemical alteration phases present in the samples, such as oxides and carbonates.

Regional observations from orbit (Goudge et al., 2015) and rover observations indicate that the Séítah formation most likely underlies the main Jezero delta. The occurrence of Séítah rocks between the main delta and its remnant Kodiak, and a lack of obvious high-temperature alteration or related geomorphic expressions at the contact/zone between Séítah and the delta front support the interpretation that Séítah crystallization predated the delta deposition. If so, the crystallization age of Séítah will provide an upper bound on the timing of deposition of the main delta. Further, this assumed stratigraphic relationship can be tested using returned sample analyses of delta sediments collected near the contact, that is, high-temperature contact alteration/metamorphism, partially reset parent-daughter systems (e.g., K-Ar) in detrital phases, and by paleomagnetic "conglomerate" tests.

The stratigraphic relationship between Máaz and the delta is presently less clear (e.g., Farley et al., 2022; Wiens et al., 2022). If Máaz is shown to also occur below the delta, its crystallization age would also provide an upper bound on delta deposition timing; however, if Máaz formed much later than Séítah, it possibly embayed a pre-existing delta, in which case its crystallization timing would provide a lower bound on delta emplacement. Observations of detrital delta sediments near Máaz can be used to test these competing relationships by seeking evidence of high-temperature alteration and/or partially reset geochronology systems near the contact. If Máaz emplacement occurred after delta deposition, we would expect thermochronological observations of proximal detrital sediments to be concordant with, or trending towards, the timing of Máaz crystallization, as determined by methods listed above in Section 5.5.1.

Geochronology applied to secondary phases (e.g., Fe-oxides, carbonates, phyllosilicates) interpreted as post-crystallization alteration products (Scheller et al., 2022; Tice et al., 2022), could quantify the timing of the alteration conditions. Laboratory applications of geochronology to such secondary alteration phases has been successful, but also involves complexities of polymineralic materials and open system behavior (e.g., Shuster et al., 2005, 2012). However, if the alteration conditions involved liquid water, such geochronology could quantify the timing, and possibly duration, of late-stage aqueous activity at the Jezero floor. For example, geochronol-

ogy using returned samples could establish whether that alteration occurred shortly after igneous emplacement (in which case, we expect concordance between secondary and primary phase crystallization timing), or much later than the original Séítah and Máaz crystallization, perhaps associated with water delivery during delta emplacement.

5.5.3. Mars Cratering Chronology Calibration

With the exception of in situ geochronology conducted at Gale Crater (Farley et al., 2014), all absolute knowledge of the timing of geologic events and features observed at the surface of Mars depends on impact cratering chronology functions that have been empirically determined from observation of the lunar surface and geochronology of returned Apollo samples, then extrapolated to Mars. This extrapolation depends critically on several assumptions about: (a) the relative fluxes of bolides to Mars and the Moon, (b) the relative crater diameters formed on Mars and the Moon for a given bolide size, and (c) that the time dependency of martian cratering history relative to the Moon.

Samples collected from Jezero crater can help to test these important assumptions and possibly provide opportunities to empirically determine the assumed parameters used for Moon-Mars extrapolations. Such tests will be important for all quantitative applications of the martian cratering chronology across the entire planet. However, such tests require knowledge of how long a particular surface was exposed to crater-forming impact events; this will not generally be equal to the time since an igneous rock crystallized on a planetary surface that has experienced active geomorphic processes. Indeed, the spatial distribution of crater densities observed at the Jezero crater floor clearly indicates that the igneous rocks have also experienced a complex exhumation history, both spatially and temporally, with lowest densities observed near the delta, highest to the NE of the landing site (Quantin-Nataf et al., 2021). Any tests or calibrations of the crater chronology function will require knowledge of when, and at what rate, this post-crystallization exhumation occurred, and more generally, how a rock crystallization age can be related to the duration of crater accumulation at a particular surface.

As the highest stratigraphic expression of the crater floor rocks observed by Perseverance, the Máaz formation (i.e., Ch'ał member) is most closely associated with crater densities observed across the crater floor. Thus, the timing of Máaz crystallization, which should be readily determinable using numerous methods of geochronology (e.g., U-Pb, $^{40}Ar/^{39}Ar$) will provide an important upper bound on the duration of crater accumulation, assuming the rocks exposed across the crater floor, off to the East of the region explored by Perseverance, are equivalent. However, since the crater floor has likely experienced post-crystallization exhumation, sedimentary burial, and subsequent exhumation, the quantitative relationship between the Máaz crystallization age and a crater accumulation duration is non-trivial; these two timescales may differ by orders of magnitude. Because the highest crater densities on the Jezero Crater floor, that is, the mapped Cf-Fr unit (cf. Stack et al., 2020), occur farthest from the delta (near Hartwell Crater; Quantin-Nataf et al., 2021), it is likely that this surface experienced the least burial and subsequent exhumation since crystallization. Thus, assuming the rocks exposed near Hartwell Crater are equivalent to upper Máaz, use of the crater density and size distribution observed near Hartwell with the crystallization age of Máaz would provide quantitative constraints on two of the key assumptions in the Mars cratering chronology, specifically the ratios of the bolide fluxes and crater diameters, respectively, between Mars and the Moon. However, due to complexities and uncertainty on the exhumation history and rates of aeolian processes that have modified the surface through time, such an analysis using the Máaz crystallization timing would provide lower bounds on these ratios. In addition, if the Séítah rocks are shown to be the equivalent of the regional olivine carbonate (Brown et al., 2020; Goudge et al., 2015; Mandon et al., 2020), other potential cratering chronology constraints may be possible using crater densities on surfaces outside Jezero Crater.

5.5.4. Dynamo History

Mars today does not have a dynamo (a global magnetic field inductively generated by convection of its metallic core); however, the discovery of remanent magnetization in the martian crust by the Mars Global Surveyor and the Mars Atmosphere and Volatile Evolution mission spacecraft and in martian meteorites from laboratory measurements indicate that Mars once had a dynamo early in its history. Crater counting age estimates of surfaces of the magnetized crust (Vervelidou et al., 2017) and $^{40}Ar/^{39}Ar$ ages of the martian meteorite Allan Hills 84001 (Weiss et al., 2004) suggest that a dynamo may have been present from the pre-Noachian until the Early Hesperian. At present, however, the intensity of the dynamo is essentially unconstrained and its lifetime uncertain by at least hundreds of Ma.

Determining the history and nature of the dynamo is important for several reasons. First, a strong dynamo may have prevented atmospheric loss, such that its decline may have played a central role in the transition from warmer and wetter conditions, that is, possibly more habitable conditions in the Noachian, eventually reaching the cold and dry conditions of today. Second, the dynamo history reflects the thermal evolution of the planetary interior including the crystallization of the core and mantle convection. Finally, the direction of the magnetic field as recorded by rocks can be used to test the hypothesis that Mars experienced plate tectonics and true polar wander, and to determine whether its dipole component underwent reversals. As such, establishing the history of the intensity and direction of the magnetic field through combined geochronology and paleomagnetic datasets using oriented rock cores from the Jezero Crater is a key goal of future returned sample studies.

The science objectives for paleomagnetic investigations require samples containing sufficiently abundant ferromagnetic minerals that can acquire remanent magnetization that is stable over billions of years. Laboratory analyses of martian meteorites (Gattacceca et al., 2014), and in situ compositional (Wiens et al., 2022), mineralogical (Morris et al., 2006), and magnetic properties measurements (Madsen et al., 2009) suggest that the mafic and ultramafic lithologies of Máaz and Séítah likely contain abundant minerals, for example, magnetite, that should be capable of recording stable paleomagnetic records. If all these samples retain primary igneous ferromagnetic oxides, this will enable paleointensity studies. Furthermore, the six cores taken from likely in-place bedrock (but even potentially the two collected at Rochette that appear to have small likely quantifiable displacement), can be used for paleodirectional studies of the magnetic field. Given that the 6 (+2?) samples were collected from bedrock with varying attitudes (with surface normals ranging over ∼15°), the relative age of their remanent magnetization relative to bedrock tilting could be established using a fold test: if the magnetization directions of samples of similar formation age are more (or less) clustered after tilt correction, this would be consistent with the hypothesis that their magnetization predates (or postdates) tilting.

6. Summary

The Perseverance rover recently completed a traverse of the floor of Jezero Crater, Mars, characterizing and collecting samples from the Séítah and Máaz formations. Eight rock samples and one atmospheric sample were collected and stored in the rover. Accompanying in situ science observations using the rover's onboard payload offer information about the composition, mineralogy, and texture of the sampled rocks. These rocks represent the first samples from Mars with known and characterized geologic context, the first collected with potential to be returned to Earth for laboratory analysis, and the first samples from rock outcrop collected on another planet.

The suite of the Séítah and Máaz formation samples collected by Perseverance represents a paradigm-shifting outcome of the Perseverance Crater Floor Campaign that will address several important objectives of the MSR Campaign, including magmatic history, water-rock interactions, environmental conduciveness to life, and isotopic ages for geologic events. Perseverance is now beginning its exploration of the delta facies and is expecting to make a cache that includes a representative set of Jezero Crater floor samples at the Three Forks depot by early 2023.

Data Availability Statement

This contribution includes a variety of geospatially located data, including context far-field and workspace images (Mastcam-Z, Figures 3–7; Figures S2–S10 in Supporting Information S1 color anaglyphs, Figure S11 in Supporting Information S1 context mapping, NASA PDS https://doi.org/10.17189/q3ts-c749), subsurface radar data (RIMFAX, Figures 3–7, NASA PDS https://doi.org/10.17189/1522644), rock target close up images (WATSON, Figures 8, 9, 12, and 13; Table S1 in Supporting Information S1, NASA PDS https://doi.org/10.17189/1522643), sample core images (CacheCam, Figure 2, NASA PDS https://doi.org/10.17189/q3ts-c749), major element compositional laser ionization breakdown spectroscopy (SuperCam-LIBS, Figure 11, Tables S2, S3, S4, S5, and S6, NASA PDS https://doi.org/10.17189/1522646), X-ray fluorescence measurements that allow compositional mapping (PIXL, Figures 9, 10, and 13; Figures S12–S16 in Supporting Information S1 distorted WATSON ACIs merged with X-ray fluorescence maps of SiO_2, Al_2O_3, and SO_3 abundance and distribution; and bulk sum analyses, Table 4, NASA PDS https://doi.org/10.17189/1522645), hydration and alteration phase identification by visible and infrared spectroscopy (SuperCam-VISIR, Figure 14, NASA PDS https://doi.org/10.17189/1522646), mineral and organic compound identification and mapping

(SHERLOC-Raman/Fluorescence, Figure 15, NASA PDS https://doi.org/10.17189/1522643), and atmospheric conditions at the time of sampling Roubion, the atmospheric sample (MEDA, Figure S1 in Supporting Information S1, NASA PDS https://doi.org/10.17189/1522849). All of the information and data presented in this contribution are included in the main text and associated Supporting Information S1. Rover instrument and calibration details can be found in the instrument payload citations included in the primary text (and references therein). Operational details, initial sample reports, and all in situ payload measurements are uploaded to NASA Planetary Data System.

Acknowledgments
The authors thank editor Bradley Thomson and reviewers Nicole E. Moore, Jade Star Lackey, and Allan Treiman for their many constructive comments. We are grateful to the entire Mars 2020 team. The Mars 2020 mission and Return Sample Science Participating Scientist Program are supported by NASA Mars Exploration Program. K.H.-L. acknowledges a UK Space Agency Aurora Research Fellowship (Grant ST/V00560X/1). M.-P.Z. is supported by Grant PID2019-104205GB-C21 funded by MCIN/AEI/10.13039/501100011033. J.F.B. is supported by NASA/JPL, Grant 1511125. A.G.F is supported by European Research Council, Grant 818602; F.G. is supported by INTA internal project DAXE (SIGS22001) and Italian Space Agency (ASI) Grant ASI/INAF n. 2017-48-H-0. C.D.K.H. and M.S. are supported by Canadian Space Agency Mars 2020 Participating Scientist Grants. S.S. is supported by Swedish National Space Agency (Contracts 137/19 and 2021-00092). A.U. is supported by NASA Mars 2020 Participating Scientist program 80NSSC21K0330 (AU). S.V. is supported by NASA Mars 2020 Participating Scientist Program (Grant 80NSSC21K0328). A.J.W. is supported by NASA Mars 2020 Participating Scientist Program (Grant 80NSSC21K0332).

References

Allwood, A. C., Lawrence, A., Wade, M. C., Foote, W. T. E., Hurowitz, J. A., Battel, S., et al. (2020). PIXL: Planetary instrument for X-ray lithochemistry. *Space Science Reviews*, *216*(8), 134. https://doi.org/10.1007/s11214-020-00767-7

Alwmark, S., Horgan, B., Udry, A., Bechtold, A., Fagents, S., Ravanis, E., et al. (2023). Diverse lava flow morphologies in the stratigraphy of the Jezero Crater Floor. *Journal of Geophysical Research: Planets*, e2022JE007446. https://doi.org/10.1029/2022JE007446

Antonelli, M. A., & Simon, J. I. (2020). Calcium isotopes in high-temperature terrestrial processes. *Chemical Geology*, *548*, 119651. https://doi.org/10.1016/j.chemgeo.2020.119651

Armytage, R. M. G., Debaille, V., Brandon, A. D., & Agee, C. B. (2018). A complex history of silicate differentiation of Mars from Nd and Hf isotopes in crustal breccia NWA 7034. *Earth and Planetary Science Letters*, *502*, 274–283. https://doi.org/10.1016/j.epsl.2018.08.013

Balta, J. B., & McSween, H. Y. (2013). Water and the composition of Martian magmas. *Geology*, *41*(10), 1115–1118. https://doi.org/10.1130/g34714.1

Bandstra, J. Z., & Brantley, S. L. (2008). Data fitting techniques with applications to mineral dissolution kinetics. In S. L. Brantley, J. D. Kubicki, & A. F. White (Eds.), *Kinetics of water-rock interaction* (pp. 211–257).

Barnes, J. J., McCubbin, F. M., Santos, A. R., Day, J. M. D., Boyce, J. W., Schwenzer, S. P., et al. (2020). Multiple early-formed water reservoirs in the interior of Mars. *Nature Geoscience*, *13*(4), 260–264. https://doi.org/10.1038/s41561-020-0552-y

Beaty, D. W., Grady, M. M., McSween, H. Y., Sefton-Nash, E., Carrier, B. L., Altieri, F., et al. (2019). The potential science and engineering value of samples delivered to Earth by Mars sample return. *Meteoritics & Planetary Science*, *54*, S3–S152. https://doi.org/10.1111/maps.13242

Bell, J. F., Maki, J. N., Alwmark, S., Ehlmann, B. L., Fagents, S. A., Grotzinger, J. P., et al. (2022). Geological and meteorological imaging results from the Mars 2020 perseverance rover in Jezero Crater. *Science Advances*, *8*(47), eabo4856. https://doi.org/10.1126/sciadv.abo4856

Bell, J. F., Maki, J. N., Mehall, G. L., Ravine, M. A., Caplinger, M. A., Bailey, Z. J., et al. (2021). The Mars 2020 perseverance rover mast camera zoom (Mastcam-Z) multispectral, stereoscopic imaging investigation. *Space Science Reviews*, *217*(1), 24. https://doi.org/10.1007/s11214-020-00755-x

Bellucci, J. J., Whitehouse, M. J., John, T., Nemchin, A. A., Snape, J. F., Bland, P. A., & Benedix, G. X. (2017). Halogen and Cl isotopic systematics in Martian phosphates: Implications for the Cl cycle and surface halogen reservoirs on Mars. *Earth and Planetary Science Letters*, *458*, 192–202. https://doi.org/10.1016/j.epsl.2016.10.028

Benison, K. C., & Bowen, B. B. (2006). Acid saline lake systems give clues about past environments and the search for life on Mars. *Icarus*, *183*(1), 225–229. https://doi.org/10.1016/j.icarus.2006.02.018

Benner, S. A., Kim, H.-J., & Biondi, E. (2018). Mineral-organic interactions in prebiotic synthesis. In C. Menor-Salván (Ed.), *Prebiotic chemistry and chemical evolution of nucleic acids, nucleic acids and molecular biology* (Vol. 35). Springer. https://doi.org/10.1007/978-3-319-93584-3_3

Beyssac, O., Forni, O., Cousin, A., Udry, A., Kah, L.C., Mandon, L., et al. (2023). Petrological traverse of the olivine cumulate Séítah formation at Jezero crater, Mars: A perspective from SuperCam onboard Perseverance. *Journal of Geophysical Research: Planets*, *128*, e2022JE007638. https://doi.org/10.1029/2022JE007638

Bhartia, R., Beegle, L. W., DeFlores, L., Abbey, W., Hollis, J. R., Uckert, K., et al. (2021). Perseverance's scanning habitable environments with Raman and luminescence for organics and chemicals (SHERLOC) investigation. *Space Science Reviews*, *217*(4), 58. https://doi.org/10.1007/s11214-021-00812-z

Bhartia, R., Hug, W. F., Salas, E. C., Reid, R. D., Sijapati, K. K., Tsapin, A., et al. (2008). Classification of organic and biological materials with deep ultraviolet excitation. *Applied Spectroscopy*, *62*(10), 1070–1077. https://doi.org/10.1366/00037020878604912

Black, B. A., Manga, M., Ojha, L., Longpre, M.-A., Karunatillake, S., & Hlinka, L. (2022). The history of water in Martian magmas from thorium maps. *Geophysical Research Letters*, *49*(11), e2022GL098061. https://doi.org/10.1029/2022GL098061

Blattler, C. L., Claire, M. W., Prave, A. R., Kirsimae, K., Higgins, J. A., Medvedev, P. V., et al. (2018). Two-billion-year-old evaporties capture Earth's great oxidation. *Science*, *360*(6386), 320–323. https://doi.org/10.1126/science.aar268

Blichert-Toft, J., Gleason, J. D., Telouk, P., & Albarede, F. (1999). The Lu-Hf isotope geochemistry of shergottites and the evolution of the Martian mantle-crust system. *Earth and Planetary Science Letters*, *173*(1–2), 25–39. https://doi.org/10.1016/s0012-821x(99)00222-8

Bogard, D. D., Clayton, R. N., Marti, K., Owen, T., & Turner, G. (2001). Martian volatiles: Isotopic composition, origin, and evolution. In R. Kallenbach, J. Geiss, & W. K. Hartmann (Eds.), *Chronology and evolution of Mars, space sciences series of ISSI* (Vol. 12). Springer. https://doi.org/10.1007/978-94-017-1035-0_17

Bogard, D. D., & Johnson, P. (1983). Martian gases in an Antarctic meteorite? *Science*, *221*(4611), 651–654. https://doi.org/10.1126/science.221.4611.651

Borg, L. E., Brennecka, G. A., & Symes, S. J. K. (2016). Accretion timescale and impact history of Mars deduced from the isotopic systematics of Martian meteorites. *Geochimica et Cosmochimica Acta*, *175*, 150–167. https://doi.org/10.1016/j.gca.2015.12.002

Borg, L. E., Nyquist, L. E., Taylor, L. A., Wiesmann, H., & Shih, C.-Y. (1997). Constraints on Martian differentiation processes from Rb-Sr and Sm-Nd isotopic analyses of the basaltic shergottite QUE 94201. *Geochimica et Cosmochimica Acta*, *61*(22), 4915–4931. https://doi.org/10.1016/s0016-7037(97)00276-7

Borg, L. E., Nyquist, L. E., Wiesmann, H., Shih, C.-Y., & Reese, Y. (2003). The age of Dar al Gani 478 and the differentiation history of the Martian meteorites inferred from their radiogenic isotopic systematics. *Geochimica et Comochimica Acta*, *67*(18), 3519–3536. https://doi.org/10.1016/s0016-7037(03)00094-2

Bosak, T., Moore, K. R., Gong, J., & Grotzinger, J. P. (2021). Searching for biosignatures in sedimentary rocks from early Earth and Mars. *Nature Reviews Earth & Environment*, *2*(7), 490–506. https://doi.org/10.1038/s43017-021-00169-5

Breuer, D., Plesa, A.-C., Tosi, N., & Grott, M. (2016). Water in the Martian interior—The geodynamical perspective. *Meteoritics & Planetary Science*, *51*(11), 1959–1992. https://doi.org/10.1111/maps.12727

Brown, A. J., Hook, S. J., Baldridge, A. M., Crowley, J. K., Bridges, N. T., Thomson, B. J., et al. (2010). Hydrothermal formation of clay-carbonate alteration assemblages in the Nili Fossae region of Mars. *Earth and Planetary Science Letters*, *297*(1–2), 174–182. https://doi.org/10.1016/j.epsl.2010.06.018

Brown, A. J., Viviano, C. E., & Goudge, T. A. (2020). Olivine-carbonate mineralogy of the Jezero Crater region. *Journal of Geophysical Research: Planets*, *125*(3), e2019JE006011. https://doi.org/10.1029/2019JE006011

Carr, M. H., & Head, J. W., III. (2010). Geologic history of Mars. *Earth and Planetary Science Letters*, *294*(3–4), 185–203. https://doi.org/10.1016/j.epsl.2009.06.042

Clavé, E., Benzerara, K., Beck, P., Meslin, P.-Y., Beyssac, O., Forni, O., et al. (2022). Carbonate detection with SuperCam in the Jezero Crater, Mars. In *Proceedings of the 53rd lunar and planetary science conference (LPSC)*. Lunar and Planetary Institute, United States of America.

Clenet, H., Pinet, P., Ceuleneer, G., Daydou, Y., Heuripeau, F., Rosemberg, C., et al. (2013). A systematic mapping procedure based on the Modified Gaussian Model to characterize magmatic units from olivine/pyroxenes mixtures: Application to the Syrtis Major volcanic shield on Mars. *Journal of Geophysical Research: Planets*, *118*(8), 1632–1655. https://doi.org/10.1002/jgre.20112

Corpolongo, A., Jakubek, R. S., Abbey, W., Asher, S. A., Baker, D., Beegle, L. W., et al. (2023). SHERLOC Raman mineral detections of the Mars 2020 Crater Floor campaign. *Journal of Geophysical Research: Planets*, e2022JE007455. https://doi.org/10.1029/2022JE007455

Crumpler, L. S., Horgan, B. H. N., Simon, J. I., Stack, K. M., Alwmark, S., Gilles, D., et al. (2023). In situ geologic context mapping transect on the floor of Jezero crater from Mars 2020 Perseverance rover observations. *Journal of Geophysical Research: Planets*, *128*, e2022JE007444. https://doi.org/10.1029/2022JE007444

Dauphas, N., & Pourmand, A. (2011). Hf-W-Th evidence for rapid growth of Mars and its status as a planetary embryo. *Nature*, *473*(7348), 489–492. https://doi.org/10.1038/nature10077

Day, J. M. D., Brandon, A. D., & Walker, R. J. (2016). Highly siderophile elements in Earth, Mars, the Moon, and asteroids. *Reviews in Mineralogy and Geochemistry*, *81*(1), 161–238. https://doi.org/10.2138/rmg.2016.81.04

Debaille, V., Brandon, A. D., Yin, Q. Z., & Jacobsen, B. (2007). Coupled ^{142}Nd-^{143}Nd evidence for a protracted magma ocean in Mars. *Nature*, *450*(7169), 525–528. https://doi.org/10.1038/nature06317

Debaille, V., O'Nell, C., Brandon, A. D., Haenecour, P., Yin, Q.-Y., Mattielli, N., & Trieman, A. H. (2013). Stagnant-lid tectonics in early Earth revealed by ^{142}Nd variations in late Archean rocks. *Earth and Planetary Science Letters*, *373*, 83–92. https://doi.org/10.1016/j.epsl.2013.04.016

Dreibus, G., & Wanke, H. (1985). Mars, a volatile-rich planet. *Meteoritics*, *20*(2), 365–381.

Ehlmann, B. L., Mustard, J. F., Fassett, C. I., Schon, S. C., Head, J. W., III, Des Marais, D. J., et al. (2008). Clay minerals in delta deposits and organic preservation potential on Mars. *Nature Geoscience*, *1*(6), 355–358. https://doi.org/10.1038/ngeo207

Eigenbrode, J. L., Summons, R. E., Steele, A., Freissinet, C., Millan, M., Navarro-Gonazlez, R., et al. (2018). Organic matter preserved in 3-billion-year-old mudstones at Gale Crater, Mars. *Science*, *360*(6393), 1096–1101. https://doi.org/10.1126/science.aas918

Elkins-Tanton, L. T. (2008). Linked magma ocean solidification and atmospheric growth for Earth and Mars. *Earth and Planetary Science Letters*, *271*(1–4), 181–191. https://doi.org/10.1016/j.epsl.2008.03.062

Etiope, G., & Whiticar, M. J. (2019). Abiotic methane in continental ultramafic rock systems: Towards a genetic model. *Applied Geochemistry*, *102*, 139–152. https://doi.org/10.1016/j.apgeochem.2019.01.012

Farley, K. A., Malespin, C., Mahaffy, P., Grotzinger, J. P., Vasconcelos, P. M., Milliken, R. E., et al. (2014). In situ radiometric and exposure age dating of the Martian surface. *Science*, *343*(6169), 1247166. https://doi.org/10.1126/science.1247166

Farley, K. A., Stack, K. M., Shuster, D. L., Horgan, B. H. N., Hurowitz, J. A., Tarnas, J. D., et al. (2022). Aqueously altered igneous rocks on the floor of Jezero Crater, Mars. *Science*, *377*(6614), eabo2196. https://doi.org/10.1126/science.abo2196

Farley, K. A., Williford, K. H., Stack, K. M., Bhartia, R., Chen, A., dela Torre, M., et al. (2020). Mars 2020 mission overview. *Space Science Reviews*, *216*(8), 142. https://doi.org/10.1007/s11214-020-00762-y

Fassett, C. I., & Head, J. W., III. (2008). The timing of Martian valley network activity: Constraints from buffered crater counting. *Icarus*, *195*(1), 61–89. https://doi.org/10.1016/j.icarus.2007.12.009

Filiberto, J., Gross, J., & McCubbin, F. M. (2016). Constraints on the water, chlorine, and fluorine content of the Martian mantle. *Meteoritics & Planetary Science*, *51*(11), 2023–2035. https://doi.org/10.1111/maps.12624

Flynn, G. J. (1996). The delivery of organic matter from asteroids and comets to the early surface of Mars. In H. Rickman & M. J. Valtonen (Eds.), *Worlds in interaction: Small bodies and planets of the solar system*. Springer. https://doi.org/10.1007/978-94-009-0209-1_58

Freissinet, C., Glavin, D. P., Mahaffy, P. R., Miller, K. E., Eigenbrode, J. L., Summons, R. E., et al. (2015). Organic molecules in the sheepbed mudstone, gale crater, mars. *Journal of Geophysical Research: Planets*, *120*, 495–514. https://doi.org/10.1002/2014JE004737

Garczynski, B. J., Bell, J. F., III, Horgan, B. H. N., Johnson, J. R., Rice, M. S., Vaughan, A., et al. (2022). Perseverance and the purple coating: A mastcam-Z multispectral story. In *Proceedings of the 53rd lunar and planetary science conference (LPSC)*. Lunar and Planetary Institute, United States of America.

Gattacceca, J., Rochette, P., Scorzelli, R. B., Munayco, P., Agee, C., Quesnel, Y., et al. (2014). Martian meteorites and Martian magnetic anomalies: A new perspective from NWA 7034. *Geophysical Research Letters*, *41*(14), 4859–4864. https://doi.org/10.1002/2014gl060464

Goderis, S., Brandon, A. D., Mayer, B., & Humayun, M. (2016). Ancient impactor components preserved and reworked in Martian regolith breccia Northwest Africa 7034. *Geochimica et Cosmochimica Acta*, *191*, 203–215. https://doi.org/10.1016/j.gca.2016.07.024

Goudge, T. A., Head, J. W., Mustard, J. F., & Fassett, C. I. (2012). An analysis of open-basin lake deposits on Mars: Evidence for the nature of associated lacustrine deposits and post-lacustrine modification processes. *Icarus*, *219*(1), 211–229. https://doi.org/10.1016/j.icarus.2012.02.027

Goudge, T. A., Mustard, J. F., Head, J. W., Fassett, C. I., & Wiseman, S. M. (2015). Assessing the mineralogy of the watershed and fan deposits of the Jezero Crater paleolake system, Mars. *Journal of Geophysical Research: Planets*, *120*(4), 775–808. https://doi.org/10.1002/2014JE004782

Gross, J., Filiberto, J., & Bell, A. S. (2013). Water in the Martian interior: Evidence for terrestrial MORB mantle-like volatile contents from hydroxyl-rich apatite in olivine–phyric shergottite NWA 6234. *Earth and Planetary Science Letters*, *369–370*, 120–128. https://doi.org/10.1016/j.epsl.2013.03.016

Haltigin, T. H., Hauber, E., Kminek, G., Meyer, M. A., Agee, C. B., Busemann, H., et al. (2022). Rationale and proposed design for a Mars sample return (MSR) science program. *Astrobiology*, *22*(S1), S-27–S-56. https://doi.org/10.1089/ast.2021.0122

Hamran, S.-E., Paige, D. A., Allwood, A., Amundsen, H. E. F., Berger, T., Provoll, S., et al. (2022). Ground penetrating radar observations on subsurface structures in the floor of Jezero Crater, Mars. *Science Advances*, *8*(34), eabp8564. https://doi.org/10.1126/sciadv.abp8564

Hamran, S.-E., Paige, D. A., Amundsen, H. E. F., Berger, T., Brovoll, S., Carter, L., et al. (2020). Radar imager for Mars' subsurface experiment—RIMFAX. *Space Science Reviews*, *216*(8), 128. https://doi.org/10.1007/s11214-020-00740-4

Harper, C. L., Jr., Nyquist, L. E., Bansal, B., Wiesmann, H., & Shih, C.-Y. (1995). Rapid accretion and early differentiation of Mars indicated by ^{142}Nd/^{144}Nd in SNC meteorites. *Science*, *267*(5195), 213–217. https://doi.org/10.1126/science.7809625

Hauri, E. H., Saal, A. E., Rutherford, M. J., & Van Orman, J. A. (2015). Water in the Moon's interior: Truth and consequences. *Earth and Planetary Science Letters*, *409*, 252–264. https://doi.org/10.1016/j.epsl.2014.10.053

Hays, L., Graham, H. V., Des Marais, D. J., Hausrath, E. M., Horgan, B., McCollom, T. M., et al. (2017). Biosignature preservation and detection in Mars analog environments. *Astrobiology*, *17*(4), 363–400. https://doi.org/10.1089/ast.2016.1627

Herd, C. D. K., Walton, E. L., Agee, C. B., Muttik, N., Ziegler, K., Shearer, C. K., et al. (2017). The Northwest Africa 8159 Martian meteorite: Expanding the Martian sample suite to the early Amazonian. *Geochimica et Cosmochimica Acta*, *218*, 1–26. https://doi.org/10.1016/j.gca.2017.08.037

Horgan, B., Rice, M., Garczynski, B., Johnson, J., StackMorgan, K., Vaughan, A., et al. (2022). Mineralogy, Morphology, and geochronological significance of the Máaz formation and the Jezero Crater floor. In *Proceedings of the 53rd lunar and planetary science conference (LPSC)*. Lunar and Planetary Institute, United States of America.

Horgan, B. H. N., Anderson, R. B., Dromart, G., Amador, E. S., & Rice, M. S. (2020). The mineral diversity of Jezero Crater: Evidence for possible lacustrine carbonates on Mars. *Icarus*, *339*(15), 113526. https://doi.org/10.1016/j.icarus.2019.113526

Humayun, M., Nemchin, A., Zanda, B., Hewins, R. H., Grange, M., Kennedy, A., et al. (2013). Origin and age of the earliest Martian crust from meteorite NWA 7533. *Nature*, *503*(7477), 513–516. https://doi.org/10.1038/nature12764

iMOST. (2018). The potential science and engineering value of samples delivered to earth by Mars sample return. (co-chairs D. W. Beaty, M. M. Grady, H. Y. McSween, E. Sefton-Nash; documentarian B.L. Carrier; plus 66 co-authors) (p. 186). white paper. Posted August, 2018 by MEPAG at Retrieved from https://mepag.jpl.nasa.gov/reports.cfm

Jakosky, B., Amato, M., Atreya, S., Marais, D. D., Mahaffy, P., Mumma, M., et al. (2021). Scientific value of returning an atmospheric sample from Mars. *Bulletin of the AAS*, *53*(4). Whitepaper #159 submitted to the Planetary Science and Astrobiology Decadal Survey 2023-2032. Topics: atmospheric/exospheric evolution; life and prebiotic organics. https://doi.org/10.3847/25c2cfeb.9799651c

Jaramillo, E. A., Royle, S. H., Claire, M. W., Kounaves, S. P., & Sephton, M. A. (2019). Indigenous organic-oxidized fluid interactions in the Tissint Mars meteorite. *Geophysical Research Letters*, *46*(6), 3090–3098. https://doi.org/10.1029/2018gl081335

John, T., Gussone, N., Padladchikov, Y. Y., Bebout, G. E., Dohmne, R., HalamaKlemd, R. R., et al. (2012). Volcanic arcs fed by rapid pulsed fluid flow through subducting slabs. *Nature GeoScience*, *5*(7), 489–492. https://doi.org/10.1038/ngeo1482

Johnson, C. M., Beard, B. L., & Albarède, F. (2004). Geochemistry of non-traditional stable isotopes. *Reviews in Mineralogy and Geochemistry*, *55*(1), 1–24. https://doi.org/10.2138/gsrmg.55.1.1

Kang, J. T., Ionov, D. A., Liu, F., Zhang, C. L., Golovin, A. V., Qin, L. P., et al. (2017). Calcium isotopic fractionation in mantle peridotites by melting and metasomatism and Ca isotope composition of the bulk silicate Earth. *Earth and Planetary Science Letters*, *474*, 128–137. https://doi.org/10.1016/j.epsl.2017.05.035

Kizovski, T. V., Schmidt, M. E., Liu, Y., Clark, B. C., Tice, M., Herd, C. D. K., et al. (2022). Minor minerals analyzed by PIXL—A major part of igneous rock petrogenesis at Jezero Crater. In *Proceedings of the 53rd lunar and planetary science conference (LPSC)*. Lunar and Planetary Institute, United States of America.

Klein, F., Grozeva, N. G., & Seewald, J. S. (2019). Abiotic methane synthesis and serpentinization in olivine-hosted fluid inclusions. *PNAS*, *116*(36), 17666–17672. https://doi.org/10.1073/pnas.1907871116

Klein, F., Grozeva, N. G., Seewald, J. S., McCollom, T. M., Humphris, S. E., Moskowitz, B., et al. (2015). Experimental constraints on fluid-rock reactions during incipient serpentinization of harzburgite. *American Mineralogist*, *100*(4), 991–1002. https://doi.org/10.2138/am-2015-5112

Kminek, G., Benardini, J. N., Brenker, F. E., Brooks, T., Burton, A. S., Dhaniyala, S., et al. (2022). COSPAR sample safety assessment framework (SSAF). *Astrobiology*, *22*(S1), S-186–S-216. https://doi.org/10.1089/ast.2022.0017

Koike, M., Nakada, R., Kajitani, I., Usui, T., Tamenori, Y., Sugahara, H., & Kobayashi, A. (2020). In-situ preservation of nitrogen-bearing organics in Noachian Martian carbonates. *Nature Communications*, *11*(1), 1988. https://doi.org/10.1038/s41467-020-15931-4

Lammer, H., Chassefière, E., Karatekin, Ö., Morschhauser, A., Niles, P. B., Mousis, O., et al. (2013). Outgassing history and escape of the martian atmosphere and water Inventory. *Space Science Reviews*, *174*(1–4), 113–154. https://doi.org/10.1007/s11214-012-9943-8

Lapen, T. J., Righter, M., Andreasen, R., Irving, A. J., Satkoski, A. M., Beard, B. L., et al. (2017). Two billion years of magmatism recorded from a single Mars meteorite ejection site. *Science Advances*, *3*(2), e1600922. https://doi.org/10.1126/sciadv.1600922

Lapen, T. J., Righter, M., Brandon, A. D., Debaille, V., Beard, B. L., Shafer, J. T., & Peslier, A. H. (2010). A younger age for ALH84001 and its geochemical link to Shergottite sources in Mars. *Science*, *328*(5976), 347–351. https://doi.org/10.1126/science.1185395

Lasaga, A. (1998). *Kinetic theory in the Earth sciences*. Princeton University Press.

Liu, Y., Tice, M. M., Schmidt, M. E., Treiman, A. H., Kizovski, T. V., Hurowitz, J. A., et al. (2022). An olivine cumulate outcrop on the floor of Jezero Crater, Mars. *Science*, *377*(6614), 1513–1519. https://doi.org/10.1126/science.abo27

Madigan, M. T., Bender, K. S., Buckley, D. H., Sattley, W. M., Stahl, D. A., & Brock, T. D. (2022). *Brock biology of microorganisms* (16th ed., p. 1124). Pearson Education limited.

Madsen, M. B., Goetz, W., Bertelsen, P., Binau, C. S., Folkmann, F., Gunnlaugsson, H. P., et al. (2009). Overview of the magnetic properties experiments on the Mars Exploration Rovers. *Journal of Geophysical Research*, *114*(E6), E06S90. https://doi.org/10.1029/2008JE003098

Maki, J. N., Gruel, D., McKinney, C., Ravine, M. A., Morales, M., Lee, D., et al. (2020). The Mars 2020 engineering cameras and microphone on the perseverance rover: A next-generation imaging system for Mars exploration. *Space Science Reviews*, *216*(8), 137. https://doi.org/10.1007/s11214-020-00765-9

Mandon, L., Quantin-Nataf, C., Royer, C., Beck, P., Fouchet, T., Johnson, J. R., et al. (2022). Infrared reflectance of rocks and regolith at Jezero Crater one year of SuperCam observations. In *Proceedings of the 53rd lunar and planetary science conference (LPSC)*. Lunar and Planetary Institute, United States of America.

Mandon, L., Quantin-Nataf, C., Thollot, P., Mangold, N., Lozac'h, L., Dromart, G., et al. (2020). Refining the age, emplacement and alteration scenarios of the olivine-rich unit in the Nili Fossae region, Mars. *Icarus*, *336*, 113436. https://doi.org/10.1016/j.icarus.2019.113436

Mangold, N., Gupta, S., Gasnault, O., Dromart, G., Tarnas, J. D., Sholes, S. F., et al. (2021). Perseverance rover reveals an ancient delta-lake system and flood deposits at Jezero Crater, Mars. *Science*, *374*(6568), 711–717. https://doi.org/10.1126/science.abl4051

Maurice, S., Wiens, R. C., Bernardi, P., Caïs, P., Robinson, S., Nelson, T., et al. (2021). The SuperCam instrument suite on the Mars 2020 rover: Science objectives and mast-unit description. *Space Science Reviews*, *217*(3), 47. https://doi.org/10.1007/s11214-021-00807-w

McCubbin, F. M., Boyce, J. W., Srinivasan, P., Santos, A. R., Elardo, S. M., Filiberto, J., et al. (2016). Heterogeneous distribution of H_2O in the Martian interior: Implications for the abundance of H_2O in depleted and enriched mantle sources. *Meteoritics & Planetary Science*, *51*(11), 2036–2060. https://doi.org/10.1111/maps.12639

McCubbin, F. M., Hauri, E. H., Elardo, S. M., Vander Kaaden, K. E., Wang, J., & Shearer, C. K. (2012). Hydrous melting of the Martian mantle produced both depleted and enriched shergottites. *Geology*, *40*(8), 683–686. https://doi.org/10.1130/g33242.1

McCubbin, F. M., Lewis, J. A., Barnes, J. J., Elardo, S. M., & Boyce, J. W. (2021). The abundances of F, Cl, and H_2O in eucrites: Implications for the origin of volatile depletion in the asteroid 4 Vesta. *Geochimica et Cosmochimica Acta*, *314*, 270–293. https://doi.org/10.1016/j.gca.2021.08.021

McCubbin, F. M., Nekvasil, H., Harrington, A. D., Elardo, S. M., & Lindsley, D. H. (2008). Compositional diversity and stratification of the Martian crust: Inferences from crystallization experiments on the picrobasalt Humphrey from Gusev Crater, Mars. *Journal of Geophysical Research*, *113*(E11), E11013. https://doi.org/10.1029/2008JE003165

McCubbin, F. M., Smirnov, A., Nekvasil, H., Wang, J., Hauri, E., & Lindsley, D. H. (2010). Hydrous magmatism on Mars: A source of water for the surface and subsurface during the Amazonian. *Earth and Planetary Science Letters*, *292*(1–2), 132–138. https://doi.org/10.1016/j.epsl.2010.01.028

McKay, D. S., Gibson, E. K., Thomas-Keprta, K. L., Vali, H., Romanek, C., Clemett, S. J., et al. (1996). Search for past life on Mars: Possible relic biogenic activity in Martian meteorite ALH84001. *Science*, *273*(5277), 924–930. https://doi.org/10.1126/science.273.5277.924

McMahon, S., Bosak, T., Grotzinger, J. P., Milliken, R. E., Summons, R. E., Daye, M., et al. (2018). A field guide to finding fossils on Mars. *Journal of Geophysical Research: Planets*, *123*(5), 1012–1040. https://doi.org/10.1029/2017JE005478

McSween, H. Y. (2015). Petrology on Mars. *American Mineralogist*, *100*(11–12), 2380–2395. https://doi.org/10.2138/am-2015-5257

Meslin, P.-Y., Forni, O., Beck, P., Cousin, A., Beyssac, O., Lopez-Reyes, G., et al. (2022). Evidence for perchlorate and sulfate salts in Jezero Crater, Mars, from SuperCam observations. In *Proceedings of the 53rd lunar and planetary science conference (LPSC)*. Lunar and Planetary Institute, United States of America.

Meyer, M. A., Kminek, G., Beaty, D. W., Carrier, B. L., Haltigin, T. H., Hays, L. E., et al. (2022). Final report of the Mars sample return science planning group 2 (MSPG2). *Astrobiology*, *22*(S1), S-5–S-26. https://doi.org/10.1089/ast.2021.0121

Millan, M., Teinturier, S., Malespin, C. A., Bonnet, J. Y., Buch, A., Dworkin, J. P., et al. (2022). Organic molecules revealed in Mars's Bagnold Dunes by Curiosity's derivatization experiment. *Nature Astronomy*, *6*(1), 129–140. https://doi.org/10.1038/s41550-021-01507-9

Mills, R. D., Simon, J. I., & DePaolo, D. J. (2018). Calcium and neodymium radiogenic isotopes of igneous rocks: Tracing crustal contributions in felsic magmas related to super-eruptions and continental rifting. *Earth and Planetary Science Letters*, *495*, 242–250. https://doi.org/10.1016/j.epsl.2018.05.017

Moeller, R. C., Jandura, L., Rosette, K., Robinson, M., Samuels, J., Silverman, M., et al. (2021). The sampling and caching subsystem (SCS) for the scientific exploration of Jezero Crater by the Mars 2020 perseverance rover. *Space Sci Rev*, *217*(1), 5. https://doi.org/10.1007/s11214-020-00783-7

Moore, W. B., Simon, J. I., & Webb, A. A. G. (2017). Heat-pipe planets. *Earth and Planetary Science Letters*, *474*, 13–19. https://doi.org/10.1016/j.epsl.2017.06.015

Moriwaki, R., Usui, T., Simon, J. I., Jones, J. H., Yokoyama, T., & Tobita, M. (2017). Coupled Pb isotopic and trace element systematics of the Tissint meteorite: Geochemical signatures of the depleted shergottite source mantle. *Earth and Planetary Science Letters*, *474*, 180–189. https://doi.org/10.1016/j.epsl.2017.06.044

Moriwaki, R., Usui, T., Tobita, M., & Yokoyama, T. (2020). Geochemically heterogeneous Martian mantle inferred from Pb isotope systematics of depleted shergottites. *Geochimica et Cosmochimica Acta*, *274*, 157–171. https://doi.org/10.1016/j.gca.2020.01.014

Morris, R. V., Klingelhofer, G., Schroder, C., Rodionov, D. S., Yen, A., Ming, D. W., et al. (2006). Mössbauer mineralogy of rock, soil, and dust at Meridiani Planum, Mars: Opportunity's journey across sulfate-rich outcrop, basaltic sand and dust, and hematite lag deposits. *Journal of Geophysical Research*, *111*(E12), E12S15. https://doi.org/10.1029/2006JE002791

Mosenfelder, J. L., Rossman, G. R., Rossman, G. R., & Johnson, E. A. (2015). Hydrous species in feldspars: A reassessment based on FTIR and SIMS. *American Mineralogist*, *100*(5–6), 1209–1221. https://doi.org/10.2138/am-2015-5034

Murphy, M. A. E., Beegle, L. W., Bhartia, R., DeFlores, L., Abbey, W., Razzell Hollis, J., et al. (2022). The first 300 sols of the SHERLOC investigation on the Mars 2020 rover. In *Proceedings of the 53rd lunar and planetary science conference (LPSC)*. Lunar and Planetary Institute, United States of America.

Oelkers, E. H. (2001). An experimental study of forsterite dissolution rates as a function of temperature and aqueous Mg and Si concentrations. *Chemical Geology*, *175*(3–4), 485–494. https://doi.org/10.1016/s0009-2541(00)00352-1

Olsen, A. A., Hausrath, E. M., & Rimstidt, D. (2015). Forsterite dissolution rates in Mg-sulfate-rich Mars-analog brines and implications of the aqueous history of Mars. *Journal of Geophysical Research: Planets*, *120*(3), 388–400. https://doi.org/10.1002/2014je004664

Paniello, R., Day, J. M. D., & Moynier, F. (2012). Zinc isotopic evidence for the origin of the Moon. *Nature*, *490*(7420), 376–379. https://doi.org/10.1038/nature11507

Peslier, A. H. (2010). A review of water contents of nominally anhydrous natural minerals in the mantles of Earth, Mars, and the Moon. *Journal of Volcanology and Geothermal Research*, *197*(1–4), 239–258. https://doi.org/10.1016/j.jvolgeores.2009.10.006

Peters, T. J., Simon, J. I., Jones, J. H., Usui, T., Moriwaki, R., Economos, R. C., et al. (2015). Tracking the Martian mantle signature in olivine-host melt inclusions of basaltic shergottites Yamato 980459 and Tissint. *Earth and Planetary Science Letters*, *418*, 91–102. https://doi.org/10.1016/j.epsl.2015.02.033

Pinet, P. C., & Chevrel, S. D. (1990). Spectral identification of geological units on the surface of Mars related to the presence of silicates from Earth-based near-infrared telescopic charge-coupled device imaging. *Journal of Geophysical Research: Plants*, *95*(B9), 14435–14446. https://doi.org/10.1029/JB095iB09p14435

Pritchett, B. N., Madden, M. E. E., & Madden, A. S. (2012). Jarosite dissolution rates and maximum lifetimes in high salinity brines: Implications for Earth and Mars. *Earth and Planetary Science Letters*, *357–358*, 327–336. https://doi.org/10.1016/j.epsl.2012.09.011

Quantin-Nataf, C., Holm-Alwmark, S., Lasue, J., Calef, F. J., Shuster, D., Kinch, K. M., et al. (2021). The complex exhumation history of Jezero Crater floor unit. In *52nd lunar and planetary science conference*. LPI Contribution No. 2548.

Reeves, E. P., & Fiebig, J. (2020). Abiotic synthesis of methane and organic compounds in Earth's lithosphere. *Elements*, *16*(1), 25–31. https://doi.org/10.2138/gselements.16.1.25

Rice, M. S., Johnson, J. R., Million, C. C., St. Clair, M., Horgan, B. N., Vaughan, A., et al. (2022). Summary of Mastcam-Z visible to near infrared (VNIR) multispectral observations from perseverance's mission in Jezero Crater, Mars. In *Proceedings of the 53rd lunar and planetary science conference (LPSC)*. Lunar and Planetary Institute, United States of America.

Robie, R. A., Hemingway, B. S., & Fisher, J. R. (1979). Thermodynamic properties of minerals and related substances at 298.15°K and 1 Bar (105 Pascals) pressure and at higher temperatures. *United States Geological Survey Bulletin*, *1452*, 456.

Royer, C., Fouchet, T., Montmessin, F., Poulet, F., Forni, O., Johnson, J. R., et al. (2022). The detection of spectral signatures with IRS/SuperCam, perseverance rover: Instrument performance. In *Proceedings of the 53rd lunar and planetary science conference (LPSC)*. Lunar and Planetary Institute, United States of America.

Rubin, A. E., Warren, P. H., Greenwood, J. P., Verish, R. S., Leshin, L. A., Hervig, R. L., et al. (2000). Los Angeles: The most differentiated basaltic Martian meteorite. *Geology*, *28*(11), 1011–1014. https://doi.org/10.1130/0091-7613(2000)28<1011:latmdb>2.0.co;2

Ruedas, T., Tackley, P. J., & Solomon, S. C. (2013). Thermal and compositional evolution of the Martian mantle: Effects of phase transitions and melting. *Physics of the Earth and Planetary Interiors*, *216*, 32–58. https://doi.org/10.1016/j.pepi.2012.12.002

Saal, A. E., Hauri, E. H., Langmuir, C. H., & Perfit, M. R. (2002). Vapour undersaturation in primitive mid-ocean-ridge basalt and the volatile content of Earth's upper mantle. *Nature*, *419*(6906), 451–455. https://doi.org/10.1038/nature01073

Santos, A. R., Agee, C. B., McCubbin, F. M., Shearer, C. K., Burger, P. V., Tartse, R., & Anand, M. (2015). Petrology of igneous clasts in Northwest Africa 7034: Implications for the petrologic diversity of the Martian crust. *Geochimica et Cosmochimica Acta*, *157*, 56–85. https://doi.org/10.1016/j.gca.2015.02.023

Scheller, E. L., Razzell Hollis, J., Cardarelli, E. L., Steele, A., Beegle, L. W., Bhartia, R., et al. (2022). Aqueous alteration processes and implications for organic geochemistry in Jezero Crater, Mars. *Science*, *378*(6624), 1105–1110. https://doi.org/10.1126/science.abo5204

Schon, S. C., Head, J. W., & Fassett, C. I. (2012). An overfilled lacustrine system and progradational delta in Jezero Crater, Mars: Implications for Noachian climate. *Planetary and Space Science*, *67*(1), 28–45. https://doi.org/10.1016/j.pss.2012.02.003

Sephton, M. A., Wright, I. P., Gilmour, I., de Leeuw, J. W., Grady, M. M., & Pillinger, C. T. (2002). High molecular weight organic matter in Martian meteorites. *Planetary and Space Science*, *50*(7–8), 711–716. https://doi.org/10.1016/s0032-0633(02)00053-3

Shahrzad, S., Kinch, K. M., Goudge, T. A., Fassett, C., Needham, D. H., Quantin-Nataf, C., & Knudsen, C. P. (2019). Crater statistics on the dark-toned, mafic floor unit in Jezero Crater, Mars. *Geophysical Research Letters*, *46*(5), 2408–2416. https://doi.org/10.1029/2018gl081402

Sharma, S., Beegle, L. W., Bhartia, R., & the SHERLOC Team. (2022). 400 sols of SHERLOC on Mars. *GeoRaman*.

Sharma, S., Roppel, R., Murphy, A., Beegle, L. W., Bhartia, R., Steele, A., et al. (2022). Mapping organic-mineral associations in Jezero Crater: Implications for Martian organic geochemistry. In *AGU Fall Conference*.

Sholes, S. F., Stack, K. M., Kah, L. C., Simon, J. I., & Mangold, N. (2022). Topographic trends of the geologic units in Jezero Crater: Lake levels, potential shorelines, and the crater floor units. In *Proceedings of the 53rd lunar and planetary science conference (LPSC)*. Lunar and Planetary Institute, United States of America.

Shuster, D. L., Farley, K. A., Vasconcelos, P. M., Balco, G., Monteiro, H. S., Waltenberg, K., & Stone, J. O. (2012). Cosmogenic ^{3}He in hematite and goethite from Brazilian "canga" duricrust demonstrates the extreme stability of these surfaces. *Earth and Planetary Science Letters*, *329–330*, 41–50. https://doi.org/10.1016/j.epsl.2012.02.017

Shuster, D. L., Vasconcelos, P. M., Heim, J. A., & Farley, K. A. (2005). Weathering geochronology by (U-Th)/He dating of goethite. *Geochimica et Comochimica Acta*, *69*(3), 659–673. https://doi.org/10.1016/j.gca.2004.07.028

Simon, J. I. (2022). Calcium isotope constraints on recycled carbonates in subduction-related magmas. In *Isotopic constraints on Earth system processes* (pp. 43–56). https://doi.org/10.1002/9781119595007.ch3

Simon, J. I., Christoffersen, R., Wang, J., Mouser, M. D., Mills, R. D., Ross, D. K., et al. (2020). Volatiles in lunar felsite clast: Impact-related delivery of hydrous materials to an ancient dry lunar crust. *Geochimica et Cosmochimica Acta*, *276*, 299–326. https://doi.org/10.1016/j.gca.2020.02.008

Stack, K. M., Williams, N. R., Calef, F., Sun, V. Z., Williford, K. H., Farley, K. A., et al. (2020). Photogeologic map of the perseverance rover field site in Jezero Crater constructed by the Mars 2020 science team. *Space Science Reviews*, *216*(8), 127. https://doi.org/10.1007/s11214-020-00739-x

Steele, A., Benning, L. G., Wirth, R., Schreiber, A., Araki, T., McCubbin, F. M., et al. (2022). Organic synthesis associated with serpentinization and carbonation on early Mars. *Science*, *375*(6577), 172–177. https://doi.org/10.1126/science.abg7905

Steele, A., Benning, L. G., Wirth, R., Siljeström, S., Fries, M. D., Hauri, E., et al. (2018). Organic synthesis on Mars by electrochemical reduction of CO_2. *Science Advances*, *4*(10), eaat5118. https://doi.org/10.1126/sciadv.aat5118

Steele, A., McCubbin, F. M., Fries, M., Kater, L., Boctor, N. Z., Fogel, M. L., et al. (2012). A reduced organic carbon component in Martian basalts. *Science*, *337*(6091), 212–215. https://doi.org/10.1126/science.1220715

Steele, A., McCubbin, F. M., & Fries, M. D. (2016). The provenance, formation, and implications of reduced carbon phases in Martian meteorites. *Meteoritics & Planetary Science*, *51*(11), 2203–2225. https://doi.org/10.1111/maps.12670

Steiner, M. H., Hausrath, E. M., Madden, M. E., Tschauner, O., Ehlmann, B. L., Olsen, A. A., et al. (2016). Dissolution of nontronite in chloride brines and implications for the aqueous history of Mars. *Geochimica et Cosmochimica Acta*, *195*, 259–276. https://doi.org/10.1016/j.gca.2016.08.035

Summons, R. E., Amend, J. P., Bish, D., Buick, R., Cody, G. D., Des Marais, D. J., et al. (2011). Preservation of Martian organic and environmental records: Final report of the Mars biosignature working group. *Astrobiology*, *11*(2), 157–181. https://doi.org/10.1089/ast.2010.0506

Sun, V. Z., Hand, K. P., Stack, K. M., Farley, K. A., Milkovich, S., Kronyak, R., et al. (2022). Exploring the Jezero Crater floor: Overview of results from the Mars 2020 perseverance rover's first science campaign. In *Proceedings of the 53rd lunar and planetary science conference (LPSC)*. Lunar and Planetary Institute, United States of America.

Swindle, T. D., Atreya, S., Busemann, H., Cartwright, J. A., Mahaffy, P., Marty, B., et al. (2022). Scientific value of including an atmospheric sample as part of Mars sample return (MSR). *Astrobiology*, *22*(S1), S-165–S-175. https://doi.org/10.1089/ast.2021.0107

Tait, K. T., & Day, J. M. (2018). Chondritic late accretion to Mars and the nature of shergottite reservoirs. *Earth and Planetary Science Letters*, *494*, 99–108. https://doi.org/10.1016/j.epsl.2018.04.040

Tait, K. T., McCubbin, F. M., Smith, C. L., Agee, C. B., Busemann, H., Cavalazzi, B., et al. (2022). Preliminary planning for Mars sample return (MSR) curation activities in a sample receiving facility (SRF). *Astrobiology*, *22*(S1), S-57–S-80. https://doi.org/10.1089/ast.2021.0105

Tanaka, K. L., Skinner, J. A., Jr., Dohm, J. M., Irwin, R. P., III, Kolb, E. J., Fortezzo, C. M., et al. (2014). Geologic map of Mars. Retrieved from http://pubs.usgs.gov/sim/3292/

Teng, F.-Z., Dauphas, N., Helz, R. T., Gao, S., & Huang, S. (2011). Diffusion-driven magnesium and iron isotope fractionation in Hawaiian olivine. *Earth and Planetary Science Letters*, *308*(3–4), 317–324. https://doi.org/10.1016/j.epsl.2011.06.003

Teng, F.-Z., Dauphas, N., & Watkins, J. M. (2017). Non-traditional stable isotopes: Retrospective and prospective. *Reviews in Mineralogy and Geochemistry*, *82*(1), 1–26. https://doi.org/10.2138/rmg.2017.82.1

Tice, M. M., Hurowitz, J. A., Allwood, A. C., Jones, M. W., Brendan, M., Orenstein, J., et al. (2022). Alteration history of Séítah formation rocks inferred by PIXL X-ray fluorescence, X-ray diffraction, and multispectral imaging on Mars. *Science Advances*, *8*(47), eabp9084. https://doi.org/10.1126/sciadv.abp9084

Tomascak, P. B. (2004). Developments in the understanding and application of lithium isotopes in the Earth and planetary sciences. *Reviews in Mineralogy and Geochemistry*, *55*(1), 153–195. https://doi.org/10.2138/gsrmg.55.1.153

Udry, A., Howarth, G. H., Herd, C. D. K., Day, J. M. D., Lapen, T. J., & Filiberto, J. (2020). What Martian meteorites reveal about the interior and surface of Mars. *Journal of Geophysical Research: Planets*, *125*(12), e2020JE006523. https://doi.org/10.1029/2020je006523

Udry, A., Howarth, G. H., Lapen, T. J., & Righter, M. (2017). Petrogenesis of the NWA 7320 enriched Martian gabbroic shergottite: Insight into the Martian crust. *Geochimica et Cosmochimica Acta*, *204*(3), 1–18. https://doi.org/10.1016/j.gca.2017.01.032

Udry, A., Sautter, V., Cousin, A., Wiens, R. C., Forni, O., Benzerara, K., et al. (2022). Mars 2020 perseverance SuperCam perspective on the igneous nature of the Máaz formation at Jezero Crater, Mars. *Journal of Geophysical Research: Planets*, *127*, e2022JE007440. https://doi.org/10.1029/2022JE007440

Usui, T., Alexander, C. M. D., Wang, J., Simon, J. I., & Jones, J. H. (2015). Meteoritic evidence for a previously unrecognized hydrogen reservoir on Mars. *Earth and Planetary Science Letters*, *410*, 140–151. https://doi.org/10.1016/j.epsl.2014.11.022

Usui, T., Alexander, C. M. O. D., Wang, J., Simon, J. I., & Jones, J. H. (2012). Origin of water and mantle–crust interactions on Mars inferred from hydrogen isotopes and volatile element abundances of olivine-hosted melt inclusions of primitive shergottites. *Earth and Planetary Science Letters*, *357–358*, 119–129. https://doi.org/10.1016/j.epsl.2012.09.008

Vervelidou, F., Lesur, V., Grott, M., Morshhauser, A., & Lillis, R. (2017). Constraining the date of the Martian dynamo shutdown by means of crater magnetization signatures. *Journal of Geophysical Research: Planets*, *122*(11), 2294–2311. https://doi.org/10.1002/2017JE005410

Wacey, D., Mcloughlin, N., & Brasier, M. D. (2009). Looking through windows onto the earliest history of life on Earth and Mars. In J. Seckbach & M. Walsh (Eds.), *From fossils to astrobiology, cellular origin, life in extreme habitats and astrobiology* (Vol. 12). Springer. https://doi.org/10.1007/978-1-4020-8837-7_3

Walton, E. L., Kelly, S. P., & Herd, C. D. K. (2008). Isotopic and petrographic evidence for young Martian basalts. *Geochimica et Cosmochimica Acta*, *72*(23), 5819–5837. https://doi.org/10.1016/j.gca.2008.09.005

Warren, P. H., & Kallemeyn, G. M. (1994). Siderophile trace elements in ALH84001, other SNC meteorites and eucrites: Evidence of heterogeneity, possibly time-linked, in the mantle of Mars. *Meteoritics & Planetary Science*, *31*(1), 97–105. https://doi.org/10.1111/j.1945-5100.1996.tb02059.x

Watkins, J. M., DePaolo, D. J., Huber, C., & Ryerson, F. J. (2009). Liquid composition-dependence of calcium isotope fractionation during diffusion in molten silicates. *Geochimica et Cosmochimica Acta*, *73*(24), 7341–7359. https://doi.org/10.1016/j.gca.2009.09.004

Weiss, B. P., Kim, S. S., Kirschvink, J. L., Kopp, R. E., Sankaran, M., Kobayshi, A., & Komeili, A. (2004). Magnetic tests for magnetosome chains in Martian meteorite ALH84001. *Proceedings of the National Academy of Sciences of the United States of America*, *101*(22), 8281–8284. https://doi.org/10.1073/pnas.0402292101

Werner, S. C. (2008). The early Martian evolution—Constraints from basin formation ages. *Icarus*, *195*(1), 45–60. https://doi.org/10.1016/j.icarus.2007.12.008

Westall, F., & Brack, A. (2018). The importance of water for life. *Space Science Reviews*, *214*(2), 50. https://doi.org/10.1007/s11214-018-0476-7

Westall, F., Foucher, F., Bost, N., Bertrand, M., Loizeau, D., Vago, J. L., et al. (2015). Biosignatures on Mars: What, where, and how? Implications for the search for Martian life. *Astrobiology*, *15*(11), 998–1029. https://doi.org/10.1089/ast.2015.1374

Wiens, R. C., Maurice, S., Robinson, S. H., Nelson, A. E., Cais, P., Bernardi, P., et al. (2021). The SuperCam instrument suite on the NASA Mars 2020 rover: Body unit and combined system tests. *Space Science Reviews*, *217*(1), 4. https://doi.org/10.1007/s11214-020-00777-5

Wiens, R. C., Udry, A., Beyssac, O., Quantin-Nataf, C., Mangold, N., Cousin, A., et al. (2022). Compositionally and density stratified igneous terrain in Jezero Crater, Mars. *Science Advances*, *8*(34), eabo3399. https://doi.org/10.1126/sciadv.abo3399

Yen, A. S., Mittlefehldt, D. W., McLennan, S. M., Gellert, R., Bell, J. F., III, McSween, H. Y., Jr., et al. (2006). Nickel on Mars: Constraints on meteoritic material at the surface. *Journal of Geophysical Research*, *111*(E12), E12S11. https://doi.org/10.1029/2006JE002797

Zastrow, A. M., & Glotch, T. D. (2021). Distinct carbonate lithologies in Jezero Crater, Mars. *Geophysical Research Letters*, *48*(9), e2020GL092365. https://doi.org/10.1029/2020GL092365

Zhang, L., Wang, Q., Ding, X., & Li, W.-C. (2021). Diverse serpentinization and associated abiotic methanogenesis within multiple types of olivine-hosted fluid inclusions in orogenic peridotite from northern Tibet. *Geochimica et Cosmochimica Acta*, *296*, 1–17. https://doi.org/10.1016/j.gca.2020.12.016